Technical Report Documentation Page

1. Report No.	2. Government Accession No.	3. Recipient's Catalog No.
FHWA/TX-93+1267-1F		

4. Title and Subtitle	5. Report Date
HYDRAULIC CHARACTERISTICS OF RECESSED CURB INLETS AND BRIDGE DRAINS	November 1992
	6. Performing Organization Code
7. Author(s)	8. Performing Organization Report No.
Edward R. Holley, Carl Woodward, Aldo Brigneti, and Clemens Ott	Research Report 1267-1F
9. Performing Organization Name and Address	10. Work Unit No. (TRAIS)
Center for Transportation Research The University of Texas at Austin Austin, Texas 78712-1075	
	11. Contract or Grant No. Research Study 3-5-91/2-1267
	13. Type of Report and Period Covered Final
12. Sponsoring Agency Name and Address	14. Sponsoring Agency Code
Texas Department of Transportation Transportation Planning Division P. O. Box 5051 Austin, Texas 78763-5051	

15. Supplementary Notes

Study conducted in cooperation with the U.S. Department of Transportation, Federal Highway Administration
Research Study Title: "Hydraulic Characteristics of Recessed Curb Inlets and Bridge Drains"

16. Abstract

One of the many concerns about roadway safety is how to remove precipitation runoff from the roadway surface quickly and efficiently. On uncurbed roadways, water simply drains into adjacent ditches. On curbed roadways, water is removed by allowing it to flow down a gutter until it reaches an inlet structure, at which point it is diverted through a subsurface drainage system. The problem is that not all inlet structures are uniformly effective.

This study analyzed the effectiveness of both grate and curb inlets; the efficiency of several types of bridge deck drains was also investigated. Overall, the study had three objectives: (1) to determine the hydraulic characteristics of recessed curb inlets for different flow conditions and curb inlet geometries; (2) to determine the hydraulic characteristics of three types of bridge deck drains with different flow conditions and geometries; and, finally, (3) to provide predictive equations for performance and capacity—so as to obtain new design guidelines for the construction of both recessed curb inlets and bridge drains.

Concerning recessed curb inlets, three geometries of inlets and three inlet lengths were tested. For the experiments, the flow rate into the recessed curb inlet, the flow rate passing the inlet section (the carryover), and water depths on the roadway surface were measured. Based on an approach that categorizes curb inlets as either 100 percent efficient or less than 100 percent efficient, a new design equation (the "captured" flow divided by the gutter flow) was developed in which a facility's efficiency is expressed as a function of the effective length of the inlet divided by the effective length required to capture all of the flow.

For all three bridge deck drains tested, regression analysis was used to determine the flow into the inlet as a function of the upstream uniform flow depth, the longitudinal roadway slope, and the cross slope. In this way, empirical equations for predicting the capacity for the flow conditions most likely to be encountered on bridges were obtained.

17. Key Words	18. Distribution Statement
Recessed curb inlets, grate inlets, bridge drains, scupper drains, roadway gutters, curb inlet geometry	No restrictions. This document is available to the public through the National Technical Information Service, Springfield, Virginia 22161.

19. Security Classif. (of this report)	20. Security Classif. (of this page)	21. No. of Pages	22. Price
Unclassified	Unclassified	88	

HYDRAULIC CHARACTERISTICS OF RECESSED CURB INLETS AND BRIDGE DRAINS

by

Edward R. Holley
Carl Woodward
Aldo Brigneti
Clemens Ott

Research Report 1267-1F

Hydraulic Characteristics of Recessed Curb Inlets and Bridge Drains
Research Project 3-5-91/1267

conducted for the

Texas Department of Transportation

in cooperation with the

U.S. Department of Transportation
Federal Highway Administration

by the

CENTER FOR TRANSPORTATION RESEARCH
Bureau of Engineering Research
THE UNIVERSITY OF TEXAS AT AUSTIN

November 1992

DISCLAIMERS

The contents of this report reflect the views of the authors, who are responsible for the facts and the accuracy of the data presented herein. The contents do not necessarily reflect the official views or policies of the Federal Highway Administration or the Texas Department of Transportation. This report does not constitute a standard, specification, or regulation.

There was no invention or discovery conceived or first actually reduced to practice in the course of or under this contract, including art, method, process, machine, manufacture, design or composition of matter, or any new and useful improvement thereof, or any variety of plant which is or may be patentable under the patent laws of the United States of America or any foreign country.

NOT INTENDED FOR CONSTRUCTION,
PERMIT, OR BIDDING PURPOSES

Edward R. Holley, P.E. (Texas No. 51638)
Study Supervisor

METRIC (SI*) CONVERSION FACTORS

APPROXIMATE CONVERSIONS TO SI UNITS

Symbol	When You Know	Multiply by	To Find	Symbol
		LENGTH		
in	inches	2.54	centimeters	cm
ft	feet	0.3048	meters	m
yd	yards	0.914	meters	m
mi	miles	1.61	kilometers	km
		AREA		
in^2	square inches	645.2	millimeters squared	mm^2
ft^2	square feet	0.0929	meters squared	m^2
yd^2	square yards	0.836	meters squared	m^2
mi^2	square miles	2.59	kilometers squared	km^2
ac	acres	0.395	hectares	ha
		MASS (weight)		
oz	ounces	28.35	grams	g
lb	pounds	0.454	kilograms	kg
T	short tons (2,000 lb)	0.907	megagrams	Mg
		VOLUME		
fl oz	fluid ounces	29.57	milliliters	mL
gal	gallons	3.785	liters	L
ft^3	cubic feet	0.0328	meters cubed	m^3
yd^3	cubic yards	0.0765	meters cubed	m^3
		TEMPERATURE (exact)		
°F	Fahrenheit temperature	5/9 (after subtracting 32)	Celsius temperature	°C

NOTE: Volumes greater than 1,000 L shall be shown in m^3.

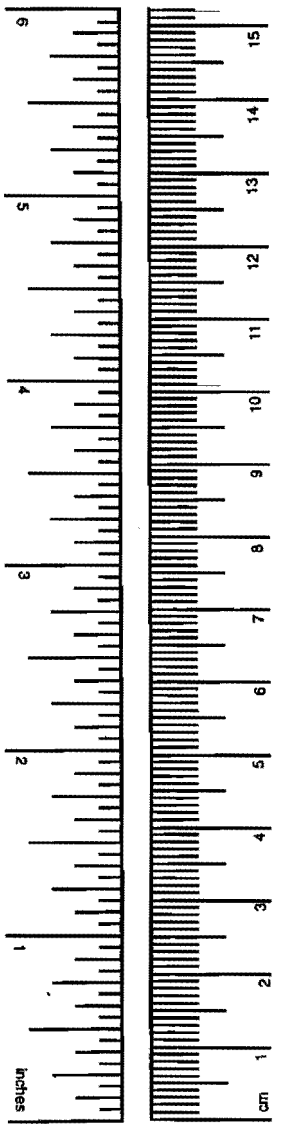

APPROXIMATE CONVERSIONS FROM SI UNITS

Symbol	When You Know	Multiply by	To Find	Symbol
		LENGTH		
mm	millimeters	0.039	inches	in
m	meters	3.28	feet	ft
m	meters	1.09	yards	yd
km	kilometers	0.621	miles	mi
		AREA		
mm^2	millimeters squared	0.0016	square inches	in^2
m^2	meters squared	10.764	square feet	ft^2
m^2	meters squared	1.20	square yards	yd^2
km^2	kilometers squared	0.39	square miles	mi^2
ha	hectares (10,000 m^2)	2.53	acres	ac
		MASS (weight)		
g	grams	0.0353	ounces	oz
kg	kilograms	2.205	pounds	lb
Mg	megagrams (1,000 kg)	1.103	short tons	T
		VOLUME		
mL	milliliters	0.034	fluid ounces	fl oz
L	liters	0.264	gallons	gal
m^3	meters cubed	35.315	cubic feet	ft^3
m^3	meters cubed	1.308	cubic yards	yd^3
		TEMPERATURE (exact)		
°C	Celsius temperature	9/5 (then add 32)	Fahrenheit temperature	°F

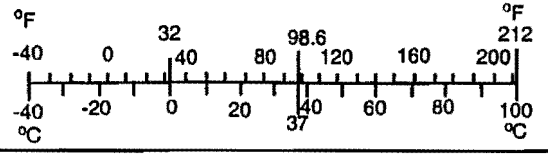

These factors conform to the requirement of FHWA Order 5190.1A.

* SI is the symbol for the International System of Measurements

TABLE OF CONTENTS

DISCLAIMERS ..... *iii*

METRICATION ..... *iv*

SUMMARY ..... *vii*

CHAPTER 1. INTRODUCTION

1.1 BACKGROUND *1*
1.2 OBJECTIVES *1*
1.3 APPROACH *1*
1.4 ACKNOWLEDGEMENTS *2*

PART I. RECESSED CURB INLETS

CHAPTER 2. LITERATURE REVIEW

2.1 FLOW OVER A BROAD-CRESTED WEIR (IZZARD, 1950) *4*
2.2 FLOW OVER A FREE DROP (LI, 1954) *5*
2.3 COMPARISONS OF THE TWO METHODS *6*
2.4 OTHER INVESTIGATIONS *7*
2.5 MODIFIED MANNING'S EQUATION *9*

CHAPTER 3. THE PHYSICAL MODEL

3.1 MODEL LENGTH SCALE *11*
3.2 MODEL CONSTRUCTION *11*
3.3 MODEL LAYOUT *12*
3.4 RECESSED CURB INLET GEOMETRY *13*
3.5 ROADWAY ROUGHNESS *13*
3.6 MEASUREMENTS *14*
3.6.1 Venturi Meter for the North Pipe *14*
3.6.2 Flow Sensor for the South Pipe *15*
3.6.3 V-Notch Weir for the Carryover *16*
3.6.4 V-Notch Weir for Total Discharge *16*
3.6.5 Water Surface Elevation Measurement *17*
3.7 DATA ANALYSIS *18*

CHAPTER 4. EXPERIMENTAL RESULTS

4.1 EXPERIMENTAL LABORATORY PROCEDURES *19*
4.1.1 Reverse Curve Transition *19*
4.1.2 Linear Transition *20*
4.1.3 20% Recessed Slope *20*
4.2 LABORATORY RESULTS FOR REVERSE CURVE TRANSITIONS *20*
4.2.1 Inlet Efficiency = 100% *20*
4.2.2 Results for Inlet Efficiency < 100% *22*
4.2.2.1 Analysis in Terms of Efficiency *22*
4.2.2.2 Analysis of Residuals *23*
4.2.2.3 Effects of Inlet Length and Froude Number *23*
4.2.2.4 Comparison to Flush Inlets *25*

4.3 LABORATORY RESULTS FOR LINEAR TRANSITIONS 26
4.3.1 Inlet Efficiency = 100% 26
4.3.2 Inlet Efficiency < 100% 26
4.4 LABORATORY RESULTS FOR 20% RECESSED SLOPE 27
4.5 FIELD TESTS 28
4.5.1 Procedures 28
4.5.2 Results 29

CHAPTER 5. CONCLUSIONS FOR RECESSED CURB INLETS 31

PART II. BRIDGE DECK DRAINS

CHAPTER 6. INTRODUCTION 33

CHAPTER 7. EXPERIMENTS AND RESULTS
7.1 THE PHYSICAL MODEL 35
7.2 MEASUREMENTS 35
7.3 DRAIN 1 (SCUPPER DRAIN) 36
7.3.1 Geometry and Description 36
7.3.2 Procedures 36
7.3.3 Results 36
7.3.4 Limits of Applicability 38
7.4 DRAIN 2 38
7.4.1 Geometry and Description 38
7.4.2 Procedures 39
7.4.3 Results 41
7.4.3.1 Effects of Piping System 41
7.4.3.2 Results for Low Flow Conditions 42
7.4.4 Limits of Applicability 44
7.4.5 Comparison of Results for Drain 2 with HEC-12 44
7.5 DRAIN 3 44
7.5.1 Geometry and Description 44
7.5.2 Procedures 45
7.5.3 Results 45
7.5.4 Limits of Applicability 46
7.5.5 Comparison of Results for Drain 3 with HEC-12 46

CHAPTER 8. CONCLUSIONS FOR BRIDGE DECK DRAINS 51

REFERENCES 53

APPENDIX A. DATA FOR RECESSED CURB INLETS 55

APPENDIX B. DATA FOR BRIDGE DECK DRAINS 65

APPENDIX C. PHOTOGRAPHS 73

SUMMARY

The hydraulic characteristics of flow into roadway drainage facilities and the flow capacity of these facilities are important considerations from the standpoints of both safety and possible nuisance. Previous studies have been done on curb inlets and bridge deck drains, but the designs of these facilities are sometimes changed for various reasons. Changes in the geometry of drainage facilities also affect the hydraulics and the flow capacity. These types of changes have meant that some drains have been installed after being designed by inference from other similar facilities since design information on the particular geometries being used was not available. This was the case for the recessed curb inlets and the three types of bridge deck drains which were studied in this project.

In order to obtain design information for these inlets and drains, a large hydraulic model was designed and constructed. The model was 64 feet long and 10.5 feet wide to represent one lane of a roadway at three-quarters scale. It was constructed so that both the cross slope and the longitudinal slope could be easily changed. The roadway surface had a uniform cross slope, not a compound slope. There was no depression in front of the curb line.

A literature review was conducted, primarily to determine the source of some of the design information which is normally used for curb inlets. This review located two different analyses which appear to be the background for dividing the flow into curb inlets into separate categories for 100% efficiency and less than 100% efficiency. Although the general forms of the two equations in the literature for 100% efficiency were the same, the numerical coefficients were different. For less than 100% efficiency, the basic forms of the equations were significantly different. Each of the authors compared the equations to experimental data, apparently indicating that the details of roadway geometry can have a significant influence on the capacity of inlets.

For the recessed curb inlets, three geometries of inlets and three inlet lengths were tested. The first geometry had reverse curve transitions 10 feet long at both ends of the inlet opening, which was recessed 1.5 feet from the curb line. (All dimensions are prototype sizes unless stated differently.) Inlet lengths of 15, 10, and 5 feet were tested. For 100% efficiency, it was possible to obtain basically the same type of design equation as is used for flush inlets by defining an effective length of the inlet to be used in place of the actual length of a flush inlet. For the reverse curve transitions, the effective length at 100% efficiency was 2 feet shorter than the total length of the curb opening. For less than 100% efficiency, the downstream transition section loses effectiveness for capturing flow. Even after water crosses the curb line and enters the region of the downstream transition, the momentum of the flow can cause it to flow back up the slope behind the curb line and back into the street. Thus, for less than 100% efficiency, a recessed inlet with the same actual opening length as a flush inlet may be only slightly more effective than a flush inlet with the same opening length. A new design equation was developed for the efficiency of the inlet (the flow captured divided by the gutter flow) as a function of the effective length of the inlet divided by the effective length required to capture all of the flow.

After completing the analysis of the tests with reverse curve transitions, a smaller number of tests were done for linear transition sections and for the slope from the gutter line to the inlet opening reduced from 30% to 20%. Neither of these changes had a significant effect on the results, other than that the effective length for the linear transition sections included the entire 10 feet of the downstream transition section, rather than only 8 feet as for the reverse curve transitions. Thus, the linear transitions are slightly more efficient than the reverse curves.

The three types of bridge deck drains were a 4-inch-by-6-inch rectangular scupper and two types of grated inlets. The scupper and the smaller grated inlet were tested at full scale, while the larger grated inlet was tested at three-quarters scale. All of the inlets were constructed of plexiglass so that the flow in the inlet boxes and in the subsequent piping could be seen. For each of the drains, the flow regimes fell into either of two categories. For the lower gutter depth and flows, the flow into the drain was ap-

parently controlled by weir flow over the lip of the inlets or orifice control as the water flowed from the inlet box into the drain pipe. (For the scupper, the only possibility was weir control since there was no subsequent piping.) For higher flows for the two grated inlets, there were back-pressure effects from the drain piping. One of the grated inlets is normally followed by 6-inch drain piping. For this inlet, several different configurations of piping were first tested to determine the effects on the flow into the inlet. It was determined that the most critical situation existed when the first elbow in the piping system was closest to the bottom of the inlet box. Thus, this configuration was used for the remainder of the tests. The tests revealed that the most likely range of inlet flows for these bridge drains fell into the low flow regime. Thus, attention was concentrated on these conditions for developing design information. For each of the drains, regression analysis was used to determine the flow into the inlet as a function of the upstream uniform flow depth, the longitudinal roadway slope, and the cross slope.

CHAPTER 1. INTRODUCTION

1.1 BACKGROUND

One of the many concerns about roadway safety is how to remove precipitation runoff from the roadway surface and adjacent areas quickly and efficiently. On uncurbed roadways, water simply drains into adjacent ditches. With curbed roadways, the basic principle of removal is to allow the water to flow down the gutter until it reaches an inlet structure. After the water enters the inlet, it flows away from the roadway through a subsurface drainage system. Similarly, runoff from bridge decks is captured by bridge deck drains. Depending on the type of bridge deck drain, the water may then fall freely through the air or it may flow downward through a piping system.

Inability of inlets and drains to adequately intercept the runoff results in water standing on the roadway and possibly on adjacent property. Standing water threatens traffic safety by causing hydroplaning of vehicles, deterioration of the pavement due to the seepage of water, and accumulation of sediments and debris in low areas.

Several types of inlet structures are used for roadways. Two of the primary types are grate inlets and curb inlets. A grate inlet uses metal bars placed in the roadway surface with the bars parallel and/or perpendicular to the flow of water. Flush inlets are simply vertical openings in the curb face and may or may not have a depression in the roadway adjacent to the inlet. According to Wasley (1960), grate inlets allow more flow to enter per given length than flush curb inlets. One drawback of grate inlets is their high probability of clogging since the opening between the bars is smaller than the opening for a curb inlet. Another potential problem is interference with traffic. Clogging is not often a problem with curb inlets. Unlike the grate inlet, the curb inlet does not interfere with traffic. A third type of inlet is a combination inlet, which uses a curb opening inlet and a grate inlet. One of the purposes of combining the two types of inlets is to achieve good efficiency while minimizing the potential for clogging.

Similarly, several types of bridge deck drains exist. These drains may be either open scupper drains with subsequent free fall of the captured runoff or grated drains in the bridge decks with a variety of geometries of the grates, of the boxes beneath the grates, and of the subsequent drain pipes.

1.2 OBJECTIVES

The primary objectives of this research were to

1. determine hydraulic characteristics of recessed curb inlets for different flow conditions and curb inlet geometries;
2. determine hydraulic characteristics of three types of bridge deck drains with different flow conditions and geometries; and
3. develop design information related to objectives 1 and 2.

1.3 APPROACH

The primary variables which influence the amount of flow captured by inlets and drains are longitudinal gutter slope, transverse pavement slope and geometry, flow rate in the gutter, Manning's roughness, flow regime (i.e., whether the flow is subcritical or supercritical), and inlet or drain size and geometry. Obtaining mathematical solutions for the amount of flow captured is a very complex problem. In fact, the computational approach is so complex that it would require verification against experimental results before complete confidence could be placed in the results of the computations. Thus, the primary approach for accomplishing the project objectives (Section 1.2) was to construct a large, versatile physical model of a roadway and to conduct a large number of experiments to cover the expected flow conditions and geometries of recessed curb inlets and bridge deck drains. Field testing of recessed curb inlets was also done to verify the

results of the laboratory tests on these inlets. Apparently, no hydraulic data previously existed for recessed curb inlets, which were being designed by inference from other types of inlets. The three bridge deck drains were also being designed without any hydraulic data on these specific geometries of drains. In addition, for the two drains with piping systems below them, attention was given to the effects of the piping on the drain capacity and hydraulic behavior.

Following Chapter 1, the remainder of the report is divided into two parts. Part I (Chapters 2-5) is for recessed curb inlets, and Part II (Chapters 6-8) is for bridge deck drains. Part I includes a description of the model facility. The data for Parts I and II are in Appendices A and B, respectively. Appendix C contains photographs. Some of the equations in this report are given in dimensionally consistent equations; such equations may be used with any set of consistent units. When specific units are needed for the equations which are not dimensionally consistent, traditional English units are used throughout.

1.4 ACKNOWLEDGEMENTS

This research was funded by the Texas Department of Transportation (TxDOT) through the Center for Transportation Research (CTR) at The University of Texas at Austin. The project number was 3-5-91/2-1267, entitled "Hydraulic Characteristics of Recessed Curb Inlets and Bridge Deck Drains." The research was conducted at the Center for Research in Water Resources. The graduate students (Carl Woodward, Aldo Brigneti, Clemens Ott, and Clint Willson) actually carried out the primary parts of the research. Various ones of them designed the physical model, supervised and assisted with the model construction, conducted the tests, analyzed the data, and wrote the first draft of different parts of this report. M. D. Englehardt and other personnel associated with the Ferguson Structural Engineering Laboratory of The University of Texas at Austin provided significant assistance with structural aspects of designing and constructing the roadway model. The project was supervised primarily by E. R. Holley and also by G. H. Ward. The supervisors were intimately involved in all aspects of the planning and execution of the project. E. R. Holley prepared the final draft of this report. Peter Smith of the Division of Bridges and Structures, TxDOT, was the Technical Panel Chair. He was extremely helpful in all phases of the research from its conception through its execution to the writing of this report.

PART I. RECESSED CURB INLETS

CHAPTER 2. LITERATURE REVIEW

As the name implies, recessed curb inlets are placed some distance behind the gutter line (Figures 2.1, C.1). A common geometry is to have reverse-curve transition sections upstream and downstream of the actual inlet opening. As the water flows down the roadway gutter at a flow rate of Q_a, the depth approaches normal depth if the roadway geometry, slope, and roughness are uniform. When the water reaches the recessed inlet section, some of it begins the transition in the direction to pass over the inlet lip at the curb line, down the recessed slope which is often steeper than the pavement cross slope, and ultimately into the inlet opening. In this report, the steeper slope between the curb line and the actual inlet opening is called the recessed slope (Figure 2.1b).

Before this project, apparently no research had been conducted on this particular type of stormwater inlet. The majority of the previous research had focused on flush inlets and grate inlets. One of the primary objectives of the literature search was to determine the source of the design information which is currently being used by TxDOT for flush inlets. The articles by Izzard and by Li (Sections 2.1 through 2.3) provided most of the related background information. In the process of searching for that information (since the references were not known at the beginning of the project), a few other references on curb inlets were also located. Some of those other studies are briefly summarized in Section 2.4.

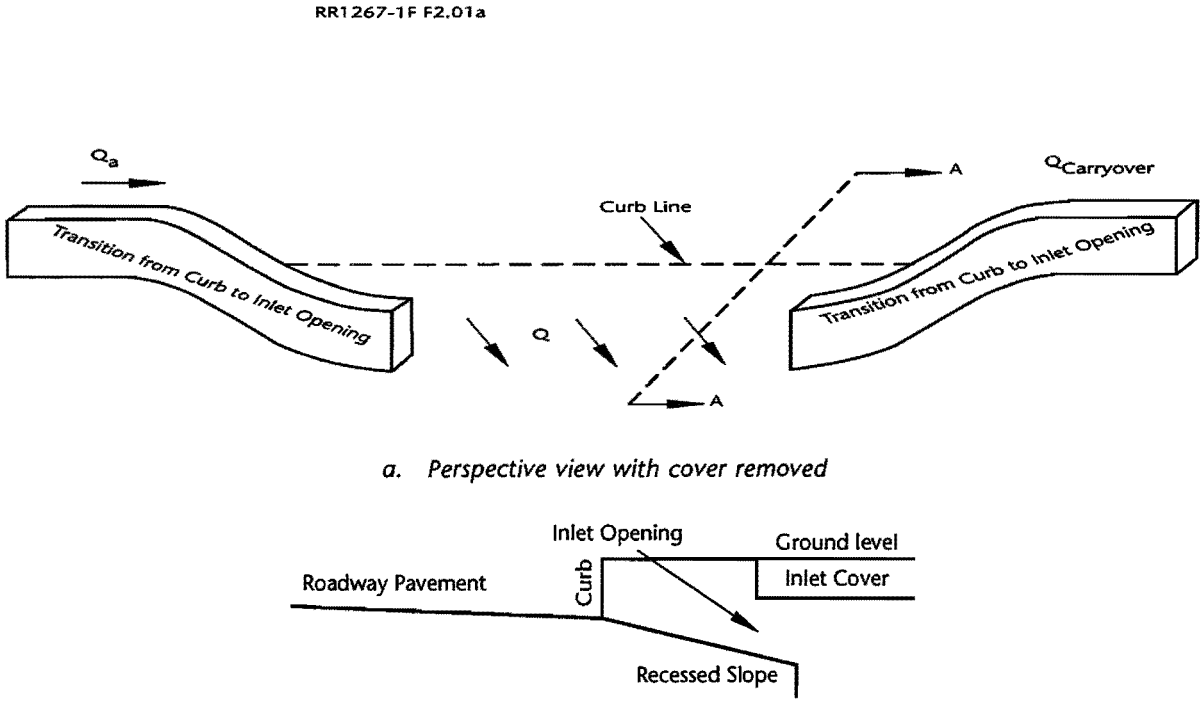

a. Perspective view with cover removed

b. Section A-A

Figure 2.1 Recessed curb inlet

2.1 FLOW OVER A BROAD-CRESTED WEIR (IZZARD, 1950)

Izzard (1950) analyzed flow into a flush curb inlet as if it were flow over a broad-crested weir. He assumed that the inlet is located in a region of constant gutter slope, that the velocity into the inlet is normal to the plane of the opening, and that the head varies linearly along the inlet opening (Figure 2.2). The head on the inlet lip is then

$$h = y\left(1 - \frac{x}{L_r}\right) \tag{2.1}$$

where y = depth at curb of gutter flow at the upstream end of the inlet,
x = distance along the inlet measured from the upstream end, so

$0 \le x \le L$

where L = length of curb opening, and
L_r = length of curb opening required for 100% efficiency, i.e., the length required for the inlet to capture all of the flow.

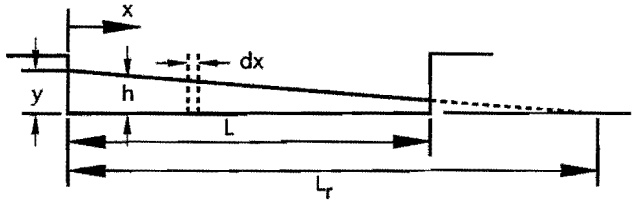

Figure 2.2 Definition sketch for Izzard's analysis

Since Izzard assumed that the curb inlet is a broad-crested weir, the depth of the flow at the inlet lip is critical depth. Thus

$$V = \left[\frac{2}{3}gh\right]^{0.5} \tag{2.2}$$

where V = velocity of flow into the inlet at any x and
g = gravitational acceleration.

The flow rate through a strip dx of the inlet opening was calculated as

$$dQ = V\,h\,dx = \left[\frac{2}{3}gh\right]^{0.5} h\,dx \tag{2.3}$$

Eliminating h using Equation 2.1 and integrating between the limits of x = 0 and x = L (Figure 2.2) gave

$$Q = \frac{2}{5}\left[\frac{2}{3}g\right]^{0.5} L_r\, y^{1.5}\left[1 - \left(1 - \frac{L}{L_r}\right)^{2.5}\right] \tag{2.4}$$

where Q = flow rate entering the inlet (cfs).

For the inlet to capture the entire flow (100% efficiency), $L = L_r$ so that

$$Q_a = \frac{2}{5}\left[\frac{2}{3}g\right]^{0.5} L_r\, y^{1.5} = 1.85\, L_r\, y^{1.5} \tag{2.5}$$

where Q_a = gutter flow approaching the inlet = flow rate into curb inlet for 100% efficiency.

For efficiencies less than 100%, an equation was obtained for the efficiency (Q/Q_a) by dividing Equation 2.4 by Equation 2.5, with the result being

$$\frac{Q}{Q_a} = \left[1 - \left(1 - \frac{L}{L_r}\right)^{2.5}\right] \tag{2.6}$$

When Izzard compared Equation 2.6 with unpublished data from the University of Illinois for curb inlets with no depression, the data were found to fit reasonably well if

$$Q_a = 0.7\, L_r\, y^{1.5} \tag{2.7}$$

(Even though the data from which Equation 2.7 was derived were unpublished at the time that they were used by Izzard, he stated that they were to be published later in a bulletin of the University of Illinois Engineering Experiment Station, presumably by J. J. Doland and/or J. C. Guillou, since the use of their unpublished data was acknowledged in another part of Izzard's paper.) Equation 2.7 is presently used by the Texas Department of Transportation (TxDOT) in its *Design Training Program* manual for curb inlets with no depression at 100% efficiency.

The analytical equation (Equation 2.5) and the empirical equation (Equation 2.7) for 100% efficiency are the same except for the numerical coefficient. Comparison of Equations 2.5 and 2.7 shows that the 100% capacity of a flush curb inlet

is actually 0.7/1.85, or about 40% of the flow which would be predicted by the assumptions made by Izzard. One of the primary reasons for the smaller numerical coefficient in Equation 2.7 is that Izzard effectively assumed that only gravity influences the motion of the water at the lip of the inlet. Actually, while gravity is tending to cause the water to flow into the inlet, the momentum of the gutter flow parallel to the curb is tending to cause the water to flow past the inlet opening.

For depressed curb inlets, Izzard presented a modification of Equation 2.7 for 100% efficiency, namely

$$Q_a = 0.7\, L_r (a + y)^{1.5} \tag{2.8}$$

where a = depression (ft) of the inlet lip below the normal gutter flow line at the face of curb.

Equation 2.8 overpredicted the flow captured by inlets tested at North Carolina State College (Conner, 1945) with a 3-inch depression and underpredicted data from inlets tested by the Corps of Engineers (1949) with a 2-inch depression.

Izzard grouped these two data sets with the unpublished data from the University of Illinois with no depression but with a composite cross slope, i.e., a steeper cross slope in the gutter than in the remainder of the roadway (as shown later in Figure 2.7), and compared Equation 2.8 with all of the data. He recognized that there was a significant amount of scatter but concluded that the agreement between Equation 2.8 and the data was adequate for design purposes. Part of the scatter of the data compared to Equation 2.8, and part of the differences between the three data sets may be due to the fact that the geometry of the depression was different in the three sets of experiments.

TxDOT's *Design Training Program* manual presently uses an equation similar to Equation 2.8 for curb inlets to capture the total approach gutter flow for undepressed and depressed curb inlets. For less than 100% efficiency, TxDOT's *Design Training Program* manual uses Equation 2.6 for undepressed curb inlets.

2.2 FLOW OVER A FREE DROP (LI, 1954)

Li (1954) derived an expression for the capacity of stormwater inlets by comparing the flow into an inlet with the flow freely dropping at the end of a channel (Figure 2.3). Assuming supercritical flow in the gutter prior to the inlet section, a uniform velocity distribution throughout the flow, and neglecting friction in the falling flow, the trajectory of a particle of water on the free surface gives the length (L_r, Figure 2.3) as

$$L_r = V_a \sqrt{\frac{2y}{g}} \tag{2.9}$$

where y = depth of flow and
g = gravitational acceleration.

If, rather than having a completely free-falling flow, there is an opening of length L in the bottom of the channel, then only the flow between the channel bottom and a depth y_1 (Figure 2.3)

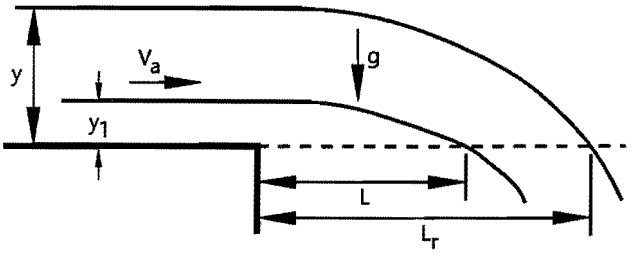

Figure 2.3 Profile view of a free drop

is captured by the opening. Using the same approach, i.e., by calculating the trajectory of a water particle at a distance y_1 from the bottom of the channel,

$$L = V_a \sqrt{\frac{2y_1}{g}} \tag{2.10}$$

From Equations 2.9 and 2.10,

$$\frac{y_1}{y} = \left(\frac{L}{L_r}\right)^2 \tag{2.11}$$

The flow into a flush curb inlet was considered by Li to be analogous to the preceding analysis, as shown in the plan view (Figure 2.4) for a curb inlet. The vertical direction in Figure 2.3 was replaced by the direction parallel to the pavement cross slope at the inlet. Thus, g was replaced by the acceleration $a = g(\cos\theta)$, which is the component of gravity parallel to the cross slope at an angle θ to the vertical (Figure 2.5). The depths were replaced by the ponded width (T) or a fraction thereof. From Equation 2.9 with y replaced by the ponded width ($T = y \tan\theta$) and g replaced by component of g parallel to pavement ($g \cos\theta$), the length of the opening required for 100% interception in a triangular cross section (Figure 2.5) is therefore

$$L_T = V_a\sqrt{\frac{2y\tan\theta}{g\cos\theta}} = V_a\sqrt{\frac{2T}{g\cos\theta}} \qquad (2.12)$$

where y = depth at curb for the gutter flow.

Using $Q_a = V_a\, y\, T/2 = V_a\, y^2(\tan\theta)/2$ and Equation 2.12 gives

$$\frac{Q}{L_T\, y\sqrt{gy}} = \sqrt{\frac{\sin\theta}{8}} \qquad (2.13)$$

for 100% efficiency with $Q = Q_a$. Li assumed that $\sin\theta \approx 1$ on the basis that θ is close to 90° in many situations. He then reduced Equation 2.13 to

$$\frac{Q}{L_T\, y\sqrt{gy}} = \sqrt{\frac{1}{8}} = 0.35 \qquad (2.14)$$

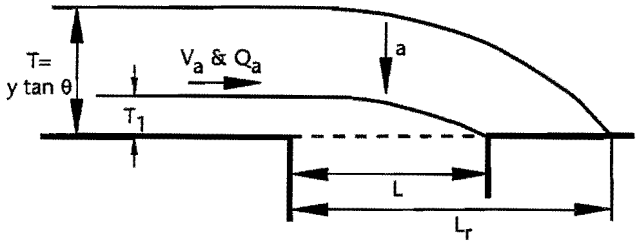

Figure 2.4 Plan view of flow at the inlet section

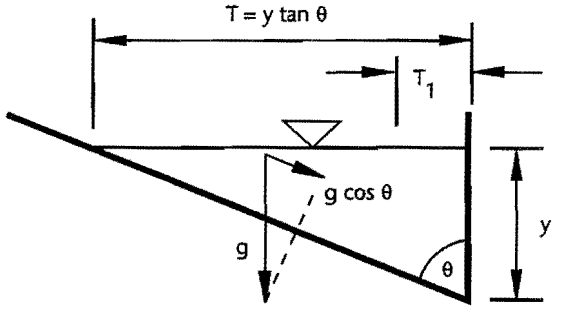

Figure 2.5 Cross section of gutter flow

A term similar to $Q/\left(L_T y\sqrt{gy}\right)$ had previously been obtained by dimensional analysis (Li et al., 1951). The numerical value on the right-hand side of the equation was empirically evaluated by Li et al. from model studies for undepressed inlets as 0.2 for tan θ = 24 and 48 (cross slopes, S_x = 1/24 = 4.2% and 1/48 = 2.1%) and as 0.23 for tan θ = 12 (S_x = 1/12 = 8.3%).

It has been noted in the literature that the term on the left-hand side of Equations 2.13 and 2.14 could be interpreted as a type of Froude number. Nevertheless, the presence of L_T in the denominator instead of T keeps it from being a traditional type of Froude number. Thus, in this report, this quantity is called a dimensionless flow rate (Q′) where

$$Q' = \frac{Q}{L_T\, y\sqrt{gy}} \qquad (2.15)$$

Both Izzard's and Li's analyses led to Q′ = constant for 100% efficiency. The parameter Q′ is discussed further in Section 4.2.1.

When the inlet capacity is less than 100%, the length (L_T) required to capture all of the flow is larger than the actual length L of the curb opening. To determine the capacity when $L < L_T$, the width of the flow captured was taken as T_1 (Figures 2.4 and 2.5). Comparing Figure 2.4 with Figure 2.3, the following expression was derived in a manner analogous to Equation 2.9:

$$\frac{T_1}{T} = \frac{T_1}{y\tan\theta} = \left(\frac{L}{L_T}\right)^2 \qquad (2.16)$$

The flow (Q) captured in the opening is the flow in the area in the width T_1 next to the curb (Figure 2.5) and was given by

$$Q = \frac{1}{2}V_a\left[y\,T - y_1(T - T_1)\right] \qquad (2.17)$$

The efficiency of the inlet after simplification was

$$\frac{Q}{Q_a} = 2\left(\frac{L}{L_T}\right)^2 - \left(\frac{L}{L_T}\right)^4 \qquad (2.18)$$

No data set was given by Li in the two references cited nor in the related comprehensive report (Storm Drainage Research Committee, 1956) on the project at Johns Hopkins University on which Li's other papers were based and for which Li was presumably one of the authors. Therefore no observations could be made to determine if the scatter seemed reasonable when compared to Izzard's.

2.3 COMPARISONS OF THE TWO METHODS

Table 2.1 shows a comparison of the equations from Izzard and Li. For 100% efficiency, the general functional dependence of Q on L_T and y is the same for Li's and Izzard's work (as given by Q′ = constant), but there is about a 60% difference in both the analytical coefficients and the empirical

coefficients. Li's larger coefficient gives a larger flow rate than Izzard's for 100% efficiency. On the other hand, for less than 100% efficiency, Li's equation gives a lower relative flow rate (Q/Q_a) than Izzard's equation, as shown in Figure 2.6.

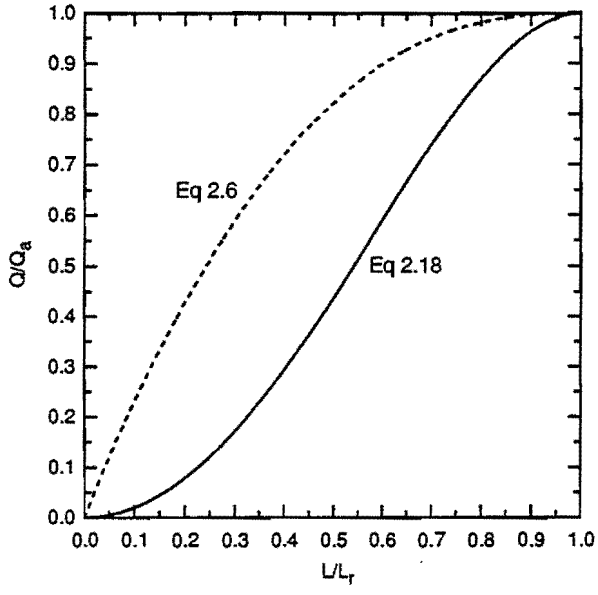

Figure 2.6 Comparison of Li's and Izzard's equations for less than 100% efficiency

The differences in the coefficients in the analytical equations are due to the different assumptions made in the analyses. The differences in the empirical coefficients may be due to the differences in cross sections of the roadway in the different studies. The Illinois data, which Izzard used for undepressed inlets, were collected for a roadway surface which had a composite gutter slope (i.e., a change in the transverse pavement slope 13.5 inches from the curb, Figure 2.7), while the roadway for Li's experiments had a uniform or constant cross slope for the experiments used to evaluate the numerical values in Table 2.1 (but not for all experiments which he used for other purposes). It is interesting that Li's experimental equation with Q′ = 1.13 to 1.30 agrees more closely with Izzard's analytical equation than the empirical coefficient obtained by Izzard.

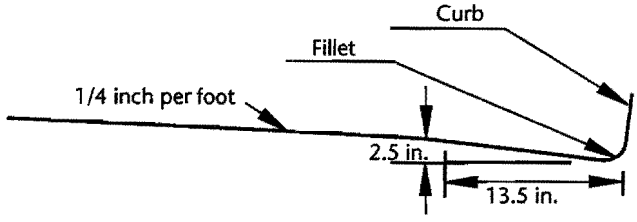

Figure 2.7 Composite cross slope of Illinois roadway model

2.4 OTHER INVESTIGATIONS

Tapley (1942) reported the results of a very early (1937) 3/32 scale model study of flow into curb inlets with a depression whose width normal to the curb decreased in the downstream direction. Tapley did a dimensional analysis to determine the variables to be used in the data analysis. Because of the early date of the experiments and the publication, most of the information was not presented in a manner consistent with present-day analyses of curb inlets. Nevertheless, the efficiency (Q/Q_a) was included in the paper. The efficiency was plotted in various ways, including being plotted as a function of the Froude number for the approach flow.

Table 2.1 Comparison of inlet discharge equations (no depression)

		Izzard (1950)	Li (1954), Li et al (1951)
100% Efficiency			
• Analytical Equations			
Dimensionless	$\frac{Q}{L_T y\sqrt{gy}} =$	$\frac{2}{5}\left[\frac{2}{3}\right]^{0.5} = 0.218$	0.35
English Units	$Q =$	$1.23\, L_T y^{1.5}$	$1.99\, L_T y^{1.5}$
• Empirical Equations			
Dimensionless	$\frac{Q}{L_T y\sqrt{gy}} =$	0.124	0.20 to 0.23
English Units	$Q =$	$0.7\, L_T y^{1.5}$	$(1.13 \text{ to } 1.30)\, L_T y^{1.5}$
< 100% Efficiency			
• Analytical Equations			
Dimensionless	$\frac{Q}{Qa} =$	$2\left(\frac{L}{L_T}\right)^2 - \left(\frac{L}{L_T}\right)^4$	$1-\left(1-\frac{L}{L_T}\right)^{2.5}$

Guillou (1948) presented a general summary of plans to construct and operate hydraulic models for gutter and inlet flows.

Wasley (1960) did a numerical study of the hydrodynamics of curb inlets. He divided the problem of the flow into a curb inlet into two parts. The first part consisted of the main gutter flow prior to the inlet section, assuming uniform flow but with the velocity varying with distance from the curb. The second part described the cross flow into the inlet as the instantaneous failure of a dam retaining a triangular reservoir. To determine a solution, the two phases were matched. The research was directed more at the dynamics of the flow and at the velocity distributions as the flow turns to enter the inlet than at a discharge relationship. A solution was obtained for the velocity distributions throughout the region where the flow is turning from being parallel to the curb and then entering the inlet opening. The experimental part of the research was primarily for determining velocity distributions for the flow into inlets, not for evaluating the flow rates into inlets. He did a dimensional analysis and concluded that

$$Q' = f(Fr, S_x) \tag{2.19}$$

where Q' is defined in Equation 2.15,
$Fr = V/\sqrt{gy}$,
V = average velocity in approach flow parallel to the curb,
y = flow depth at the curb, and
S_x = cross slope.

The experiments yielded values of Q' which were in a narrow range from 0.18 to 0.21 for Q > 0.3 cfs. Thus, his experimental results agreed more closely with those of Li for a constant cross slope than with those of Izzard. He also noted the differences between Izzard's and Li's expressions as shown in Table 2.1. For Q < 0.3, Wasley's experimental values of Q' decreased approximately linearly with decreasing values of Q. These decreases may be due to the rather small Reynolds numbers on the hydraulically smooth roadway surface (for which he estimated n = 0.009). He did not include viscosity in the dimensional analysis, so there was no Reynolds number in Equation 2.19. The gutter flow depths ranged from 0.01 ft (for a flow of only 0.003 cfs!) to 0.38 ft (for a flow of 3.0 cfs). He used longitudinal slopes of 0.005, 0.01, 0.03 and 0.05 and cross slopes of 1/12, 1/24, and 1/96. The model was considered to be full-scale; it was 50 feet long and 6 feet wide with a constant cross slope (i.e., not a composite cross slope) which could be changed and with the upstream end of the inlet section being 32 feet from the upstream end of the model roadway. Rather than having an inlet with a fixed length, there was no downstream end to the inlet section; the length required to capture 100% of the flow was taken from the end of the curb (i.e., the beginning of the inlet opening) to the downstream end of the region occupied by the flow as it crossed the inlet lip.

Wasley (1961) presented a summary of his previous report. This journal article did not include the values of Q' from his experiments. Liggett (1961) and McKown and Yu (1962) raised several questions about the assumptions made in his analysis, and Wasley (1962) responded to those questions.

Bauer and Woo (1964) presented new design curves for depressed curb inlets based on experimental results from full-scale and 1/4-scale models. They proposed a "standard" depression which was 2 inches deep, 2 feet wide (normal to the curb) and which had inclined transition sections 2 feet long. The upstream transition began 2 feet before the inlet opening and ended at the upstream end of the inlet opening. The downstream transition began at the downstream end of the opening and extended 2 feet downstream. There was a uniform cross slope except for the depression. Experiments were run with S (longitudinal slope) = 0.01 and 0.04 and S_x = 0.015 and 0.06 in the full-scale model and with S = 0 and 0.002 and S_x = 0.016 and 0.058 in the 1/4-scale model. The full-scale model was used with two different roughnesses (n = 0.01 and n = 0.016). The results for efficiency (Q/Q_a) were presented as a function of $L/(Fr_w T)$ where $Fr_w = V/\sqrt{gy_w}$, y_w = upstream depth at a distance W from the curb, W = width of the depression normal to the curb, and T = ponded width in the uniform approach flow. There was a family of curves for different values of S_x and W/T. No expression was given for the flow captured by the inlets on grade at 100% efficiency. For sag inlets, they gave

$$q = 1.7(y + a)^{1.85} \tag{2.20}$$

for their standard depression. They concluded that Izzard's (1950) results "substantially underestimate the capacity of inlets with depression widths greater than one foot" due to the lack of data for this type of depression in Izzard's analysis.

Forbes (1976) discussed a method for calculating the flow captured by curb inlets and looked also at the effects of extending a depressed gutter upstream of the inlet. He concluded that such an extended depression could increase the efficiency of curb inlets.

Izzard (1977) reanalyzed previously published data. He stated for depressed inlets that Q/Q_a is

a function of S_x and $L/(Fr_wT)$, which is the same parameter used by Bauer and Woo (1964). However, he also shows results in terms of other dimensional parameters and groups or parameters. Two of his figures show that 50% or more of the data for Q/Q_a in those figures was significantly larger than the predicted values. He stated only that he did not use those data points in his analysis. Although he referred to Bauer and Woo's (1964) paper, he did not specifically address their observation that his results underestimated the capacity of inlets.

2.5 MODIFIED MANNING'S EQUATION

The usual form of Manning's equation for open channel flow using English units (Equation 3.4) can be written for flow in triangular channels such as street gutters. Assuming that the cross slope is uniform and that the wetted perimeter is equal to the ponded width, or equivalently that the hydraulic radius is y/2, Manning's equation can be rearranged as

$$Q = \frac{0.47 y^{8/3} S^{1/2}}{n S_x} \tag{2.21}$$

where Q = flow rate in the gutter (cfs),
y = flow depth (ft),
S = longitudinal slope, and
S_x = cross slope.

Izzard (1946) obtained an alternative form of Manning's equation. He applied the usual form of the equation in a local sense rather than an average sense, as it is normally used. That is, he assumed that the velocity at each distance (ζ) from the curb could be calculated by Manning's equation for the velocity based on the local depth (η) at that point being equal to the hydraulic radius. Thus, at each ζ where the depth is η, he had

$$V = \frac{1.49}{n} \eta^{2/3} S^{1/2} \tag{2.22}$$

The flow through an incremental area at each ζ was then $(V\eta)d\zeta$. Using Equation 2.22, he integrated $V\eta d\zeta$ with respect to ζ and across the flow area with a uniform cross slope. The result was

$$Q = \frac{0.56 y^{8/3} S^{1/2}}{n S_x} \tag{2.23}$$

This is the form of Manning's equation which is traditionally used for gutter flows. The only difference from Equation 2.21 is the numerical coefficient. Thus, for a given set of hydraulic conditions (Q, y, S, and S_x), η calculated from measurements and Equation 2.23 would be 19% larger than when calculated from Equation 2.21.

CHAPTER 3. THE PHYSICAL MODEL

A physical model was constructed to study and evaluate the performance of recessed curb inlets (Figure C.2) and bridge deck drains (which are discussed in Part II of this report). Throughout the testing of the inlets, the flow in the gutter approached uniform conditions prior to the inlets. All dimensions throughout this report are prototype scale unless specified otherwise.

The model was designed for several different types of criteria. Flow rates up to 10 cfs were to be tested. Longitudinal and transverse pavement slopes up to 10% could be tested to cover a wide range of conditions. Depths were not to exceed 6 inches since this is the maximum curb height. Finally, the recessed curb inlet openings were to have lengths of 5, 10, and 15 feet. The model was designed and constructed meeting all these conditions plus some structural constraints discussed in Section 3.2.

3.1 MODEL LENGTH SCALE

As mentioned in Chapter 1, the complexity of flows such as inlet flows makes it difficult to solve such problems analytically. Therefore, the model was built to study the flows. An important consideration in the design of the model was the length scale ratio. Several factors which needed to be considered in choosing the length scale included establishment of uniform flow upstream of the inlet opening, available pump capacity, available space in the laboratory, construction constraints, cost, and avoidance of surface tension effects at small scales.

The model and the prototype had to have equal Froude numbers in order to obtain hydraulic similitude. This condition is met by the relationships (Roberson, Cassidy, and Chaudhry, 1988):

$$V_r = \Lambda_r^{1/2} \tag{3.1}$$

$$Q_r = \Lambda_r^{5/2} \tag{3.2}$$

where Λ_r = length scale ratio,
V_r = velocity ratio, and
Q_r = discharge ratio.

Each ratio is defined as the model value divided by the corresponding prototype value.

With all the constraints considered, a length scale of 3/4 was chosen, i.e., the model size was 3/4 of the prototype size. At 3/4 scale, a depth of 6 inches in the prototype is 4.5 inches in the model, and a prototype flow rate of 10 cfs is 4.9 cfs in the model.

3.2 MODEL CONSTRUCTION

Construction of the model was done in two primary phases. The first phase consisted of design and construction of a steel structure on which the roadway would rest. The second phase was the design and construction of a wood deck which was placed on top of the steel beams to represent the roadway. Several photographs of the model are in Appendix C. All of the dimensions in this section are model dimensions.

It was desired to be able to vary both the longitudinal slope and the cross slope. These objectives were met by constructing the support structure as follows (Figure 3.1): Two longitudinal beams (W18x35, 60 feet long) were used to support the roadway channel (Figure C.3). They were parallel to each other at a spacing of 6 feet, and the pair of beams was centered laterally under the roadway deck which was added later. At a distance of 13.8 feet from each end of the longitudinal beams, a cross (lifting) beam (W12x16) was welded perpendicular to and underneath the longitudinal beams. The location of the cross (lifting) beams was chosen so that the deflections at the two ends of the channel and at the point halfway along the length between the two cross beams would be equal for a uniformly distributed load. A portal frame constructed from W12x16 members was placed across the roadway deck and in line with the upstream lifting beam (Figure C.1). A manual, 5-ton chain hoist was attached from near each end

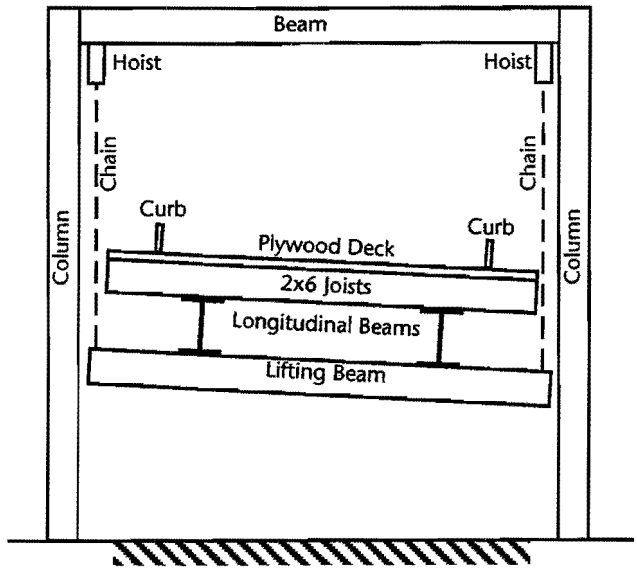

a) Upstream Portal Frame

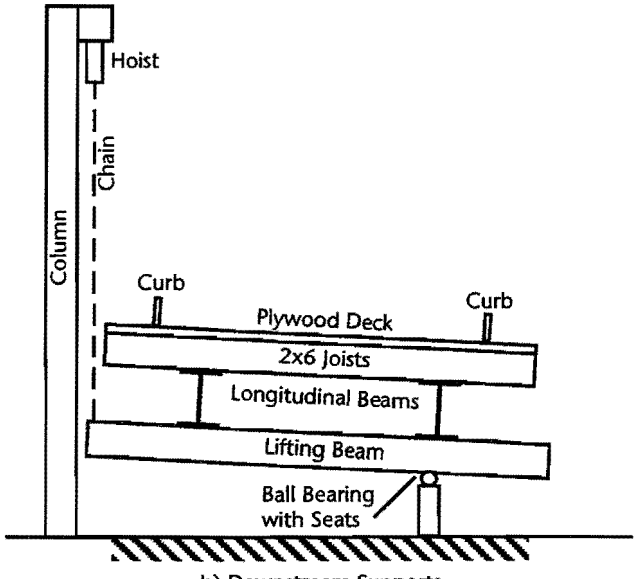

b) Downstream Supports

Figure 3.1 Schematic diagram of primary structural aspects of roadway model

of the top beam of the portal frame to the top of the upstream lifting beam. On one side of the downstream cross beam, the support was a pivot consisting of a 2-inch ball bearing in seats on top of a short column (Figure C.4). A taller column with a third chain hoist was at the other end of the downstream cross beam (Figure C.1). With the use of the frames, pivot, and manual chain hoists, the longitudinal gutter and transverse pavement slopes could be changed easily.

The structure was designed to allow no more than a 1/8-inch deflection at any location along the roadway for the dead load plus the live load (water plus personnel). This constraint was imposed to ensure that neither the hydraulics of the flow nor the measurements would be affected by deflections or changes in deflections as the amount of water or other loads on the structure changed.

The second phase was a wood deck which was placed on top of the longitudinal steel beams. The wood structure consisted of 2x6 floor joists spaced at longitudinal intervals of 2 feet. A 3/4-inch plywood deck was installed on the joists to be the pavement surface (Figures C.3 and C.4). The deck was subsequently roughened to represent the hydraulic roughness of a pavement (Section 3.5). The total wood structure was 14 feet wide and 64 feet long. The joists were framed to support a 2-foot overhang at each end of the channel, giving a total length of 64 feet. The curbs were then placed on both sides of the model roadway at a spacing of 10.5 feet, which is the model width of a 14-foot lane. The curbs for the roadway were constructed of painted, wolmanized 2x6's. The roadway deck was wide enough to allow walkways approximately 1.5 feet wide on each side of the roadway. After this construction phase was complete, the entire model in contact with water was waterproofed with a liquid sealant (which was also used to attach the roughness elements).

3.3 MODEL LAYOUT

A plan view of the physical model is shown in Figure 3.2. (See also Figure C.2.) Water was pumped from a half-million-gallon reservoir to the headbox. Immediately downstream of the headbox was a series of baffles to adjust and dampen the flow conditions in the model. The distance from the headbox to the upstream portion of the recessed inlet section varied from 26 to 36 feet, depending on the inlet length. For supercritical flow, this distance was long enough to allow the water to reach uniform depth prior to entering the inlet section.

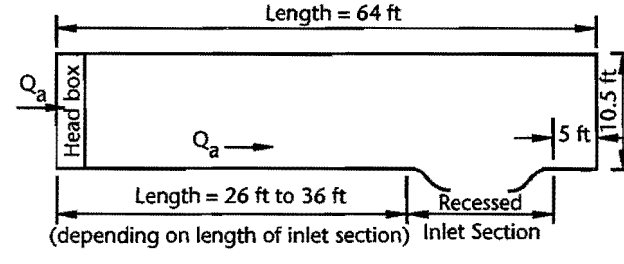

Figure 3.2 Plan view of physical model (model dimensions)

The model was designed to test different recessed curb inlet sizes with two standard transitions, namely a reversed-curve transition (Figures 3.3a, C.1, and C.2) and a linear transition (Figure 3.3b). The size of the inlet opening could be set to 15, 10, or 5 feet by moving the upstream transition sections either up or downstream. The downstream transition remained fixed for the duration of the tests.

Walkways and instrument carriages were constructed to lie on top of the curbs to allow personnel to traverse the roadway and to make measurements (Figure C.2).

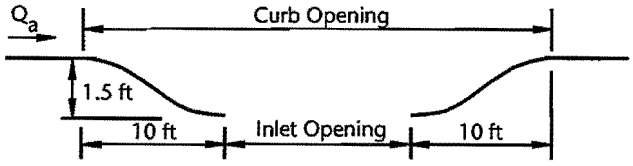

Figure 3.3a Reverse curve transition (prototype dimensions)

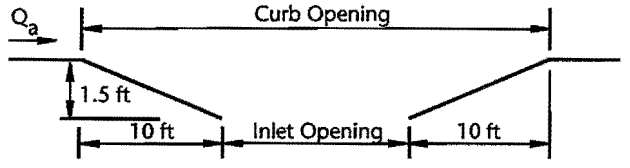

Figure 3.3b Linear transition (prototype dimensions)

3.4 RECESSED CURB INLET GEOMETRY

The transition sections upstream and downstream of the inlet opening were all 10 feet long. For the primary series of tests, the transitions were reversed curves (Figure 3.3a) with a geometry based on drawings supplied by TxDOT and on several installed recessed curb inlets in Austin. The radius of each curve was chosen to be 16 feet, which matched both the drawings and the inlets inspected in the field. The most upstream and downstream circular arcs were tangent to the curb line. The two arcs next to the inlet opening were tangent to a line parallel to the curb line and 1.5 feet away from the curb line. The transitions for the first tests were placed on a recessed slope (Figure 2.1b) of 30% which began at the gutter line and extended to the line of the inlet opening at 1.5 feet from the curb line. Throughout the duration of the first tests, the transition geometry stayed constant while the size of the inlet opening was set at 15, 10, or 5 feet.

The second transition tested was also 10 feet in length, but it had linear transition sections (Figure 3.3b). This transition was placed on the same recessed slope of 30%. For the second set of tests, the transition length and geometry were constant and the inlet opening was 15 feet. The reason that other opening sizes were not tested is discussed in Section 4.2.1.

A third set of tests was done with the original, reversed curve transitions with a 15-foot inlet opening, but with a recessed slope of 20% rather than 30%.

3.5 ROADWAY ROUGHNESS

As mentioned in Section 3.1, similitude requires that prototype and model Froude numbers be equal. This requirement and Manning's equation lead to (Henderson, 1966)

$$n_r = \Lambda_r^{1/6} \tag{3.3}$$

where n_r = ratio of Manning's roughness coefficient for the model to that for the prototype.

Manning's n is defined by Manning's equation:

$$V = \frac{1.49}{n} R_h^{2/3} S_f^{1/2} \tag{3.4}$$

where V = mean flow velocity,
R_h = hydraulic radius of flow in the roadway = cross-sectional area of flow (A) divided by wetted perimeter (P_w), and
S_f = friction slope.

The original objective was to reproduce the equivalent of a prototype n value between 0.015 and 0.020. It was decided to first try to represent a prototype Manning's n of 0.015 in the model. The corresponding model n using Equation 3.3 and $\Lambda_r = 3/4$ is 0.0143. Since there is a known relationship between the size of sand grains on a surface and n, it was further decided to cover the roadway surface with sand grains to produce the desired n value.

Henderson (1966) gives the relationship between median sand grain size (d) and Manning's roughness coefficient (n) as

$$n = 0.034\, d^{1/6} \tag{3.5}$$

with d in feet. For n = 0.0143, this equation gives d = 0.00554 feet or 1.7 millimeters. The closest available grain size for presorted sand was 2 mm or 0.00656 feet. Assuming that the nominal size is the mean grain size, the corresponding n value from Equation 3.5 is 0.0147.

The 2-mm sand grains were attached to the 3/4-inch plywood deck by first applying a thick

coat of waterproofing, which also served as an adhesive, and then scattering the sand grains uniformly over the surface. Another coat of waterproofing was applied to secure the sands grains to the surface (Figure C.5).

Experiments were conducted to quantify the resulting roughness. First, the recessed inlet section was blocked along the curb line, and then the cross slope was set to zero. The tests were conducted at longitudinal slopes of 0.001, 0.03, and 0.05 with two known discharges for each slope. The water depths were measured at 1/3 points along the length of the roadway. The standard step method (Henderson, 1966) was used to determine n. A spreadsheet was used to generate water surface profiles for trial values of n. The correct n value was the one which caused the calculated profiles to agree most closely with the measurements. By this procedure Manning's roughness coefficient was determined to be 0.019 in the model or 0.020 for the prototype. This n value was confirmed by many measurements made during the tests of inlet capacity. It is unknown why the actual Manning's roughness was larger than what was calculated from Equation 3.5. Calculations indicated that there is no significant change in n with changing depths for the range of depths in these experiments.

3.6 MEASUREMENTS

During the experimentation, it was necessary to measure the flow rate into the model, the flow rate into the recessed curb inlet, the flow rate passing the inlet section (the carryover), and water depths on the roadway surface.

Figure 3.4 is a schematic diagram of the system by which the water was pumped into the model from a half-million-gallon reservoir outside the laboratory. Two vertical turbine pumps (designated north and south) pumped from the reservoir into the two ends of an overhead 12-inch-diameter steel pipe loop in the laboratory. The pumps could be operated separately or simultaneously. For this model placement, each pump, operated separately, could discharge up to 4 cfs. With both pumps operating, the total flow was 7 cfs. (These maximum flow rates were much smaller than for some other operations in the laboratory because this model was elevated above the laboratory floor. The end of the pipe delivering flow to the model was about 12 feet above the laboratory floor, thus increasing the heads against which the pumps had to operate.) The discharge into the model was controlled by a 12-inch-diameter butterfly valve just prior to the headbox.

The flow into the model was measured by either or both the venturi meter and the flow sensor (Figure 3.4). V-notch weirs were used to measure the carryover and the total outflow from both the inlet and the carryover. It was not practical to separately measure the flow captured by the inlet. Thus, this flow was determined by subtracting the carryover from the total flow. All of the flow measurement devices were calibrated at the start of the project, and the calibrations were checked periodically during the project to assure accuracy of the flow measurements.

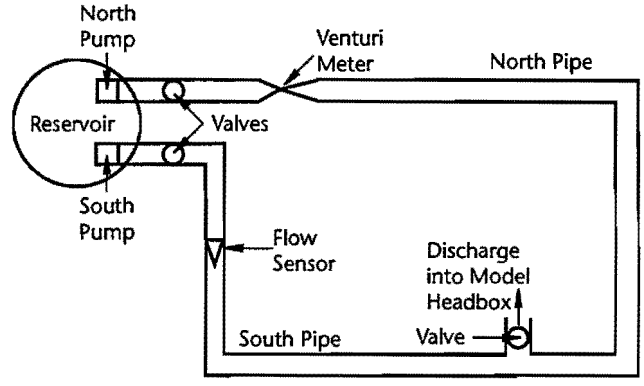

Figure 3.4 Schematic diagram of piping system

3.6.1 Venturi Meter for the North Pipe

Flow from the north pump into the model was measured by a venturi meter in the north line of the system. The standard equation for discharge through a venturi meter (Roberson and Crowe, 1985) is

$$Q = \frac{CA_2\sqrt{(2g\Delta h)}}{\sqrt{1-(A_2/A_1)^2}} \tag{3.6}$$

where
- Q = discharge,
- C = discharge coefficient,
- A_1 = area of approach pipe,
- A_2 = area of venturi throat,
- Δh = difference in piezometric head between the entrance and throat of the venturi, and
- g = acceleration of gravity.

For a given venturi meter, A_1 and A_2 are constants. For a well-made venturi, the discharge coefficient will be constant for pipe Reynolds numbers above about 2×10^5. The pipe Reynolds number (Re) is defined as

$$Re = \frac{VD}{\upsilon} \tag{3.7}$$

where V = mean flow velocity,
D = diameter, and
υ = kinematic viscosity.

Since D and υ are constant (except for small changes in υ due to temperature changes), the discharge coefficient should be constant for all velocities greater than a certain value, or, equivalently, for all discharges greater than a certain value.

The venturi in the north pipe has an entrance diameter of 12 inches and a throat diameter of 6 inches. For a venturi meter of this size, the discharge coefficient should be constant for throat velocities greater than 2 fps in the 12-inch pipe or for discharges greater than 1.6 cfs. Accordingly, Equation 3.6 can be simplified to

$$Q = K\,\Delta h^{0.5} \tag{3.8}$$

where $K = CA_2\sqrt{2g/\left[1-(A_2/A_1)^2\right]}$.

K should be constant for discharges greater than 1.6 cfs.

The venturi was calibrated volumetrically using part of the return floor channel as a volumetric tank. The available volume for calibration was 2,640 ft^3. Figure 3.5 shows the calibration data. The piezometric head difference (Δh) was measured in feet of water. The slope of the calibration line is K (Equation 3.8). A calibration line through the origin has a slope of 1.35. The correlation coefficient for the least squares determination of the line is 0.999. This value of K corresponds to a constant discharge coefficient of 0.833. This appears to be a reasonable value since the contraction section of the venturi is a normal pipe contraction and thus is not very well streamlined. There is no obvious change in the calibration even for flow rates less than 1.6 cfs.

3.6.2 Flow Sensor for the South Pipe

Flow from the south pump was measured by a Model 220B flow sensor connected to a Model 1000 digital flow monitor, both manufactured by Data Industrial Corporation of Pocasset, Massachusetts. The flow sensor has a nonmagnetic sensing mechanism with a six-bladed forward-swept impeller. As the flow turns the impeller, a low-impedance 8-volt DC signal is transmitted to the digital flow monitor. The frequency of the signal is proportional to the flow rate being measured. The flow monitor provides both an instantaneous flow reading and a total flow reading. Actual flow rates were determined by taking a time-integrated average using the total flow output from the flow monitor as sampled by a data acquisition system. For accurate measurement, the diameter of the pipe in which flow is being measured must be set on the flow monitor.

The flow sensor was calibrated volumetrically in the same manner as the venturi meter. Figure 3.6 is the calibration curve for the flow sensor with the pipe diameter set for 11.54 inches, the inside diameter of a 12-inch steel pipe. The correlation coefficient for the least squares determination of the line is 0.998. This curve was used to calculate the discharge flowing from the south pump into the model. The calibration indicated that the actual discharge was 0.99 times the discharge indicated by the flow sensor.

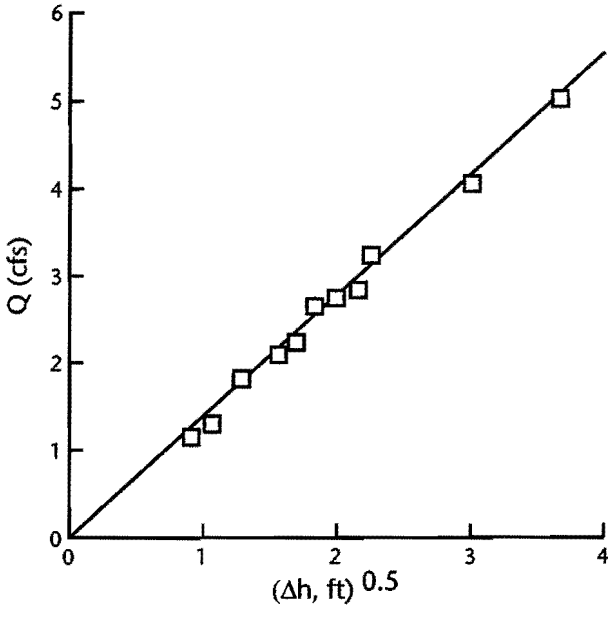

Figure 3.5 Calibration of venturi meter

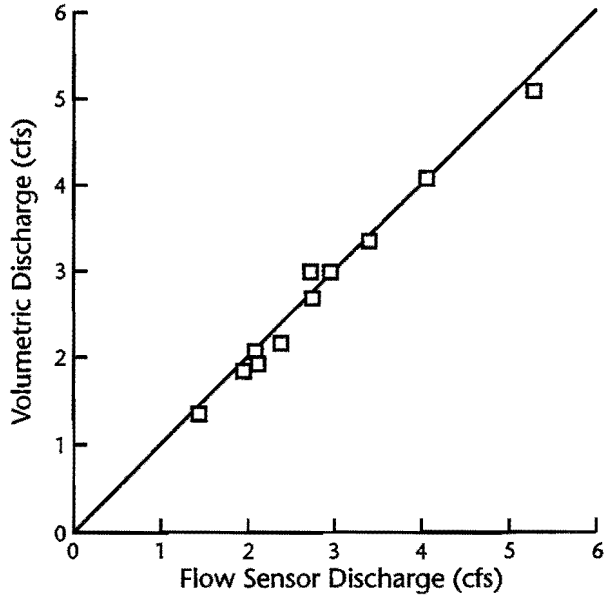

Figure 3.6 Calibration of flow sensor

3.6.3 V-Notch Weir for the Carryover

The carryover discharge was measured by a V-notch weir at the outflow point from a basin at the downstream end of the roadway. The head-discharge equation for a V-notch sharp-crested weir (Bos, 1976) is

$$Q = C_{ev}\frac{8}{15}\sqrt{2g}\tan\left(\frac{\theta}{2}\right)h_1^{2.5} \qquad (3.9)$$

where C_{ev} = effective discharge coefficient for a V-notch weir,
θ = angle included between the sides of the V-notch, and
h_1 = head on the weir.

To apply this equation to both fully and partially contracted sharp-crested weirs, it was modified to a form proposed by Kindsvater and Carter (1957), namely

$$Q = C_{ev}\frac{8}{15}\sqrt{2g}\tan\left(\frac{\theta}{2}\right)h_e^{2.5} \qquad (3.10)$$

where h_e = effective head.

The effective head is $(h_1 + K_h)$, where K_h represents the combined effects of surface tension and viscosity. For V-notch weirs, values of K_h have been determined empirically as a function of the notch angle. This particular V-notch weir had a notch angle of 125°, giving a K_h of approximately 0.003 feet (Bos, 1976).

For water at temperatures between 5°C and 30°C, C_{ev} for a V-notch sharp-crested weir can be a function of three variables, namely h_1/P, P/B_1, and θ, where P is the height of the bottom of the weir notch above the invert of the channel in which the weir is placed and B_1 is the width of the approach channel. For this weir, P = 1.021 feet, B_1 = 5.50 feet, and θ = 125°. Since these parameters were constant, C_{ev} for this application should be a function of only h_1/P.

Measurement of h_1 should be made upstream of the V-notch weir at a distance equal to 3 to 4 times the maximum possible value of h_1. Baffles were placed upstream of the measurement section to dampen the flow. A bubbler and a gas-water manometer were used to measure the head upstream of the weir and provided accurate measurement of h_1. The source of the gas for the bubbler was bottled oxygen with a constant outlet pressure of almost zero so that the bubbling rate was very low.

Calibration tests were conducted to determine Q as a function of h_1 and then C_{ev} as a function of h_1/P. The flow sensor was used to determine the flow rate over the V-notch weir, and h_1 was measured as described above. Measured values of Q as a function of h_1 are plotted in Figure 3.7. C_{ev} was calculated from Equation 3.10 and plotted in Figure 3.8 as a function of h_1/P. The range of C_{ev} values in Figure 3.8 is quite small. The standard deviation of the C_{ev} values is approximately 0.01. After a thorough literature search, no data were found for θ = 125° to compare with these values of C_{ev}.

During the course of the experimental work, the calibration of the V-notch weir was checked against the volumetric tank used to calibrate the venturi meter and flow sensor. The V-notch weir discharge measurements always agreed with the volumetric measurements within 2%.

3.6.4 V-Notch Weir for Total Discharge

The total discharge into the model was measured with the venturi meter and/or the flow sensor. As a double check, the total outflow from the model was measured by a 90° V-notch weir placed outdoors in the return channel to the outside reservoir. Equation 3.10 was used again for this weir, for which K_h had a value of approximately 0.003 feet (Bos, 1976). As with the previous weir, P and B_1 were constants with P = 1.125 feet and B_1 = 5.00 feet. Therefore, C_{ev} for this application should be a function of h_1/P only.

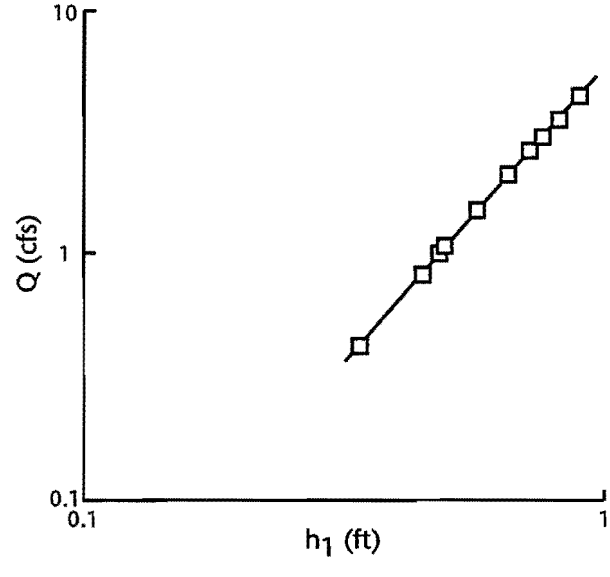

Figure 3.7 Calibration of carryover weir

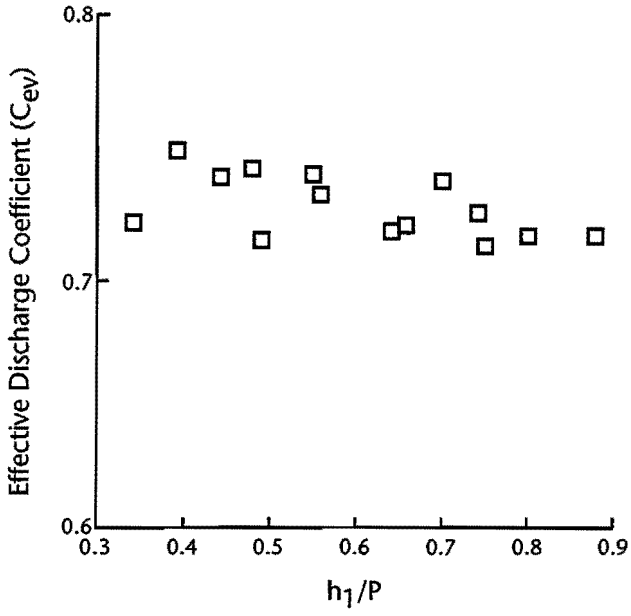

Figure 3.8 Discharge coefficients for carryover weir

Measurement of h_1 was at an upstream distance of four times the maximum value of h_1. Like the carryover weir, a bubbler and a gas-water manometer were used to measure the head and provided accurate measurement of h_1.

Calibration tests were conducted to determine Q as a function of h_1 and C_{ev} as functions of h_1/P. The flow sensor and venturi meter were used to determine the flow rate over the V-notch weir since the part of the floor channel used as a volumetric tank was upstream of this weir. Measured values of Q as a function of h_1 are plotted in Figure 3.9. C_{ev} was calculated from Equation 3.10 and plotted in Figure 3.10 as a function h_1/P. The solid line in Figure 3.10 is the effective discharge coefficient as a function of h_1/P for a standard 90° V-notch sharp-crested weir with a constant P/B value of 1.125 feet/5.00 feet = 0.23, as given by Bos (1976). Even though the differences between the data points and the solid line in Figure 3.10 are as great as 6%, these differences relate only to a comparison with a supposedly standard weir. The accuracy of the weir calibration itself, as shown in Figure 3.9, was much better than the comparison with a standard weir.

As with the carryover weir, the calibration was checked periodically against the calibrated venturi meter and flow sensor. The V-notch weir discharge measurements always agreed with the volumetric measurements within 2%.

3.6.5 Water Surface Elevation Measurement

Measurements were made of the water surface elevation in the gutter of the roadway at several cross sections upstream and one downstream of the recessed inlet section and on the recessed slope just before and after the actual inlet opening. The majority of the water surface elevation measurements were made using point gauges. The water surface elevations just before and after the actual recessed inlet opening were measured by mounting a tape measure to the recessed transition and visually reading the depth on the tape. At times, the water surfaces on the roadway were too rough for direct measurement, so cylindrical stilling wells were used for measuring the depths. A static tube was placed with one of its ends just flush with the inside of the curb so as not to interfere with flow next to the curb. The other end of the static tube was connected to the stilling well just outside the curb on the walkway. With the use of the stilling well, the water depths could be measured more accurately than was possible for the gutter flow itself.

Two personnel walkways and two instrument carriages were used to span the model (Figure C.2). The walkways and the instrument carriages could be moved longitudinally along almost the entire length of the roadway. One carriage was placed upstream of the recessed inlet section and the other downstream. A horizontal instrument bar equipped with a linear bearing was mounted on the instrument carriage. A point gauge was mounted on the linear bearing. Since the linear bearing could be moved laterally along the instrument carriage, it was possible to move the point gauge across the full width of the roadway.

Measurement tapes were mounted on the curbs so that the point gauge carriage could be accurately positioned along the roadway. Another tape was placed along the instrument bar so that the point gauge could be accurately positioned laterally.

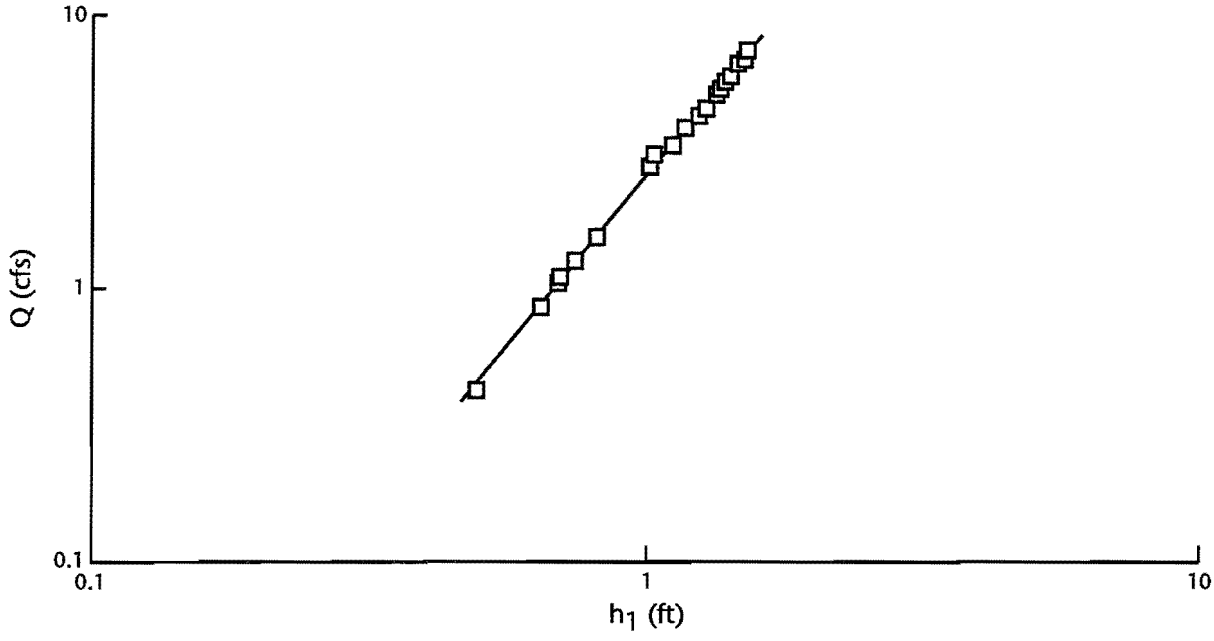

Figure 3.9 Calibration of 90° total flow weir

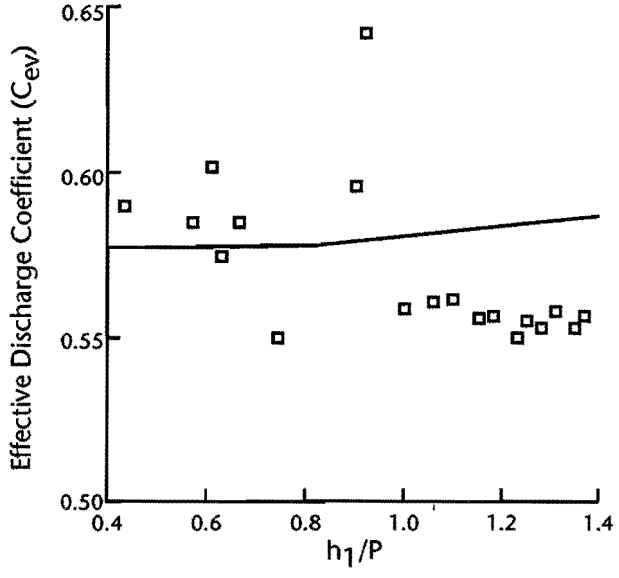

Figure 3.10 Discharge coefficients for 90° total flow weir

3.7 DATA ANALYSIS

A computer spreadsheet was utilized to convert the 3/4-scale model values to prototype values. Input to the spreadsheet included:

1. flow sensor and venturi meter data to calculate the flow rate entering the model;
2. carryover V-notch weir and total discharge V-notch weir measurements to calculate the flow of each;
3. water surface elevations to calculate the gutter depth for the approach flow;
4. ponded width upstream of the recessed inlet section;
5. depth of flow just before and after the actual inlet opening; and
6. gutter depth and ponded width downstream of the recessed inlet section.

CHAPTER 4. EXPERIMENTAL RESULTS

For the recessed curb inlets, 143 tests were conducted in the model described in Chapter 3. The majority of the tests focused on evaluating the discharge captured by recessed curb inlets with reverse curve transitions. Other testing was directed at the effects of a linear transition on inlet capacity and the effects of the steepness of the recessed slope between the curb line and the actual inlet opening (Section 3.4). The model results were used to develop empirical relationships to predict the interception capacity of these recessed curb inlets. Results from the model tests and the empirical relationships developed from the model data are presented in this chapter. In addition, 13 field tests were done to check the validity of the laboratory results. The laboratory testing is discussed in Sections 4.1 through 4.3. The results of the field tests are presented in Section 4.4.

4.1 EXPERIMENTAL LABORATORY PROCEDURES

4.1.1 Reverse Curve Transition

The reverse curve transitions were placed on the recessed slope portion of the model. The downstream transition was permanently fixed in place. The movable upstream transition, which was used to adjust the length of the inlet opening, was first set to the largest opening length (15 feet).

The actual testing was begun by setting the desired longitudinal gutter and transverse (or cross) slopes. At each inlet opening size, a variety of slopes was tested. Even though the model could have longitudinal gutter and transverse pavement slopes up to 0.10 (i.e., 10%), the longitudinal slopes (S) during testing ranged from 0.001 to 0.075, and the transverse slopes (S_x) from 0.01 to 0.06. Table 4.1 shows the combinations of slopes tested for the recessed inlets with reverse curve transitions. The test designations describe the inlet type and size and the slopes. The first letter indicates the type of transition (A = reverse curve transitions), the first two digits give the length of the inlet opening (15 = 15-foot opening), the next two digits give the cross slope (02 for S_x = 0.02 or 2%), and the last two digits give the longitudinal slope in percent (0.5 for S = 0.005 or 0.5%). The combinations covered a reasonable range of slopes for various topographical conditions. Several flow rates were used with each set of slopes shown in Table 4.1.

Table 4.1 Test designations for reverse curve transitions for 15-foot opening

S	S_x			
	0.01	0.02	0.04	0.06
0.001	A15010.1	A15020.1	A15040.1	A15060.1
0.005	A15010.5	A15020.5	A15040.5	A15060.5
0.010	A150101	A150201	A150401	A150601
0.020	A150102	A150202	A150402	A150602
0.050	A150105	A150205	A150405	A150605
0.075	A150107.5	A150207.5	A150407.5	A150607.5

After setting the slopes, the flow rate into the headbox was adjusted until the inlet efficiency was 100%. After the flow in the model had reached the desired steady state, measurements were taken. Flow sensor and/or venturi meter data were collected to determine the flow rate entering the model. Total-flow V-notch weir measurements were used to determine the flow rate captured by the inlet, for comparison with the inflow. Water depth measurements were made in the approach gutter. These gutter depths were measured at several cross sections to determine if the flow had reached uniform depth upstream of the inlet. Other measurements included ponded width upstream of the inlet section, depth of flow on the recessed slope just before and after the actual recessed inlet opening, and gutter depth and ponded width downstream of the recessed inlet section.

After the 100% efficiency test for the set slopes was completed, two to four more tests were made for the same slopes at less than 100% efficiency (Figures C.2 and C.6), i.e., by increasing the inflow to the model. The same measurements were made as those during the 100% efficiency tests. In

addition, the flow for the carryover weir was measured, and the flow captured by the inlet was obtained as the difference between the total flow and the carryover flow. After the final test at less than 100% efficiency was completed for the set slopes, the process was repeated for a new longitudinal gutter slope and transverse pavement slope in Table 4.1. The amount of testing for less than 100% efficiency depended on whether several limiting conditions were met, namely, a maximum gutter depth of 6 inches (prototype), a maximum ponded width of 14 feet (prototype), or the maximum flow rate from the pumps (7 cfs prototype).

After all the tests in Table 4.1 were completed for a range of flow rates, the inlet opening length was changed, and testing was begun again. Test designations similar to those in Table 4.1 were used for the 10-foot and 5-foot inlet openings. The efficiencies during the testing ranged from 15% to 100%.

4.1.2 Linear Transition

The general procedure used for data collection was the same as outlined above. The objective for testing a linear transition was to determine if the geometry of the transition affected the capacity of the inlet. Therefore, spot testing of conditions shown in Table 4.1 was done first to determine if more extensive testing would be required. Table 4.2 shows the range of longitudinal gutter slopes and transverse pavement slopes tested. The letter B at the beginning of the designation indicates a linear transition. The remainder of the digits have the same significance as those in Table 4.1. Linear transitions were selected since they are generally preferred over curved transitions for supercritical flow (Ippen, 1949).

Table 4.2 Test designations for linear transitions for 15-foot opening

S	S_x	
	0.02	0.04
0.010	B150201	B150401
0.020	B150202	B150402
0.040	B150204	B150404

4.1.3 20% Recessed Slope

Again, the general procedure was the same as outlined in Section 4.1.1. The objective was to determine if a change in the recessed slope had a significant effect on the inlet capacity. Thus, spot testing was again done to determine if more extensive testing would be required. Table 4.3 shows the test conditions, with the letter C indicating a 20% recessed slope. The remainder of the digits have the same significance as those in Tables 4.1 and 4.2. These tests were done with the original reverse curve transition. Two tests were conducted with S = 0.01, but, unfortunately, there were experimental problems with both of these tests so that the results could not be used.

Table 4.3 Test designations for 20% recessed slope for 15-foot opening

S	S_x	
	0.02	0.04
0.020	C150202	C150402
0.040	C150204	C150404

4.2 LABORATORY RESULTS FOR REVERSE CURVE TRANSITIONS

A total of 115 tests were conducted for reverse curve transitions. For all of these tests, the transition length and transition geometry remained constant while the size of the inlet opening was set to 15, 10, or 5 feet. Data from the model experiments are presented in Table A.1 in Appendix A.

The objective of the data analysis was to obtain design information similar to that already in use by TxDOT for other types of curb inlets, as well as to determine if other variables for recessed curb inlets were significant. As discussed in Chapter 2, the results for flow captured by a curb inlet are normally divided into two parts, 100% efficiency and less than 100% efficiency. TxDOT uses equations similar to Equation 2.7 for 100% efficiency and Equation 2.6 for less than 100% efficiency for flush inlets. Therefore, analysis of the recessed curb inlet data was first done in a similar manner, and then other approaches were evaluated for possible improvements in accuracy of correlations.

4.2.1 Inlet Efficiency = 100%

With flush undepressed curb inlets, the effective inlet opening length (i.e., the length in the curb line through which water flows into the inlet) equals the physical length of the actual inlet opening. However, recessed curb inlets have transitions both upstream and downstream of the inlet opening, and these transitions can affect the flow rate into the inlet opening. Thus, the effective length (L_{eff}) of the opening is larger than the actual recessed inlet opening length and perhaps is smaller than the length of the opening in the curb (Figure 4.1). To determine the effective inlet length for 100% efficiency, different values of L_{eff} were tried for determining q_L (where $q_L = Q/L_{eff}$) until the data from the 100% efficiency tests closely matched Equation 2.7, which was rewritten as

$$q_L = 0.70y^{1.5} \quad (4.1)$$

where q_L = flow per ft of inlet (cfs/ft) at 100% efficiency = Q/L_{eff},
y = flow depth in approach gutter (ft), and
Q = Q_a (i.e., inlet flow = approach flow for 100% efficiency).

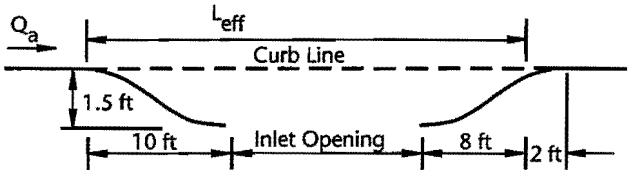

Figure 4.1 Plan view of inlet section

For all three inlet opening lengths (5, 10, and 15 feet), the optimum length of the effective inlet opening to match Equation 4.1 was the full upstream transition (10 feet) plus the full inlet opening plus 8 feet of the downstream transition. That is, the 5-, 10-, and 15-foot inlets were effectively 23, 28, and 33 feet long at 100% efficiency. Thus, any flow that entered the last 2 feet of the transition ultimately flowed downstream as carryover rather than back into the inlet. On the other hand, flow that entered the first 8 feet of the downstream transition actually turned around and flowed back upstream into the inlet opening. These conclusions are consistent with visual observations during the tests for 100% efficiency.

When q_L was first plotted against the measured depth (y) of flow in the gutter, there was a large amount of scatter because of normal random errors in the measured y values due to surface waves affecting the point gauge readings. The scatter was reduced significantly if the gutter depths were determined from Manning's equation (Equation 2.22) using the measured values of Q_a, n, S and S_x. TxDOT uses this equation to calculate depths in the approach gutter. To be consistent with the present TxDOT methods and to reduce the scatter in the data, the analysis of the recessed curb inlets was based on calculated depths.

Figure 4.2 shows Equation 4.1 and the data collected for the reverse curve transition using calculated y values. The standard error of the data relative to Equation 4.1 is 0.026 cfs/ft.

Dividing both sides of Equation 4.1 by $\sqrt{g}$ to make it dimensionally correct and using the definition of q_L allows Equation 4.1 to be rewritten in the same form as Equation 2.15, namely

$$\frac{Q}{yL_{eff}\sqrt{gy}} = 0.124 \quad (4.2)$$

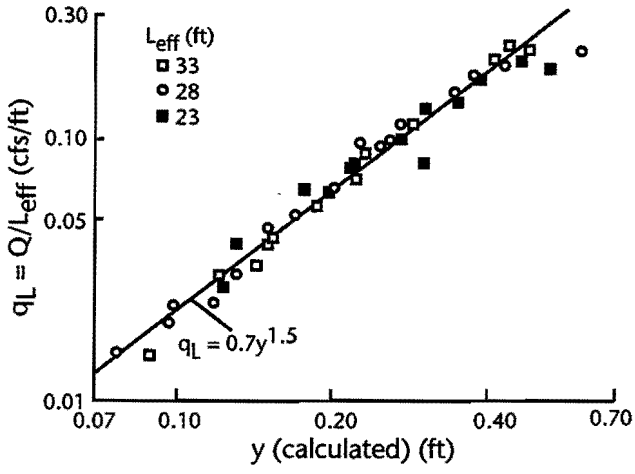

Figure 4.2 Capacity of recessed inlets with reverse curve transitions for efficiency = 100%

The left-hand side of Equation 4.2 is the dimensionless flow rate (Q') into the inlet. Thus, the data indicate that this Q' is constant for the 100% capacity tests for the recessed curb inlets. The same is true for flush curb inlets since Equation 4.1 is applicable for flush inlets when q_L is defined based on the actual inlet length. (Compare Table 2.1.) Even though Q' can also be interpreted as a type of Froude number, it is not the traditional open channel Froude number because of L_{eff} in the denominator. However, Equation 4.2 can be rearranged to give

$$Fr = 0.351\frac{L_{eff}}{T} \quad (4.3)$$

where T = ponded width = y/S_x.
Fr is the traditional open channel Froude number defined as

$$Fr = \frac{Q}{\frac{1}{2}yT\sqrt{g\frac{y}{2}}} \quad (4.4)$$

This definition is based on having the length scale equal to the hydraulic mean depth, which is y/2 for flow in a triangular cross section; the flow area is yT/2 in Equation 4.4.

Equation 4.3 is valid only for 100% efficiency. This equation says that the Froude number for the approach flow for the condition of 100% efficiency increases as L_{eff}/T increases, or that increasing L_{eff}/T allows the inlet to capture all of the flow for larger and larger Froude numbers. This kind of relationship might be expected since the Froude number can be interpreted as the ratio of the inertial force, which is trying to carry the flow

past the inlet, to the gravity force, which is trying to cause flow into the inlet. When L_{eff}/T is small, the inertia in the flow must also be small for the gravitational force to be able to accomplish the necessary radial acceleration to turn the flow into the inlet.

To further study the inlet capacity at 100% efficiency, a correlation analysis was conducted for all the variables involved in the experiments. These variables included longitudinal gutter slope (S), transverse pavement slope (S_x), ponded width (T) of the approach flow, approach gutter flow (Q_a), inlet flow (Q, which equals Q_a for 100% efficiency), effective length of the inlet (L_{eff}), and Froude number (Equation 4.4). The only correlation which resulted from this analysis was a correlation between L_{eff}/T and Fr. There was no significant correlation between other variables. Thus, this part of the analysis confirmed that no other variables are needed in Equation 4.3. Other regression equations were obtained, but none of them fit the data as well as Equations 4.1 through 4.3, which are different forms of the same relationship.

4.2.2 Results for Inlet Efficiency < 100%

The objectives in the analysis of this experimental data were to obtain a predictive equation which would be consistent with present TxDOT procedures and to determine if any different, improved design correlations could be developed.

Analysis in Terms of Efficiency

The experimental data for less than 100% efficiency are presented in Figure 4.3. The relative flow rate (Q/Q_a) was plotted against the ratio of the effective inlet opening length to the effective inlet opening length that would be required for 100% interception (L_{eff}/L_r). Fitting a third-order polynomial to the experimental values, with the constraints that the curve go through the points (0,0) and (1,1), gave

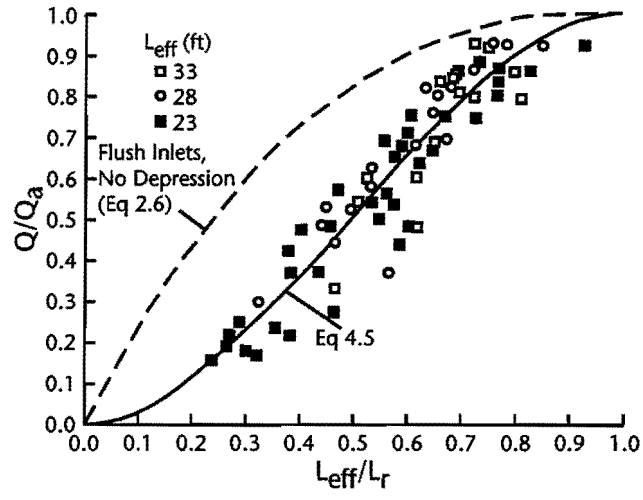

Figure 4.3 Flow into recessed curb inlets with reverse curve transitions with efficiency < 100%

This curve is shown in comparison with the data in Figure 4.3. Figure 4.4 shows the difference between Equation 4.5 and Equation 2.18. For a given relative flow rate (Q/Q_a), Equation 2.18 underestimates the relative length of the curb inlet relative to Equation 4.5.

The values of Q/Q_a (observed) are plotted against Q/Q_a (predicted) from Equation 4.5 in Figure 4.4. The scatter in Figure 4.3 is also evident in Figure 4.4. The standard error of the data in Figure 4.4 relative to Equation 4.5 is 0.087. That is, the standard error in Q is 8.7% of Q_a. The standard error is a statistical measure of the scatter of the data points relative to the curves in Figures 4.3 and 4.5.

Several other functions were also fitted to the data in Figure 4.3 to determine if an improved fit could be obtained. Fourth through sixth order polynomials, with the constraints that they pass through the points (0,0) and (1,1) and that they not have negative slopes at (0,0) and (1,1), gave essentially the same curve and standard error as Equation 4.5. The standard error for Equation 2.18 compared to the data in Figure 4.3

$$\frac{Q}{Q_a} = 0.0526\left(\frac{L_{eff}}{L_r}\right) + 2.86\left(\frac{L_{eff}}{L_r}\right)^2 - 1.92\left(\frac{L_{eff}}{L_r}\right)^3 \qquad (4.5)$$

is 0.093 compared to 0.087 for Equation 4.5. Figure 4.5 shows a comparison of Equations 2.18 and 4.5. Using the general form of Equation 2.18 with least squares fitting of the coefficients gave $Q/Q_a = 2.23\ (L_{eff}/L_r)^2 - 1.23\ (L_{eff}/L_r)^4$ and a standard error of 0.090. In addition to having a larger standard error than Equation 4.5, this equation also gives Q/Q_a slightly greater than unity for $0.9 < L_{eff}/L_r < 1.0$. Thus, it was concluded that Equation 4.5 gave the best fit possible for polynomials giving Q/Q_a as a function of L_{eff}/L_r.

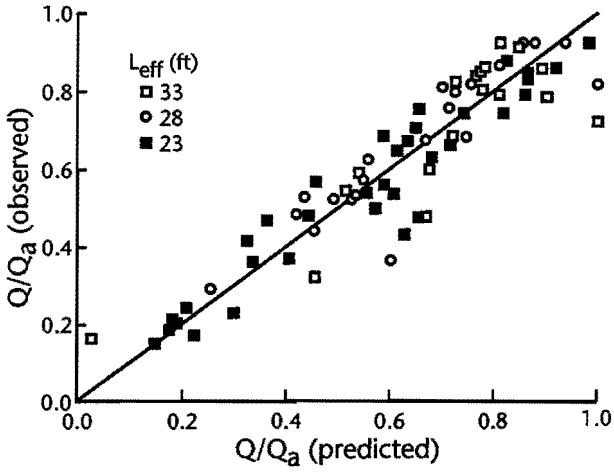

Figure 4.4 Comparison of Q/Q_a observed and predicted from Equation 4.5 for reverse curve transitions

Analysis of Residuals

Because of the magnitude of the standard error and the scatter of the data points in Figure 4.3, a correlation analysis was done on the residuals of the data relative to Equation 4.5 to try to determine if other parameters might be important for this data set. All of the variables listed at the end of Section 4.2.1 were used in the analysis. The Froude number (Fr), L_{eff}/T and the longitudinal gutter slope (S) were found to be slightly correlated to the residuals. After completion of a step-wise regression (which eliminated L_{eff}/T as a parameter), the best fit equation for the residuals was found to be

$$\text{Residuals} = 0.0577 - 0.114\text{Fr} + 4.49\text{S} \quad (4.6)$$

The t-statistics for the coefficients in Equation 4.6 were t = 1.27 for 0.577, t = -2.62 for -0.114, and t = 3.72 for 4.49. The standard error of the observed residuals vs. the predicted residuals from Equation 4.6 is 0.071, or the standard error in Q is 7.1% of Q_a. The R-squared correlation for Equation 4.6 is only 0.237. When Equation 4.6 was added to the polynomial in Equation 4.5, the standard error was reduced only from 0.087 to 0.071. Therefore, this effort to reduce the magnitude of the residuals had a very small effect on reducing the error in the predictions.

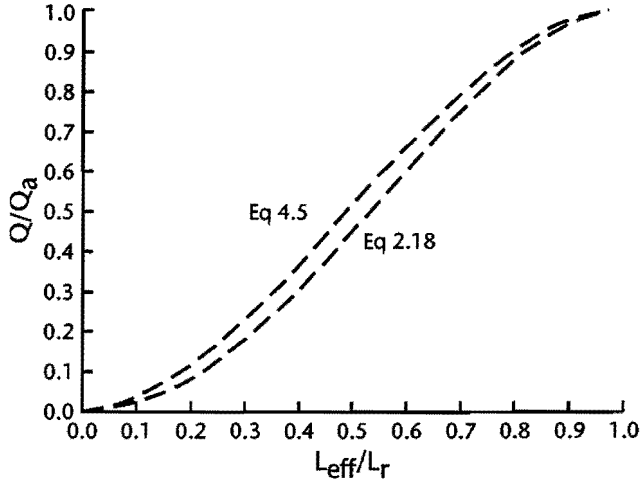

Figure 4.5 Comparison of Equation 2.18 and Equation 4.5 for efficiency < 100%

Effects of Inlet Length and Froude Number

To further study the experimental data to determine if an improved correlation could be developed, Equation 4.5 was rearranged to give

$$\frac{Q}{L_{eff}} = \frac{Q_a}{L_r}\left[0.0526\frac{L_{eff}}{L_r} + 2.8638\left(\frac{L_{eff}}{L_r}\right)^2 - 1.9164\left(\frac{L_{eff}}{L_r}\right)^3\right]\frac{L_r}{L_{eff}} \quad (4.7)$$

Q/L_{eff} is the flow rate entering the inlet divided by the effective length for 100% efficiency (33, 28, or 23 feet). Q_a/L_r is the flow rate in the approach gutter divided by the calculated effective length required to capture the entire gutter flow. The values of Q/L_{eff} (observed) are plotted against Q/L_{eff} (predicted) from Equation 4.7 in Figure 4.6. The standard error of the data relative to a line with a 1:1 slope is 0.012 cfs/ft. This numerical value of 0.012 cfs/ft for Q/L_{eff} should not be compared to the previous standard error of 0.087 for Q/Q_a since the two error measures relate to different variables. Futhermore, most of the reduction in the magnitude of the standard error from Equation 4.5 to Equation 4.7 is due to the fact that the Q/L_{eff} values are much smaller than the Q/Q_a values. Values of Q/L_{eff} range from 0.005 to 0.029 with an average of 0.10, while values of Q/Q_a range from 0.16 to 0.93 with an average of 0.62.

In Figures 4.3 and 4.5 (which are plotted in terms of Q/Q_a), there is no readily apparent segregation of the data according to inlet length, nor is there any significant correlation with other variables as discussed in conjunction with Equation 4.6. However, when the variables were rearranged to obtain Figure 4.6 in terms of Q/L_{eff}, there was a slight segregation according to effective length or inlet length. This segregation is even more apparent when Q/L_{eff} is plotted vs. Q_a/L_r in Figure 4.7. In this figure, the triangles (data for L_{eff} = 23 feet) which are below the majority of the other data have high Froude numbers (Fr = 2.6-3.0). Therefore additional analysis was done taking a different approach to determine if the standard error of Equation 4.7 could be further reduced.

A non-linear regression analysis was done to reduce the segregation among the different effective lengths and to take account of the high Froude numbers. After many trial regressions and interpretations of the residuals, the best equation which could be obtained was

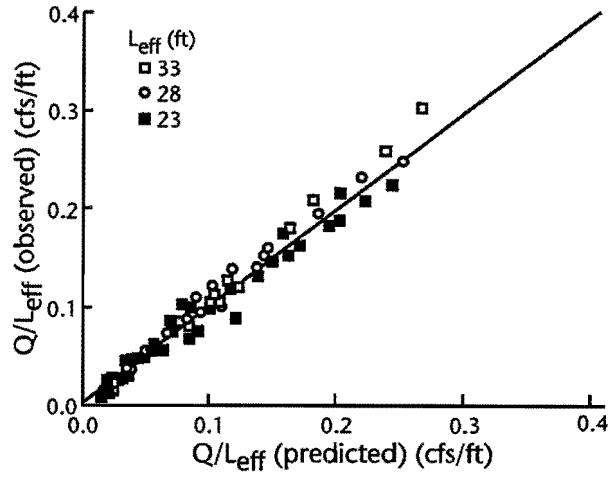

Figure 4.6 Comparison of Q/L_{eff} observed and predicted from Equation 4.7 for reverse curve transitions

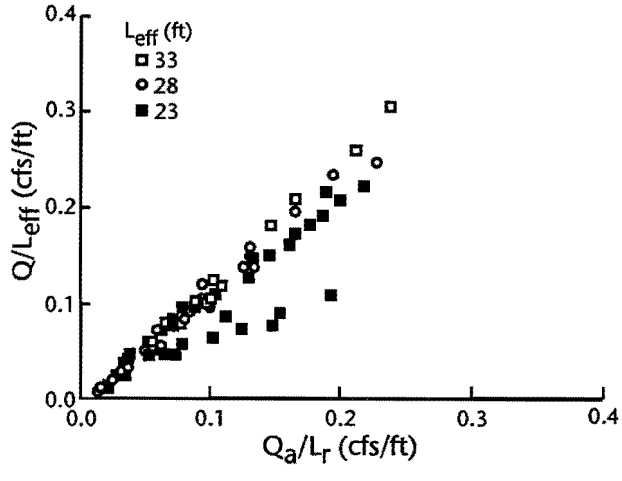

Figure 4.7 Correlation of Q/L_{eff} with Q_a/L_r for reverse curve transitions

$$\frac{Q}{L_{eff}} = \frac{1.044\,\frac{Q_a}{L_r}(1-0.382\lambda) - 0.132\lambda Fr^{2.26} + 0.112\lambda - 0.0099}{0.893\lambda^2 + 0.129\lambda + 0.824} \qquad (4.8)$$

where $\lambda = (33 - L_{eff})/33$.

The t-statistics for the dominant coefficients in Equation 4.8 are t = 31.7 for 1.044, t = –1.39 for –0.132, and t = 3.49 for 2.26. R-squared for Equation 4.8 is 0.940.

The values of Q/L_{eff} (observed) vs. Q/L_{eff} (predicted) from Equation 4.8 are shown in Figure 4.8. The standard error of the data relative to Equation 4.8 is 0.0086 cfs/ft. Thus, even though Equation 4.8 is a bit cumbersome, it reduced the standard error by 40% compared to

Equation 4.7 (from 0.012 cfs/ft for Equation 4.7 to 0.0086 cfs/ft for Equation 4.8). The amount of segregation of different inlet openings was significantly reduced, and the effects of large Froude numbers for L_{eff} = 23 feet were reduced as well.

Equation 4.8 and Figure 4.8 are presented as evidence of some degree of correlation with Froude number and inlet (or effective) length. Even though Equation 4.8 was the best correlation which could be determined, it has a major problem, namely, that it sometimes predicts negative values of Q when the conditions are outside the range of conditions for which the data used to obtain Equation 4.8 were collected. Thus, Equation 4.8 should not be used for predictive calculations.

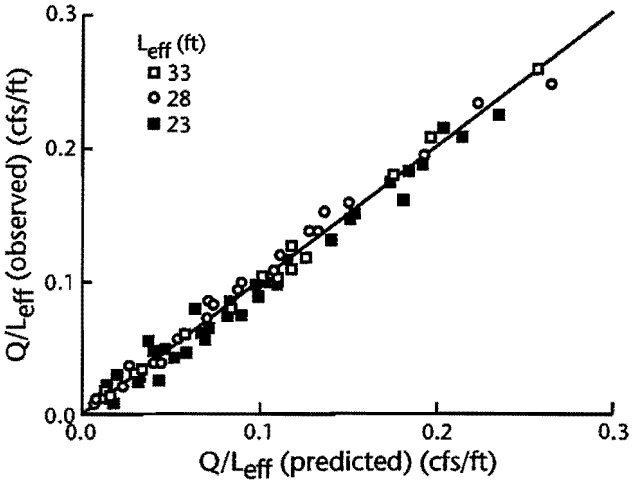

Figure 4.8 Comparison of Q/L_{eff} observed and predicted from Equation 4.8 for reverse curve transitions

Comparison to Flush Inlets

Equation 4.5 can be used for comparing the efficiency of flush inlets with no depression (Equation 2.6) and recessed curb inlets. For an example, the following conditions were taken:

Q_a = 5.0 cfs
S = 0.02
S_x = 0.02
n = 0.02
y = 0.252 feet

The curb depth was calculated from Equation 2.22. These values and Equation 4.1 can be used to obtain q_L = 0.0886 cfs/ft for 100% efficiency. The value of L_T is then $L_T = Q_a/q_L$ = 56.4 feet.

Table 4.4 shows a comparison of the calculated capacity of different inlets. Equation 2.6 was used for flush inlets with no depression, while Equation 4.5 was used for recessed inlets. Comparisons were made in two ways:

1. the opening for the flush inlet being the same as the actual inlet opening for the recessed inlet, and
2. the flush opening being the same as the curb opening for the recessed inlet (although it is recognized that this would be a very long flush inlet opening).

The first set of comparisons in Table 4.4 is for a recessed inlet with a 15-foot inlet opening, an effective length of 33 feet, and a curb opening of 35 feet. For the second set, all of the lengths are 5 feet shorter. As the table shows, when the lengths of the flush openings are equal to the lengths of the actual recessed openings, the flush inlets capture 87% and 80% as much flow as the recessed inlet, or conversely, the recessed inlets capture 15% to 25% more than flush inlets for these two examples. The flush inlets with openings equal to the curb opening for the recessed inlets are significantly more efficient than the recessed inlets.

The reason for the decreased efficiency of a recessed inlet with the same curb opening as a flush inlet is as follows: For a flush inlet, once any water moves from the gutter past the curb line and into the inlet opening, it has flowed over the lip of the inlet box and has definitely been captured by the inlet. On the other hand, for a recessed inlet, water can and does cross the curb line into the downstream transition section and then flows back into the downstream gutter (Figures C.7 and C.8). That is, the momentum of the water can be great enough for it to flow back up the recessed

Table 4.4 Comparison of flush and recessed inlets for efficiency < 100%

Type	L (ft)	L_{eff} (ft)	Efficiency (%)	Relative Efficiency (%)	Q (cfs)
Recessed		33	62	100	3.1
Flush	15		54	87	2.7
Flush	35		91	147	4.6
Recessed		28	49	100	2.5
Flush	10		39	80	1.9
Flush	30		85	173	4.3

slope in the downstream transition section and back into the gutter, rather than turning in the downstream transition section and basically flowing back upstream to get into the inlet opening as happens for 100% efficiency. This type of sweep-out exists for all flow conditions but should be expected to be greater as the Froude number of the gutter flow increases.

Another way of viewing the situation is that the effective lengths of the recessed inlets decrease as the Froude number for the approach flow increases. In a sense, this is the effect that causes the data in Figure 4.3 to be significantly below the curve for flush inlets. Thus, another possible approach for analyzing the data for less than 100% efficiency might be to use Equation 2.6 rather than Equation 4.5 and then to calculate a value of L_{eff} for each flow condition with an efficiency of less than 100%. For predictive purposes, these values of L_{eff} would then need to be correlated with gutter flow conditions (as represented by Fr and possibly also S, S_x, etc.). In a sense, this alternative approach might be more representative of the hydraulic conditions since reductions in L_{eff} would correspond to flow sweeping out of the downstream part of the recessed section. Nevertheless, this alternate approach was not investigated both because it would be more cumbersome than just using Equation 4.5 and because using Equation 4.5 is more consistent with the present TxDOT approach of using Equation 2.6 for flush inlets.

4.3 LABORATORY RESULTS FOR LINEAR TRANSITIONS

Fifteen tests were conducted to investigate the effects of a linear transition on curb inlet capacity as compared to the reverse curve transition. For all of these tests, the length of each transition section was 10 feet, and the inlet opening was 15 feet long. The objective of these tests was to determine if linear transitions cause a significant change in the hydraulic behavior of recessed inlets compared to reverse curve transitions. The data (Table A.2, Appendix A) were evaluated primarily by comparison to the relationships developed for the recessed inlets with reverse curve transition sections.

4.3.1 Inlet Efficiency = 100%

In the analysis of the data for 100% efficiency, different effective lengths (L_{eff}) were tried until the data closely matched Equation 4.1. This is the same approach that was used with the data for reverse curve transitions. Using calculated depths as before, the effective length of the 15-foot inlet opening was the full upstream transition plus the inlet opening plus the full downstream transition. Therefore, with a linear transition, a 15-foot inlet opening was effectively a 35-foot inlet at 100% efficiency. Thus, the linear transition is slightly more effective at turning the water which enters the most downstream part of the transition and causing this water to flow back upstream and into the inlet opening at 100% efficiency. The experimental data for 100% efficiency are presented in Figure 4.9. The standard error of Equation 4.1 compared to the linear transition data is 0.005 cfs/ft.

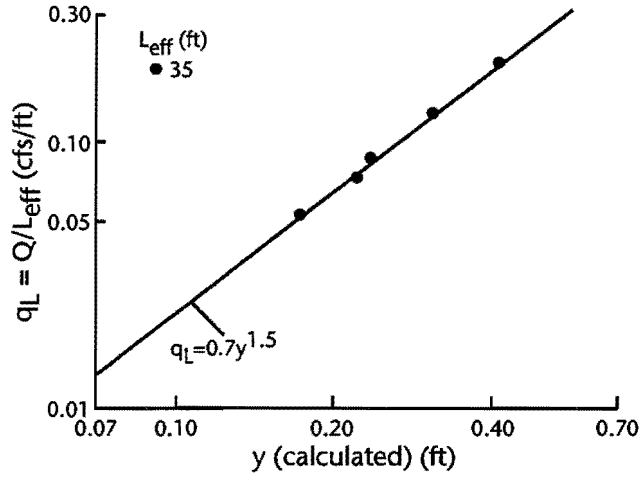

Figure 4.9 Capacity of recessed inlets with linear transitions for efficiency = 100%

4.3.2 Inlet Efficiency < 100%

The data for the linear transition with less than 100% efficiency were analyzed in the same manner as the data for the reverse curve transition. The relative flow rate was compared to L_{eff}/L_T, i.e., the effective inlet length divided by the effective inlet length required for 100% interception. The experimental data agree with Equation 4.5 rather well using L_{eff} = 35 feet (Figure 4.10). The standard error of the Q/Q_a data for the linear transition compared to Equation 4.5 is 0.054. Because of this small standard error, it was concluded that more extensive testing with linear transitions was not justified and that Equations 4.1 and 4.5 can be used for linear transitions if the effective lengths of the openings include the full 10 feet of the downstream transition, rather than only 8 feet as for reverse curve transitions.

The standard error in Figure 4.10 is smaller than that for the reverse curve transition, probably because only one opening length was tested for a linear transition and because the range of flow conditions was smaller. Even though the standard error is small, it is evident that the data in Figure 4.10 are consistently above the curve for Equation 4.5. It is difficult to know what significance to place on the fact that the data are all above the curve. An inspection of Figure 4.3 shows that the average trend of the data for reverse curve transitions with L_{eff} = 33 feet is also above the curve in that figure. On the other hand, it seems logical that the linear transition might be somewhat more efficient, since it has more area on the most downstream part of the recessed slope (Figures 3.2 and 3.3), and thus it potentially could be more difficult for the flow in this most downstream part of the transition to sweep out of the transition section and back into the gutter. However, the differences in Figure 4.10 between the data and the curve are small. Furthermore, there is a relatively large amount of scatter for the more extensive set of data in Figure 4.3. The fact that the data points in Figure 4.10 are all above the curve may be a coincidence; if more data had been collected, they might have been scattered about the curve in the same manner as the data in Figure 4.3. Nevertheless, it seems safe to conclude that the linear transitions are at least as efficient as the reverse curve transitions and perhaps slightly more efficient, since the effective length is 2 feet greater and since the data in Figure 4.10 are above the curve.

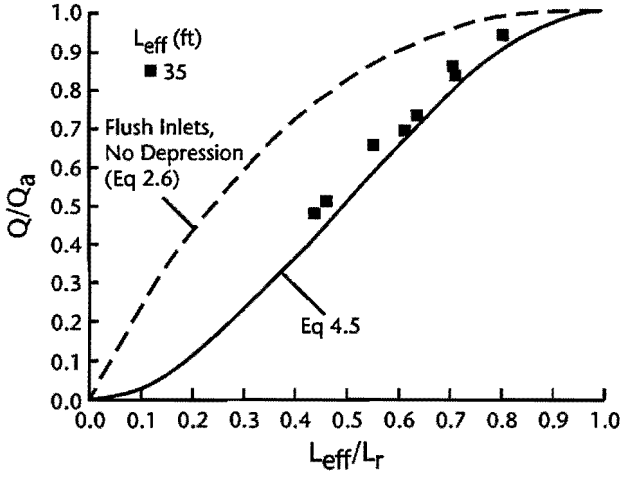

Figure 4.10 Recessed curb inlets with linear transitions for efficiency < 100%

4.4 LABORATORY RESULTS FOR 20% RECESSED SLOPE

Thirteen tests were conducted to investigate the effects of the steepness of the recessed slope. For all of the previous tests with both the reverse curve transition and the linear transition, the recessed slope was 30%. For this series of tests, the original reverse curve transition was used with a 20% recessed slope between the curb line and the actual inlet opening; the length of each transition section was 10 feet, and the inlet opening was 15 feet long. The objective of these tests was to determine if a change in the recessed slope had a significant effect on the hydraulic behavior of the recessed inlets. Thus, the data (Table A.3, Appendix A) were evaluated primarily by comparison to the relationships developed for the recessed inlets with a reverse curve transition sections and a 30% recessed slope. In the data analysis, it was assumed that the change in slope would not make a significant difference in the behavior of the inlets. Thus, the data were analyzed in the same way as for the 30% recessed slope using L_{eff} = 33 feet, and the results for the 20% slope were then compared to the results for the 30% recessed slope. The results for 100% efficiency are in Figure 4.11, while the results for less than 100% efficiency are in Figure 4.12. In both cases, there is very good agreement between the new data points and the previously developed curves. Thus, it was concluded that the change in the recessed slope from 30% to 20% did not have a significant effect on the behavior of the inlets. The data points for less than 100% efficiency are slightly above the curve, as they were for the linear transition, as discussed in Section 4.3.2.

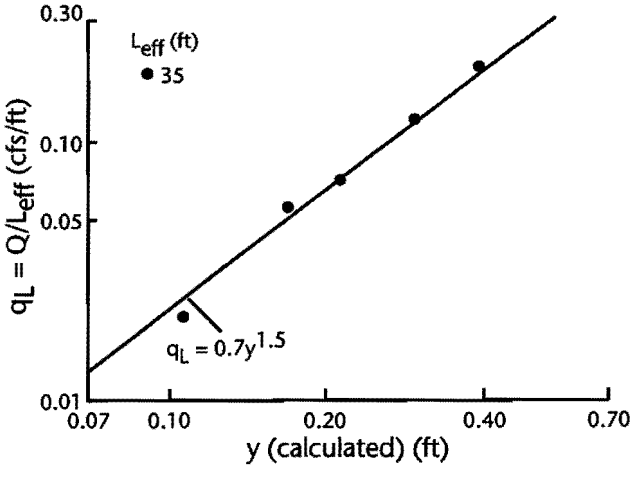

Figure 4.11 Capacity of recessed inlets with 20% recessed slope for efficiency = 100%

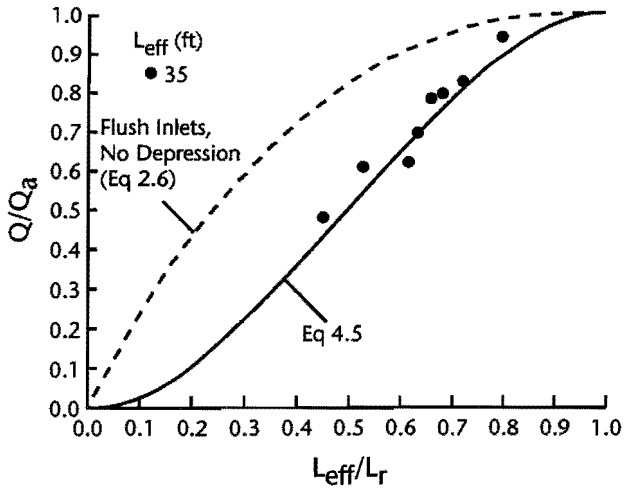

Figure 4.12 Recessed curb inlets with 20% recessed slope for efficiency < 100%

4.5 FIELD TESTS

4.5.1 Procedures

In order to verify the laboratory tests, field tests were done using existing recessed curb inlets in Austin, Texas (Figure C.9). Reconnaissance was done to identify inlets which were located in sections of streets which had well-defined and uniform gutter geometries with essentially a constant slope upstream of the inlet. An attempt was made to locate inlets with a range of longitudinal and cross slopes and with different inlets lengths (10 and 15 feet). Since city water from fire hydrants was to be used for the water supply, it was also necessary that there was a high pressure hydrant located appropriately for the tests. All of the selected inlets had reverse curve transitions which were geometrically very similar in both size and shape to the ones used in the laboratory tests.

After selecting the inlets, the streets were surveyed to determine the longitudinal and cross slopes. The approach gutter was marked at 0, 10, 20, 30, 40, 50, 75, and 100 feet from the upstream end of the upstream transition section. At each longitudinal station, marks were placed in the deepest part of the gutter and on parallel lines 3 feet and 6 feet from the curb. Levels were shot at each of these locations. The average of the longitudinal slopes along these three lines was taken as the longitudinal slope for analysis of the data. The average of the four cross slopes nearest to the inlet was taken as the cross slope for the analysis. All of the pavements were asphalt.

The tests were conducted by releasing water from the fire hydrant upstream of the inlet and adjusting the flow rate until 100% capacity was achieved, as it was in the laboratory model tests, i.e. until a further increase in the flow rate resulted in carryover. After establishing the flow rate, depths were measured at the marked stations along the curb to determine the uniform flow depth. For the first five tests, the depth measurements were made with a metal tape measure. For the remainder of the tests, a piece of 4-by-4 lumber 12 feet long was used to span the water flowing down the gutter. A point gage mounted to the lumber was used to measure the depths along the gutter. Even with the point gage, these measurements had the same difficulties as the laboratory point gage measurements (Section 3.6.5) since waviness of the water surface made it difficult to obtain measurements with a high degree of accuracy. The data were analyzed as for the laboratory tests. The effective length of each opening was taken as 2 feet shorter than the measured length of the total curb opening.

For the first five tests, the flow rate was determined from the calibration information which the City of Austin uses for rating fire hydrants. For this type of measurement, a pressure gage is attached to a cap on one of the smaller outlets on the fire hydrant. The pressure reading is used to determine the flow from the largest outlet, based on previous laboratory calibrations. Since this type of flow measurement is normally used for determining the maximum flow capacity of a hydrant and since the flows for these inlets tests were much below the maximum capacity, there was some question about the applicability and precision of the existing calibration (for the purposes of the inlets tests, not for the City's purposes). Thus, a flow measurement device (Figure C.10) was built for the remaining tests and calibrated at the Center for Research in Water Resources. The device was basically the contraction part of a venturi meter mounted on a trailer so that it could easily be moved from site to site. A fire hose was used to bring water from the hydrant to a 10-foot-long horizontal section of 4-inch steel pipe. At the downstream end of this pipe, there were two pressure gages immediately before a standard 4-inch-by-3-inch pipe contraction and a 1-foot-long section of 3-inch pipe. The meter was calibrated by volumetric measurement of the flow rates at the laboratory and of the corresponding pressures upstream of the contraction. The discharge coefficient (Equation 3.6) was found to be 1.0.

It was not feasible to conduct field tests with less than 100% efficiency because of the difficulty of measuring the carryover flow in the field.

4.5.2 Results

Thirteen field tests were conducted. Each test was done at a different inlet. The results from these tests are summarized in Table A.3 in Appendix A, and the q_L versus y values are shown in Figure 4.13 in comparison with Equation 4.1. The points are plotted using the test designations shown in Table A.3. As Figure 4.13 shows, the field data are in general agreement with Equation 4.1 and with the laboratory data. The field data have more scatter than the laboratory data, but this condition is generally expected in comparing laboratory and field data. Thus, it was concluded that the field tests confirmed the laboratory results for the 100% efficiency tests.

The results were used to calculate Manning's n for each pavement (Table A.3) using Equation 2.23. Most of the values are approximately 0.02, as would be expected. The reason for the lower values of about 0.015 is not known. The pavements were not inspected closely enough to evaluate whether some of them were physically smoother than others. The last test (Test D) had a rather high cross slope. The calculation of n is very sensitive to the value of the cross slope, so an error in S_x could have made a significant difference in the n value.

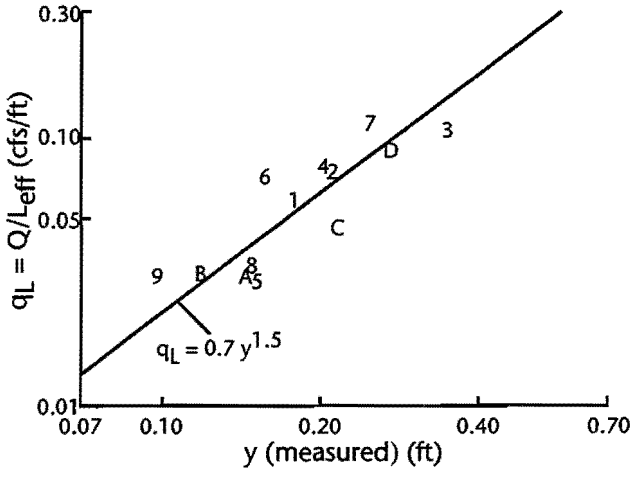

Figure 4.13 Capacity of recessed field inlets for efficiency = 100%

CHAPTER 5. CONCLUSIONS FOR RECESSED CURB INLETS

The objective of this part of the study was to investigate the hydraulic characteristics of recessed curb inlets. This study was primarily experimental. A physical model was built and used to evaluate the performance of recessed curb inlets with different geometries and varying flow conditions. This was a 3/4-scale model which was 10.5 feet wide and 64 feet long (model dimensions). It was built so that both the longitudinal and cross slopes could be easily changed. Most of the data came from measurements using this model (143 tests). Thirteen field tests were done to check the validity of the laboratory results. Most of the laboratory experiments and all of the field tests were done for inlets with 10-foot-long reverse curve transition sections both upstream and downstream of the inlet opening. Linear transition sections were also tested in the laboratory.

The physical model was designed and built to have the following capabilities:

1. flow rates up to 10 cfs;
2. longitudinal and transverse pavement slopes up to 0.10;
3. depths in the gutter up to 6 inches;
4. recessed curb inlet openings of 5, 10, and 15 feet;
5. Manning's n of 0.019; and
6. no more than a 1/8-inch deflection at any location.

All of the values are for the prototype except the 1/8-inch deflection.

The first set of laboratory tests was for reverse curve transition sections and a 30% recessed slope, i.e., a 30% slope from the curb line to the inlet opening. The analyses of the data from these tests focused on developing design information for 100% and less than 100% efficiency. The second set of laboratory tests had linear transition sections rather than reverse curve sections. For the third set, the original reverse curve transition sections were re-installed on a 20% recessed slope. The second and third sets of tests were more limited in number than the first set and were done primarily to determine if these changes in geometry had a significant effect on the performance of the inlets.

For 100% efficiency, it was found that the discharge into the inlet with a reverse curve transition could be accurately quantified using a slightly modified form of the relationship traditionally used for flush curb inlets. This relationship gives the discharge per unit length of inlet as a function of only the depth in the approach gutter. The modification was to replace the actual opening length for a flush inlet with an effective opening length for a recessed inlet. For reverse curve transitions, it was found that the effective length of the inlet equaled the full 10-foot length of the upstream transition plus the actual inlet opening (5, 10, or 15 feet) plus 8 feet of the 10-foot-long downstream transition. The resulting relationship had a standard error of 0.026 cfs/ft relative to the data. For linear transitions, the same relationship existed when the full 10-foot length of the downstream transition, rather than just 8 feet, was used in evaluating the effective length. The change in the recessed slope from 30% to 20% did not have a significant effect on the results. The significance of the effective length is that the flow into the upstream and downstream transition sections enters the inlet (8 feet of the downstream transition for reverse curve transitions and all of the downstream linear transition) for 100% efficiency. Thus, water which enters the downstream transition actually turns around and flows back upstream into the inlet at 100% efficiency flow conditions.

The field tests could be done only at 100% efficiency since the carryover flow could not be measured in the field. The field results naturally had more scatter than the laboratory results, but they generally confirmed the laboratory results.

The discharge into the inlets when their efficiency was less than 100% was quantified in two ways. The first version gave the relative flow rate (Q/Q_a = flow into the inlet divided by the flow in the approach gutter) as a function of L_{eff}/L_r = effective length of the inlet at 100% efficiency divided by the required effective

length to capture all of the gutter flow. The standard error of the Q/Q_a data relative to the equation which defined this relationship was 0.087. Due to the scatter of the data when analyzed in terms of these variables, a second approach was used. The data were replotted in terms of Q/L_{eff} = the flow into the inlet divided by the inlet's effective length (33, 28, or 23 feet for reverse curve transitions) as a function of Q_a/L_r = the flow rate in the approach gutter divided by the effective length required to capture the entire flow. This type of plotting revealed a slight segregation of the data by inlet length and Froude number of the approach flow. Many types of correlations were tried to account for the effects of these additional variables. The best relationship did provide an improved correlation, but the resulting equation was so complicated that it sometimes predicted negative flows into the inlet for conditions outside the range of conditions tested in the laboratory. Thus, it was recommended that the relationship between Q/Q_a and L_{eff}/L_r be used rather than the one between Q/L_{eff} and Q_a/L_r.

The results for less than 100% efficiency with a linear transition and with a 20% recessed slope were essentially unchanged from the original data set.

When recessed inlets capture less than 100% of the approach gutter flow, they are relatively less efficient than when they capture 100%. At less than 100% capture, some of the flow which enters the downstream transition section has enough momentum to flow back up the recessed slope and into the downstream gutter rather than flowing into the inlet. This effect was included in the predictive relationship which was developed for less than 100% efficiency.

PART II - BRIDGE DECK DRAINS

CHAPTER 6. INTRODUCTION

The drainage facilities installed in a bridge are important for ensuring that traffic remains possible and safe during and after precipitation events. The storm water that falls on a bridge deck must be drained rapidly and efficiently in order to prevent its accumulation. At the same time, drains should not represent an obstacle to traffic, and they should be positioned in a way consistent with the bridge structure and geometry.

One of the objectives of this project was to gain an improved understanding of the hydraulics of three different types of bridge deck drains used in Texas and to produce design information for these drains. There were no previous studies of performance and efficiency for these particular drains. One drain was a rectangular scupper drain, which is basically a small opening in the bridge deck. The other two consisted of a grate installed on the bridge deck, followed by an inlet box and a piping system that drains the water through the bridge structure. Because of the lack of experimental data for these particular drains, they were previously being designed without adequate information.

The hydraulic characteristics of the drains, including the effects that the inlet boxes and drain pipes could have on their behavior, were studied using a hydraulic laboratory model. Experimental data on the capacity of the drains were obtained for different longitudinal and cross slopes of the simulated bridge deck for flow rates up to 3 cfs.

The capacity and performance of on-grade grate inlets used for street drainage have been studied before. Currently, the Federal Highway Administration uses the manual "Drainage of Highway Pavements," Hydraulic Engineering Circular No. 12, by Johnson and Chang (1984) for the design and analysis of grate inlets. That publication has methods for analyzing seven different grate inlets. Because those design charts and methodologies are meant primarily for street drains, their applicability to the design of bridge drains is limited. The reason is that bridge grates are followed by an inlet box and a piping system that are significantly different in dimension and geometry from inlet boxes and subsequent sewer pipes for street drains. The back-pressure effect that bridge inlet boxes and drain pipes can have on the capacity of the bridge grate inlets is what makes the methodology for street inlets not fully applicable for bridge deck drains. Johnson and Chang (1984) also presented design information for a circular 4-inch scupper drain. It is not clear from the publication whether the design information for these drains was based solely on calculations or on data. For this reason, and since the 4-inch-by-6-inch scupper drain, which is sometimes used, has almost twice the area of a 4-inch circular drain, these rectangular scuppers were included in the experimental program.

CHAPTER 7. EXPERIMENTS AND RESULTS

7.1 THE PHYSICAL MODEL

Experimental testing of the three bridge drains was done with the same model used for the experiments for recessed curb inlets discussed in Part I of this report. The model represented one traffic lane on a bridge deck. Even though the model was used as a 3/4-scale model for the study of recessed curb inlets, it was used as a full-scale model for the study of two of the bridge drains because of the lower flow rates involved and the smaller size of the drains. For the bridge drains, the cross slope was obtained by tilting the model roadway surface downward toward the left since these drains were on the left side of the model (Figure C.11) while it was tilted toward the right for the recessed curb inlets. In hydraulics, the normal convention is to define left and right looking in the direction of flow. Each of the drains was located approximately 40 feet downstream of the head box.

7.2 MEASUREMENTS

The flow measurement devices were the same as those used for the tests with the recessed curb inlets (Section 3.6). The inflows to the model were small enough that all of the flow could be obtained with only one pump (Figure 3.4), so only the north pump and the venturi meter were used for obtaining and measuring the inflows. Each time that the venturi meter and the weirs were recalibrated, the results were within 1% to 2% of the original calibration.

For Drains 2 and 3 discussed below, the flow into the inlet was determined as the difference between the total flow rate and the carryover flow, as for the recessed curb inlets. However, for the scupper drain, the flow into the drain was so small that it was measured volumetrically. For these measurements, a 12-inch flexible hose was mounted beneath the scupper to divert the flow. The hose was mounted in a manner to allow free flow of the water into and through the scupper. Normally, the flow just passed through the hose to the return system. When it was desired to measure the flow rate, the bottom end of the hose was pulled over a cylindrical tank which had a diameter of 6.5 feet and a height of 2 feet. A stop watch was used to measure the filling time, which was typically 1 to 2 minutes. The flow rate was determined from the initial and final depth readings and the filling time. After a measurement, the tank was emptied by siphoning.

The depths and ponded widths were measured as for the recessed curb inlets in an attempt to determine these values for uniform flow. However, gradually varied flow existed in some regions of the flow so that it was not always possible to measure these quantities for uniform flow. Depending on the flow conditions, the gradually varied flow regions were of different lengths and in different locations. For supercritical flow, there was gradually varied flow immediately downstream of the head box and immediately downstream of the drain. For subcritical flow, gradually varied flow existed immediately upstream of the drain and before the downstream end of the model where there was a free overfall. All of this behavior is in accordance with the theory of free surface flow. Nevertheless, uniform flow was sometimes established in only short lengths of the model. The location of these regions for each test depended on the longitudinal slope, cross-slope and total flow rate. For this reason, even though the desire was to measure the uniform flow depth upstream of the drain and to measure the flow width (ponded width) for uniform flow, this was not always possible. The depths were measured, but the correlations which are given later between the flow rates into the drains and the depths were based on calculated uniform flow depths.

The normal depth (y) next to the curb for the gutter flow was calculated in each case using the modified Manning's formula for free surface flow in a triangular channel (Equation 2.23). When the measured flow depths were compared with the calculated normal depths for the approach flow, it was found for subcritical flows that the measured depths were smaller than the

calculated flow depths, in accordance with the theory of gradually varied flow for subcritical flow since an M2 curve existed upstream of the drain. For supercritical flows, the measured depths and the calculated normal depths were essentially the same (±5%) since uniform flow existed upstream of the drains. For all of the tests, the calculated normal depths were used for the analysis instead of the measured depth.

7.3 DRAIN 1 (SCUPPER DRAIN)

7.3.1 Geometry and Description

The first bridge deck drain was a rectangular scupper drain, which is basically an opening in the bridge deck. The water enters the drain and goes immediately into a free fall. The scupper drain was located nearly flush with the edge of the bridge deck. The model was used as a full-scale model for the scupper drain. The interior dimensions of the scupper were 4 inches (normal to the direction of flow) by 6 inches (in the direction of flow). The vertical length of the drain was 1 foot. It was constructed of 3/4-inch plexiglass. The top edge of the scupper was flush with the roadway surface.

7.3.2 Procedures

The procedures were as follows:

1. The model was set at the desired longitudinal and cross slopes.
2. A constant total flow rate was established into the upstream end of the model using the venturi meter to determine the flow rate.
3. The flow depth and the ponded width were measured upstream and downstream of the drain.
4. When the flow over the total-flow V-notch weir reached a steady condition, the head on the weir was measured.
5. The flow rate into the scupper drain was measured volumetrically, as described in Section 7.2.

For the scupper drain, 74 tests were conducted. The data are shown in Table B.1, Appendix B. The tests had longitudinal slopes of 0.001, 0.005, 0.01, 0.02, 0.04 and 0.06 and transverse slopes of 0.01, 0.02, 0.04, 0.06 and 0.08. The range of total flows (gutter flows) was from 0.03 cfs to 3 cfs.

7.3.3 Results

A graph of the calculated normal depth (y) next to the curb upstream of the drain versus the flow rate (Q_1) captured by the scupper drain is shown in Figure 7.1. All of the data points obtained during the testing appear on the graph. They are plotted in groups according to the longitudinal slope (S) for each case. Thus, each symbol in Figure 7.1 represents the data for all of the cross slopes which were tested for the indicated longitudinal slope. A visual inspection of Figure 7.1 reveals the following:

- Up to at least y = 0.10 feet (or Q_1 = 0.16 cfs), there is essentially a linear relationship between log(Q_1) and log(y) for each value of S. The scatter about each line in the figure may be due to the effect of the cross slope (S_x).
- From y = 0.10 feet to 0.40 feet, this linear relationship is not present for all longitudinal slopes (S). A change in the slope of the data points (called a break point) for log(Q_1) versus log(y) for each S exists, with the break point occurring at smaller values of y or Q_a for larger longitudinal slopes. That is, the change in slope of the data occurs for S = 0.06 for a certain value of y, then it occurs for S = 0.04 for a larger value of y, and so on. The right-hand end of each solid line in the figure is at the point where the break in the slope of the data points appears to occur.
- The range of flows used during the testing does not permit a definite evaluation of the characteristics of the relationship between Q_1 and y for the data past the break point in the slope of the data (i.e., for the largest y values for each longitudinal slope).
- In the transition region to the right of and above the break points in the slopes of the data, the curves for the different values of S cross. For the lines shown, the data for S = 0.06 are the lowest points on the graph, but it appears that they would be the highest values if there were enough data to define the variations for larger depths and larger flow rates.
- Comparing Figure 7.1 with the similar graph presented by Johnson and Chang (1984) for the 4-inch circular scupper drain, it can be seen that the results are generally similar.
- For flow conditions below the break points, the slopes of the data points for each of the longitudinal roadway slopes are essentially the same.

For the smaller flow depths and for subcritical flow, the flow into the scupper drain behaves as flow over a weir along each of the four sides. For supercritical flow, the same thing occurs, except that the water does not flow into the drain from the downstream side. At a certain flow depth, the

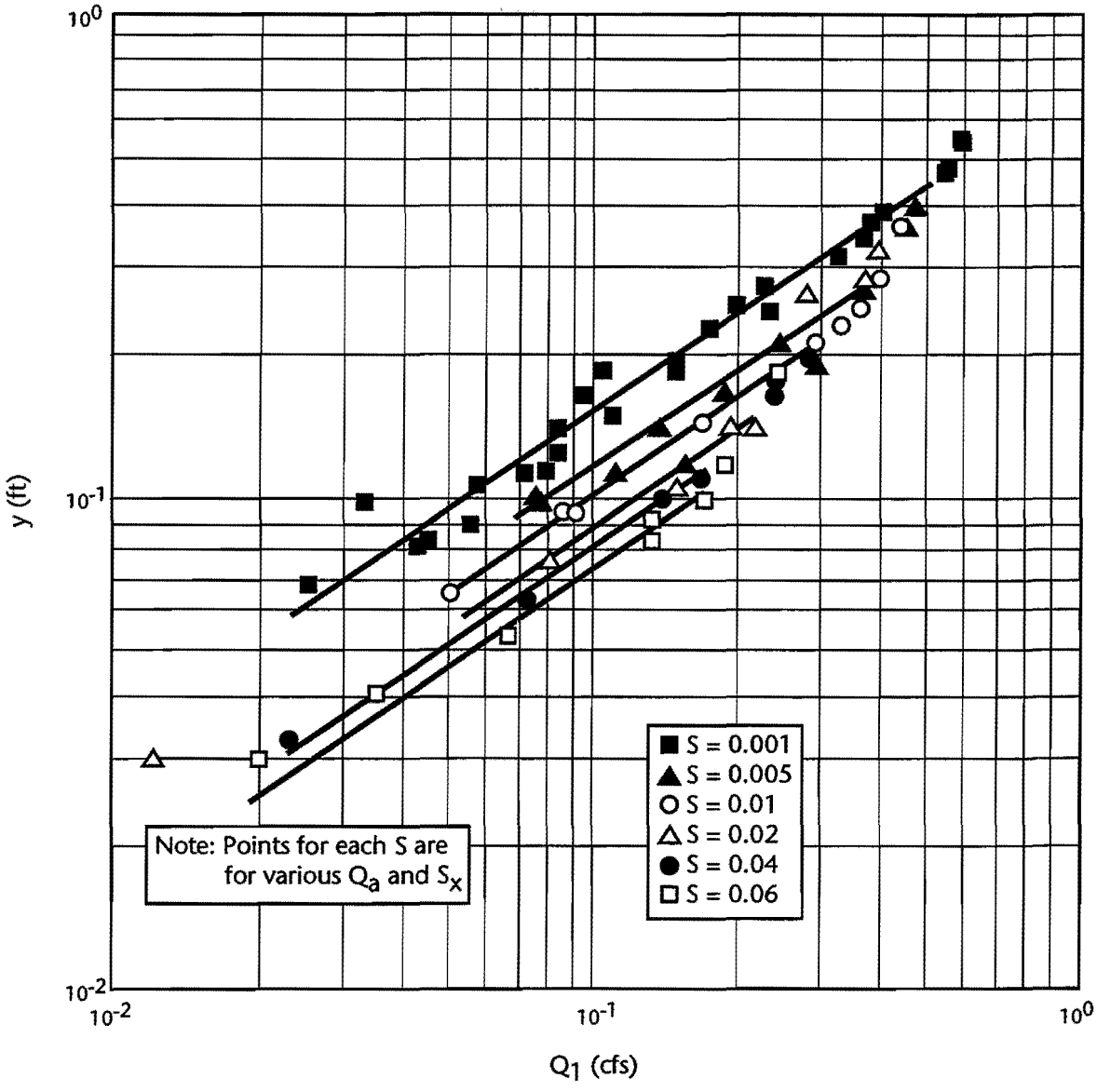

Figure 7.1 Results for scupper drain

scupper drain starts to behave as an orifice. The break point that occurs in the slope of the data points on the graph corresponds to this change in behavior for each slope.

A regression analysis for the data for the cases of weir-like behavior (before the break point in the slopes of the data) was done. The variables used for the analysis were

S = longitudinal slope
S_x = cross slope
Q_a = total flow rate (cfs)
Q_1 = captured flow rate (cfs)
y = calculated normal depth (feet)
V = velocity upstream of drain (ft/sec)
Fr = Froude number upstream of drain
T = ponded width upstream of drain (feet)

The two best equations were

$$Q_1 = 12.3 y^{1.83} \frac{S^{0.29}}{S_x^{0.18}} \quad (7.1)$$

and

$$Q_1 = 14.9\, y^{1.62}\, S^{0.28} \quad (7.2)$$

Equation 7.1 has a correlation coefficient (R-squared) value of 0.979 and a standard error of 0.042 cfs. The t-values for the variables were

Coefficient	t-value
constant	19.4
y	35.8
S	27.3
S_x	-6.5

These t-values show that the influence of the variables involved is not statistically negligible.

Equation 7.2 has a correlation coefficient (R-squared) value of 0.955 and a standard error of 0.060 cfs. The t-values for the variables are

Coefficient	t-value
constant	14.9
y	28.3
S	18.6

As can be seen, both equations are statistically good, with Equation 7.1 having a slightly smaller standard error. The primary difference between the two equations is the presence of the variable S_x in Equation 7.1. The inclusion of S_x improves the correlation coefficient by 2.5%. Plots of measured values of Q_1 against predicted values using Equations 7.1 and 7.2 are presented in Figures 7.2 and 7.3. The good match between the predicted values and the measured values of Q_1 can be seen.

7.3.4 Limits of Applicability

It must be emphasized that these equations apply only to the zone of weir-like behavior, and therefore their applicability is restricted. An analysis of the break points that occur in slopes of the data points on the graph for each longitudinal slope gives the following condition for the occurrence of weir-like behavior for S between 0.001 and 0.06:

$$y \leq \frac{0.034}{S^{0.39}} \qquad (7.3)$$

Thus, for $0.001 \leq S \leq 0.06$ and $0.01 \leq S_x \leq 0.08$, there is a weir-like behavior for the scupper drain (Drain 1) for depths which meet the restriction in Equation 7.3; Equations 7.1 and 7.2 can be used for these conditions. It is essential that these limits be observed since the capacity of the drain decreases relative to Equations 7.1 and 7.2 for depths larger than those given by Equation 7.3.

7.4 DRAIN 2

7.4.1 Geometry and Description

The second bridge deck drain tested (Drain 2) had a grate inlet (Figures 7.4, C.12, and C.13). The grate was 9.25 inches long (in the flow direction) and 36.75 inches wide and was supported by an inlet box.

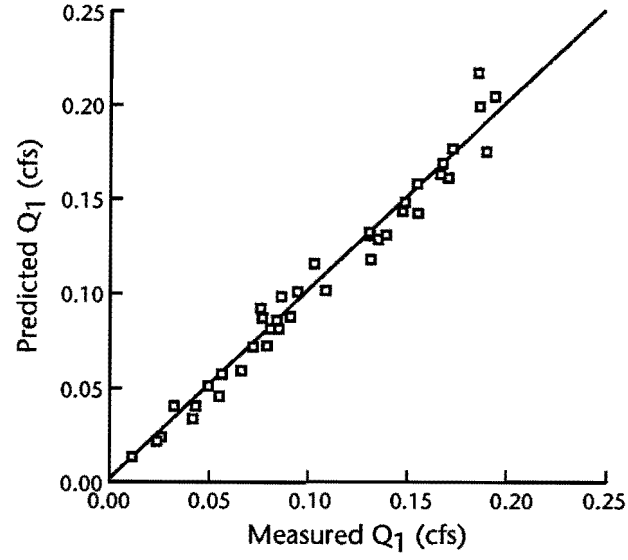

Figure 7.2 Scupper flows, measured and predicted from Equation 7.1

The bottom of the inlet box was inclined towards the entrance to the 6-inch drain pipe, which drains the water to the bottom of the bridge structure. The deep part of the box and the outlet from the box were next to the curb in these tests. Thus, when the cross slope of the bridge deck was increased, the slope of the bottom of the inlet box was also increased. The edge of the drain was located essentially flush with the bridge curb.

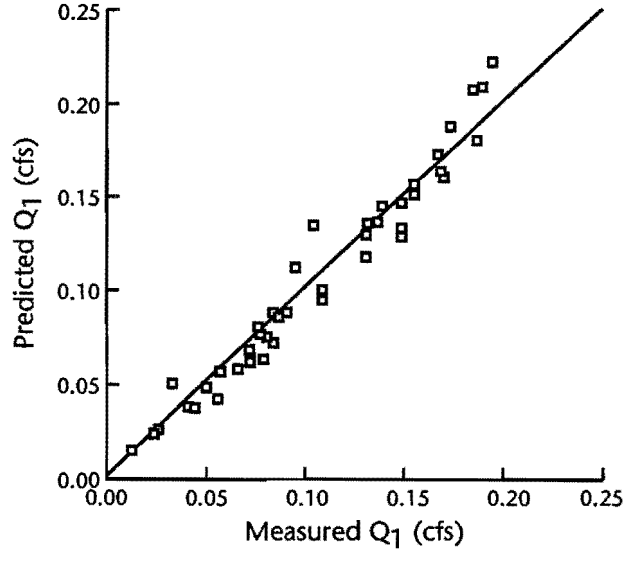

Figure 7.3 Scupper flows, measured and predicted from Equation 7.2

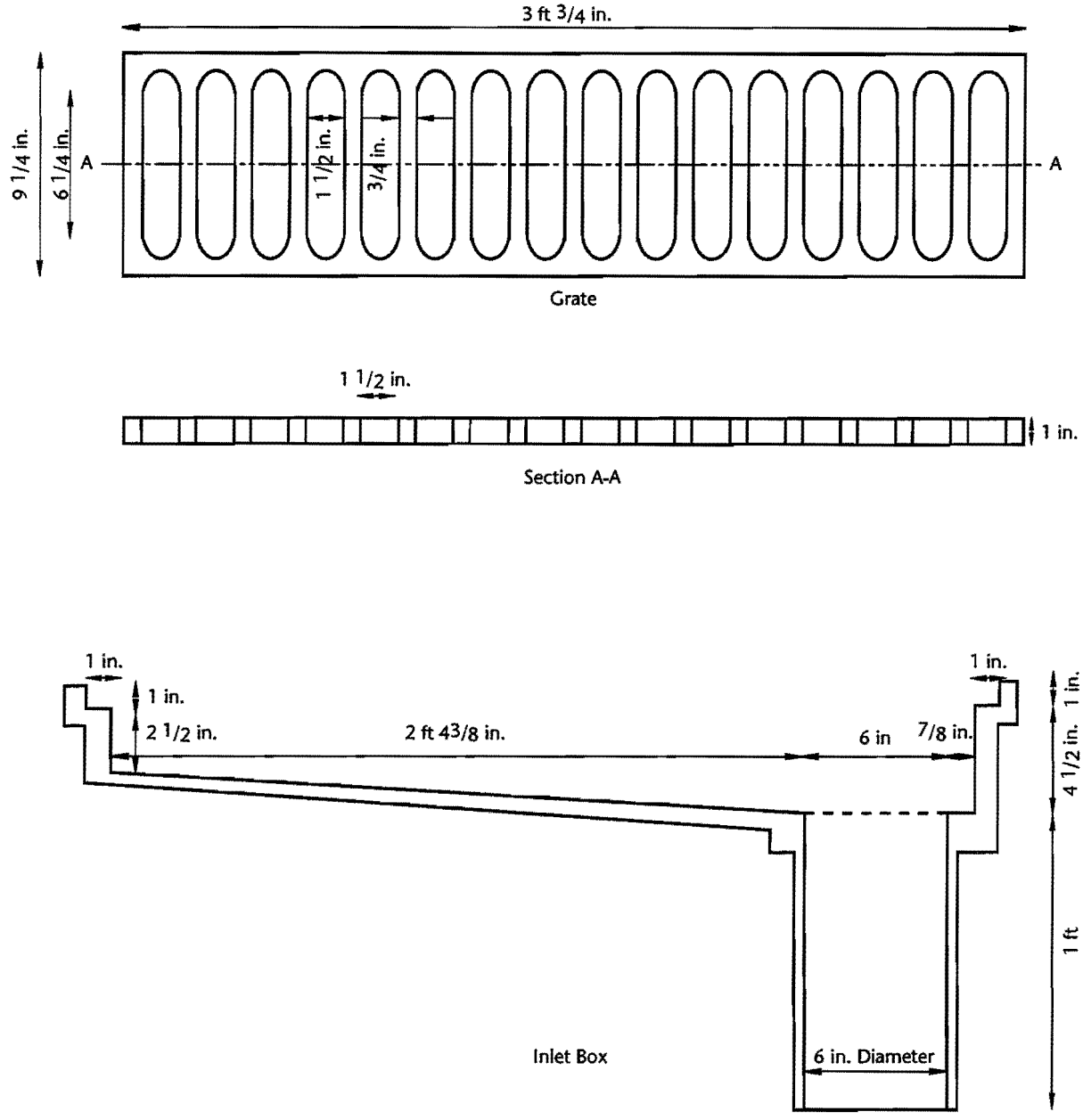

Figure 7.4 Drain 2

The model was used at full scale for these experiments. The drain was built entirely of plexiglass (Figure C.12) so that the behavior of the flow inside the inlet box could be observed visually.

7.4.2 Procedures

Ninety-nine tests were conducted for Drain 2. The influence of the piping system below the inlet box on the capacity of the drain was an important part of the study. For this reason, several different configurations of drain pipes were tested. In the prototype, the vertical distance between the bottom of the inlet box and the outlet of the piping system (which is usually near ground level) can be a few tens of feet. In the model, the vertical distance between the bridge deck and the laboratory floor was about 7 feet. Because of these space limitations, only short piping systems could be tested.

Seven different configurations of the drain pipe (Figure 7.5) were tested initially to determine their influence on the capacity of the drain. For configurations A through E, the view is looking across the roadway normal to the flow direction. For F and G, the view is looking upstream. These tests were made using a longitudinal slope of 0.001 and cross slopes of 0.06 and 0.08. These slopes

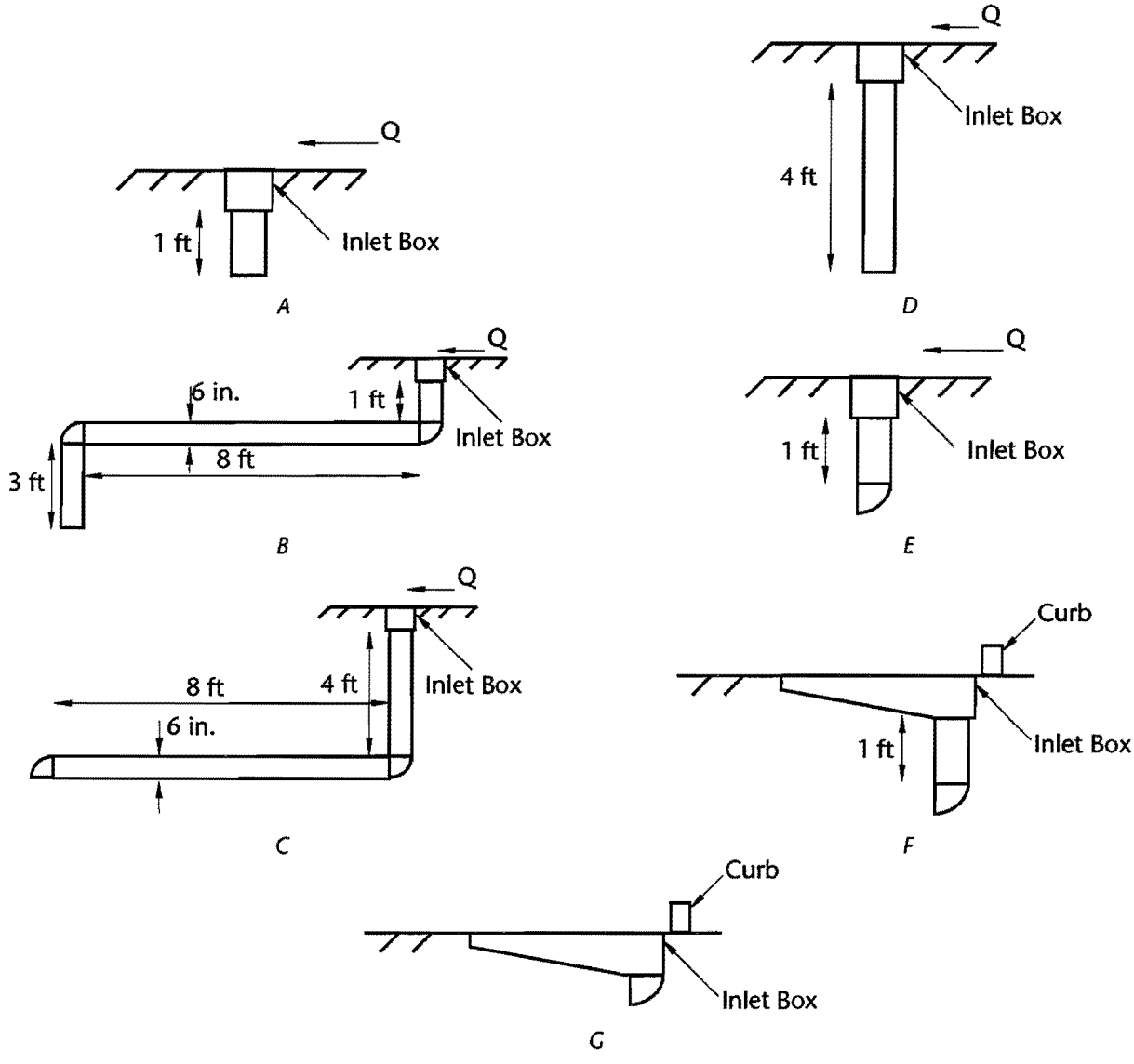

Figure 7.5 Piping configurations for Drain 2

were chosen because they were the ones which were expected to produce the largest drain flows and thus the largest possible influence of the drain piping. The drain should capture the maximum flows for small longitudinal slopes when the water is flowing slowly down the gutter and for the large cross slopes when the water is deeper over the top of the drain. The total (gutter) flows ranged from 1 cfs to 2.7 cfs. Thirty-two of the total of 99 tests for Drain 2 were conducted primarily for investigating the effects of the seven configurations of the drain pipes.

When the final configuration to be studied in more detail was selected, 67 more tests were run. The longitudinal slopes used were 0.001, 0.005, 0.01, 0.02, 0.04, 0.06 and 0.08. Cross slopes were 0.01, 0.02, 0.04, 0.06 and 0.08. The total flows varied from 0.4 cfs to 1.5 cfs.

The procedure followed for each one of the 99 tests was similar to the one described for the scupper drain in Section 7.3.2, except that in this case the flow captured by the drain was not measured directly but was calculated as the difference between the total flow rate and the carryover flow rate. The flows were large enough for the carryover to be measured accurately, and the flow captured by the inlet was too large to be accurately measured with the tank used for the scupper drain.

During each test, a visual inspection of the flow conditions inside the drain pipe and through the grate was made. In this way it could be determined whether the flow inside the drain piping was pressure flow or free flow and what the conditions at the grate were.

The data for these tests are shown in Table B.2, Appendix B.

7.4.3 Results

7.4.3.1 Effects of Piping System

As mentioned above, tests were first done to study the influence of the drain piping on the capacity of the drain. When pressure flow in the pipe controls the capacity of the drain, then basic hydraulic principles imply that the highest flow rate occurs for the largest head difference across the drain pipe. This head difference is equal to the head at the pipe entrance plus the vertical distance (Z) between the inlet and the outlet minus friction and elbow losses minus the velocity head at the outlet.

Figure 7.6 shows the flow (Q_2) captured by the drain for each of the seven piping configurations. As stated previously, the data in Figure 7.6 were obtained only for S = 0.001 and S_x = 0.06 and 0.08. This figure is not intended to give a comprehensive evaluation of flow conditions. Rather, it is intended to give an indication of the type of influence of the drain piping. The full range of flows was not covered for each piping configuration, and there is scatter of the data in Figure 7.6; a possible cause for the scatter is discussed later. Nevertheless, the general features of the behavior seem apparent. For each piping configuration, the relationship between y and Q_2 starts with one slope for the lower values of y and Q_2 and then, at some point which varies with the piping configuration, there is a definite break in the slope, with the subsequent slope being much steeper. The flatter slopes of the data points presumably correspond to weir control as the water flows over the lip of the inlet or orifice control as the water leaves

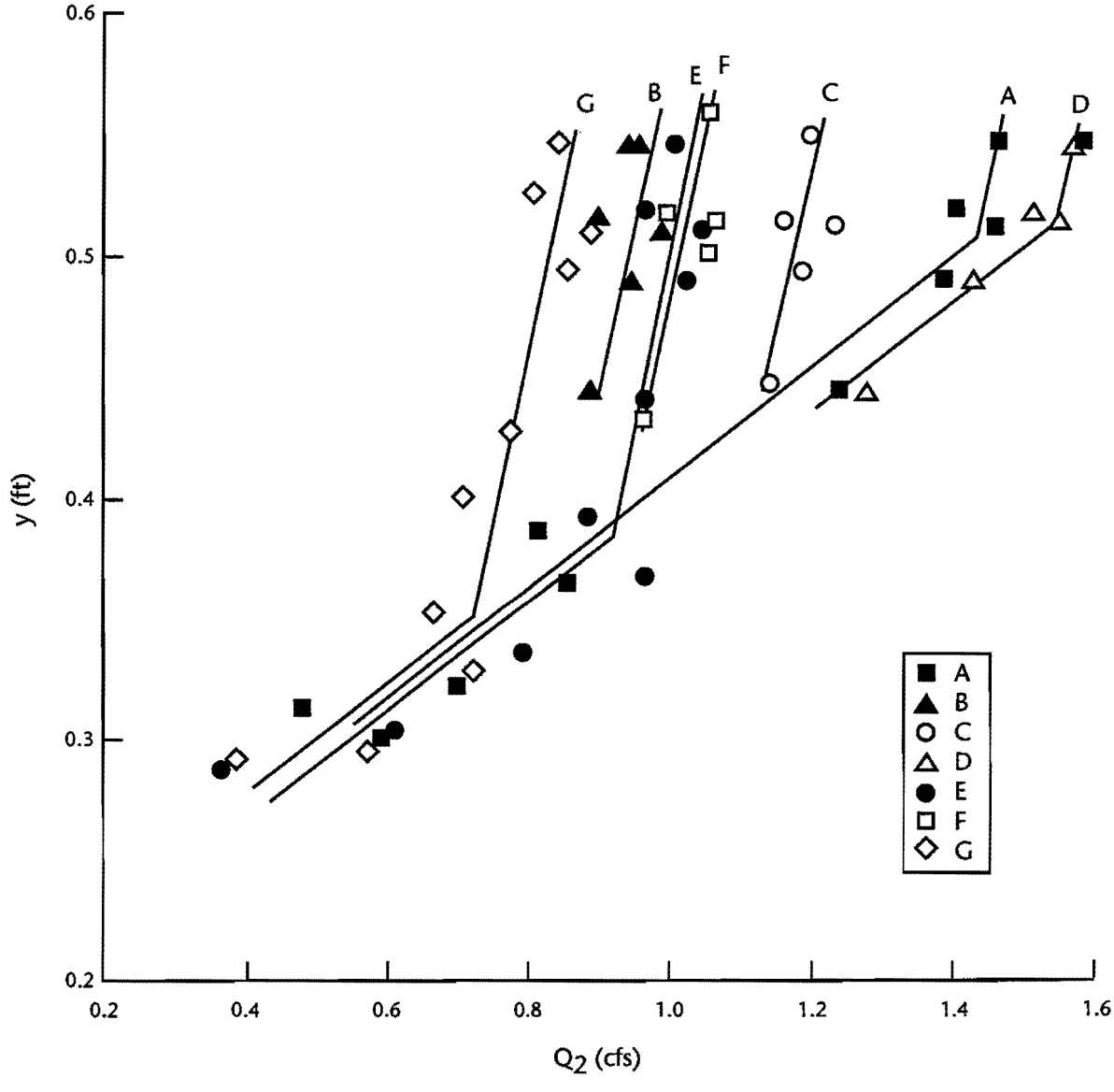

Figure 7.6 Effects of piping on Drain 2

the inlet box and enters the piping system. The steeper slopes correspond to back-pressure effects from the piping system controlling the flow. For the regions of the steeper slopes in Figure 7.6, the pipe was flowing full. Using the letter designations of the drain configurations shown in Figure 7.5 to identify the flow for the different configurations, an inspection of Figure 7.6 shows for the regions of back-pressure control that

1. $Q_2(A) < Q_2(D)$, which is in accordance with hydraulic theory. The vertical distance (Z) between inlet and outlet is larger in D than in A, so that there is a larger head difference across the pipe, and there are no elbows in either one to affect the head losses in the piping system.
2. $Q_2(B) < Q_2(C) < Q_2(D)$, with significant differences for the three cases even though the vertical distance between the inlet and outlet is the same for all three cases. Configuration B is shown in Figure C.14. The fact that $Q_2(D)$ is the largest is in accordance with hydraulics theory since it has no elbows to cause losses and since it has the shortest pipe. It is curious that $Q_2(C)$ is larger than $Q_2(B)$, despite the fact that both configurations have the same pipe length, the same number of elbows, and the same Z. The essential difference between B and C is that the first elbow is closer to the inlet for B than for C.
3. $Q_2(B) < Q_2(E)$, but the difference is small. It is somewhat surprising that $Q_2(B)$ is not significantly larger than $Q_2(E)$, since B appears to have a significantly larger head difference across the pipe than E due to the extra 3-foot drop for B. The additional head loss for B due to the extra pipe length and the extra elbow is only about 0.6 feet. The essential feature which is the same for B and E is the distance from the inlet to the first elbow.
4. $Q_2(E) \approx Q_2(F)$, with the difference in the pipe configurations for E and F being only the direction that the elbow is turned.
5. $Q_2(G) < Q_2(F)$, with the vertical distance to the elbow for G (Figure C.12) being smaller than for F. It is difficult to know whether the reduction in flow for G is due to the elbow being closer to the inlet box or due to the reduction in head difference across the pipe with the outlet being 1 foot higher for G.
6. The flow differences for the various piping configurations are much greater for back-pressure control than for weir (or orifice) control.

From these observations, it appears that the distance to the first elbow has a very strong influence on the amount of flow captured by the drain when back-pressure conditions exist, with less flow being captured by the inlet for smaller distances to the first elbow. The hydraulic reasons for this effect are not clear, but this distance appears to be very important for establishing the flow into the piping system, especially when the distance between inlet box and elbow is small. Based on these results, it was decided to conduct a complete set of tests for configuration G, since this configuration had the smallest capacity.

The results give good confirmation that configuration G has the smallest capacity of the configurations tested in the laboratory. Nevertheless, it is possible that the behavior would be different if the head difference across the drain piping were on the order of 15 feet to 20, as it might be for a bridge with the piping outlet near ground level.

7.4.3.2 Results for Low Flow Conditions

The discussion in Section 7.4.3.1 above relates primarily to conditions when the piping system causes a back-pressure effect which controls the capacity of the inlet. Even for the worst case (configuration G), there is no back-pressure effect up to a flow of about 0.7 cfs. For the other configurations, higher flows can be captured with no back-pressure effects. Thus, for the most common ranges of flows for these bridge drains, it can be anticipated that low flow conditions (no back-pressure effects) will prevail. For contrast with these intercepted flows for Drain 2, the maximum flow shown by Johnson and Chang (1984) on the design graph for a 4-inch circular scupper drain is only 0.17 cfs and low flow conditions are shown to stop at about 0.07 cfs. For the 4-inch-by-6-inch rectangular scupper discussed in Section 7.3, low flow conditions existed up to at least 0.2 cfs (Figure 7.1 and Equation 7.3).

The remainder of the experimental program for Drain 2 was directed toward determining the capacity for low flow conditions for a range of longitudinal and cross slopes. For these additional tests, the maximum gutter flow rate was 2.6 cfs, and the maximum drain flow rate was 0.8 cfs (for all but three of the tests). The gutter flow rates were selected, in combination with the slopes, to give drain flows which would be in the low flow regime with no effects of back pressure and to cover the expected range of gutter flows.

The results of the additional tests for configuration G plus the low-flow tests for all of the previous piping configurations are shown in Figure 7.7. There is a general segregation of the data according to longitudinal slope (S), but there is

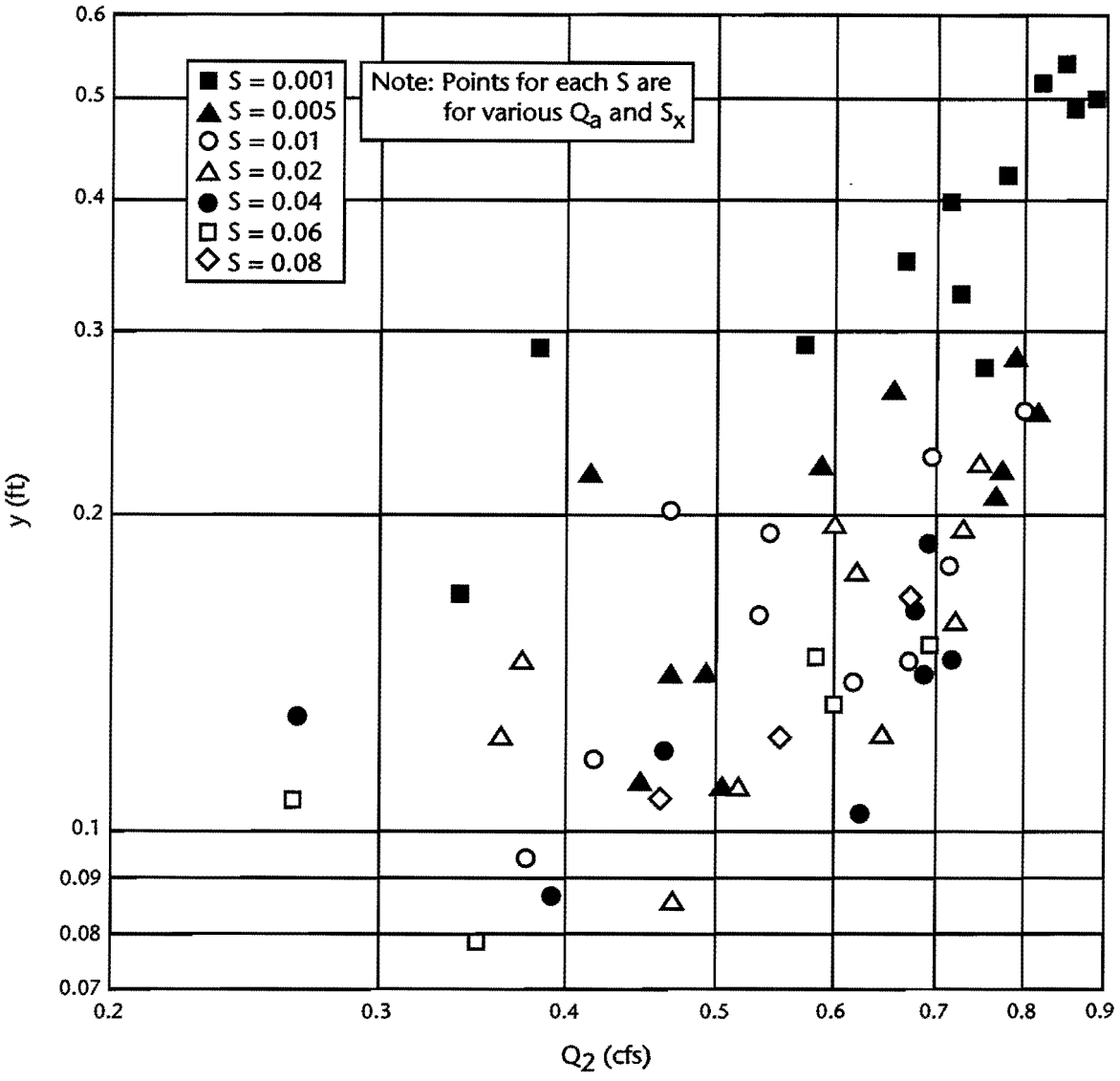

Figure 7.7 Results for Drain 2 for low flow conditions

also a large amount of scatter of the data points for each S. The reason for the large scatter seems to be that the cross slope (S_x) is also very significant but cannot be shown on a two-dimensional graph. The regression equation discussed below confirms the importance of S_x. Perhaps the reason that S_x is more important for Drain 2 than for the scupper drain is that Drain 2 is about 3 feet wide. Thus, the ponded width (and thus S_x) can have a major effect on the frontal flow for the drain.

A regression analysis was done for the data for low flow conditions. The variables used for the analysis were

S = longitudinal slope
S_x = cross slope
Q_a = total flow rate (cfs)
Q_2 = captured flow rate (cfs)
y = calculated normal depth (feet)
V = velocity upstream of drain (ft/sec)
Fr = Froude number upstream of drain
T = ponded width upstream of drain (feet)

The best equation obtained from the regression analysis was

$$Q_2 = 20.6y^{2.49}\left(\frac{S}{S_x^2}\right)^{0.44} \qquad (7.4)$$

S and S_x were used in the regression as individual parameters; the regression showed that the magnitude of the exponent for S_x was a negative two times the exponent for S. Equation 7.4 has a correlation coefficient (R-squared) value of 0.948 and a standard error of 0.030 cfs. The t-values for the variables are

Coefficient	t-value
constant	20.5
y	26.8
S	22.3
S_x	-22.3

Thus, Equation 7.4 is statistically good and can be used for low flow behavior. A plot of the measured values of Q_2 versus the predicted values from Equation 7.4 is shown in Figure 7.8.

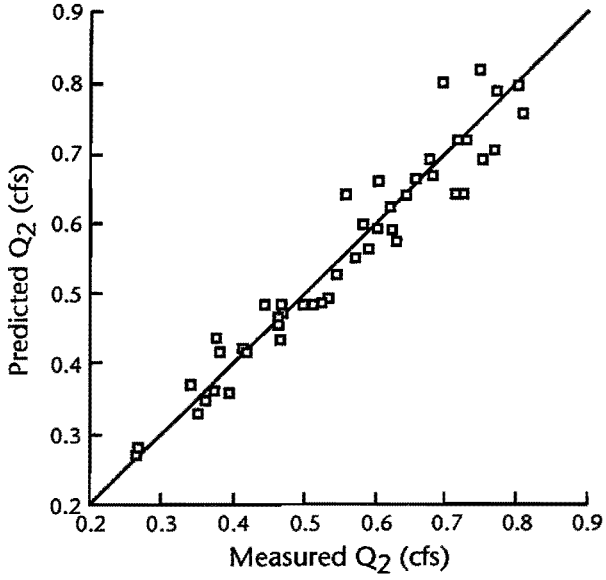

Figure 7.8 Drain 2 flows, measured and predicted from Equation 7.4 for low flows

7.4.4 Limits of Applicability

It must be emphasized that this equation applies only to the zone of low flow behavior, and therefore its applicability is restricted. There was not enough data for flows above the low flow range to obtain a good evaluation of the limits of applicability of the low flow regime directly from an analysis of the data. Thus, two approaches were taken for evaluating this limit. The first one came from an observation of flow in the inlet box during the tests. For each set of slopes, the flow depth at which back-pressure effects were first observed was noted. From these results, an approximation to the applicable limit was obtained as

$$y \leq 0.3 \frac{S_x^{0.39}}{S^{0.18}} \qquad (7.5)$$

Based on Figures 7.6 through 7.8, it seems reasonable that the limit is no greater than a drain flow of 0.8 cfs. Thus, for $0.001 \leq S \leq 0.08$ and $0.01 \leq S_x \leq 0.08$, it seems prudent to take the limit as the more restrictive of Equation 7.5 or $Q_2 < 0.8$ cfs until a better definition of the limit is obtained. Equation 7.4 should be used only for these conditions. It is essential that this limit be observed since the capacity of the drain can decrease relative to Equation 7.4 when the low flow range is exceeded.

7.4.5 Comparison of Results for Drain 2 with HEC-12

The empirical results obtained for Drain 2 were compared with the predictions from the design method given in HEC-12 (Johnson and Chang, 1984) for grate inlets. None of the grates in HEC-12 is exactly like the grate on Drain 2. Thus, for the calculations, the design method was used for a P-1-7/8 grate since this grate has no transverse rods and thus seemed to be the most nearly similar to the grate on Drain 2. Based on this type of grate and the length of the grate for Drain 2, a splash-over velocity of 5 fps was assumed. Calculations were made for all combinations of Q_a = 0.1, 0.2, 0.4, 0.6, 0.8 cfs; n = 0.015, 0.02; S = 0.005, 0.01, 0.02, 0.03, 0.04, 0.05, 0.06, 0.07, 0.08; and S_x = 0.01, 0.02, 0.03, 0.04, 0.05, 0.06, 0.07, 0.08. For most of the larger values of S_x, the ponded width was less than the width of the grate since the maximum flow was 0.8 cfs in accordance with the limitations stated in Section 7.4.4. For each case, the efficiency (E_{HEC-12}) of the grate was calculated from HEC-12 and compared to the efficiency (E_{emp}) obtained from the empirical results with E_{emp} = Q from Equation 7.4 divided by Q_a. The results are summarized in Table 7.1. For most of the cases, HEC-12 predicts that the flow captured by the grate is larger than the captured flow obtained from the experiments. The difference between E_{HEC-12} and E_{emp} is much greater for n = 0.015 than for n = 0.020.

7.5 DRAIN 3

7.5.1 Geometry and Description

Like Drain 2, the third drain tested (Drain 3) was also a grate on an inlet box (Figures 7.9 and C.15). The inlet box was followed by a transition, also called an inlet connector, to a drain pipe. The piping system normally goes to the bottom of the bridge pier where the pipe outlet is located near ground level. After falling through the grate, the water follows the slope of the bottom of the inlet box. In this case, the inlet box and connector had a slope of 0.089 relative to the deck surface, directed towards the center of the bridge. This meant that the absolute slope of the bottom of

Table 7.1 Comparison of calculations from HEC-12 with empirical results for Drain 2

	$\frac{E_{HEC-12}}{E_{emp}}$							
	n=0.020				n=0.015			
S_x	Average	Standard Deviation	Maximum	Minimum	Average	Standard Deviation	Maximum	Minimum
0.01	0.95	0.125	1.12	0.64	1.13	0.072	1.50	090
0.02	1.07	0.079	1.17	0.84	1.43	0.092	1.56	1.16
0.03	1.09	0.066	1.20	0.94	1.44	0.085	1.58	1.28
0.04	1.09	0.062	1.19	0.96	1.43	0.080	1.56	1.26
0.05	1.08	0.060	1.18	0.95	1.42	0.078	1.54	1.25
0.06	1.07	0.060	1.17	0.94	1.40	0.075	1.52	1.23
0.07	1.06	0.059	1.16	0.94	1.39	0.072	1.50	1.22
0.08	1.06	0.059	1.15	0.93	1.38	0.069	1.48	1.22
Average	1.06	0.071			1.38	0.078		

the inlet box and connector decreased as the cross slope of the bridge deck increased.

This drain was larger than the first two drains tested. The grate had a length of about 3 feet in the flow direction and a width of 2 feet. It had 11 longitudinal bars and 5 transverse or stringer bars. Due to the larger dimensions of Drain 3, a scale of 3/4 was used for these tests. All of the dimensions and flow rates are given as prototype values. The drain was built of plexiglass so that the behavior of the water flow inside the inlet box and the inlet connector could be observed visually.

7.5.2 Procedures

Sixty-one tests were done for Drain 3. The longitudinal slopes were 0.001, 0.005, 0.01, 0.02, 0.04, 0.06, and 0.08. The cross slopes were 0.01, 0.02, 0.04, 0.06, and 0.08. The total prototype flow ranged from 0.3 cfs to 3.5 cfs. The data for Drain 3 are shown in Table B.3, Appendix B.

The experimental procedures were similar to those for Drain 2 except that various piping configurations were not tested since the connector design was an essential part of the inlet design. A visual inspection of the flow conditions at the grate (Figure C.16), inside the inlet box, in the inlet connector, and through the grate was also made.

7.5.3 Results

The results are shown in Figure 7.10, which is similar to Figure 7.7 for Drain 2. There is a general segregation of the data according to longitudinal slope (S), but there is also a large amount of scatter of the data points for each S. The reason for the large scatter seems to be that the cross slope (S_x) is also significant but cannot be shown on a two-dimensional graph. The regression equation presented below confirms the importance of S_x. As for Drain 2, perhaps the reason that S_x is more important for Drain 3 than for the scupper drain is that Drain 3 is much wider than the scupper drain. Thus, the ponded width (and thus S_x) can have a major effect on the frontal flow for the drain.

A regression analysis was done for the data for the cases of low flow behavior (before back-pressure effects from the conduit below the inlet box). The variables used for the analysis were

S = longitudinal slope
S_x = cross slope
Q_a = total flow rate (cfs)
Q_3 = captured flow rate (cfs)
y = calculated normal depth (feet)
V = velocity upstream of drain (ft/sec)
Fr = Froude number upstream of drain
T = ponded width upstream of drain (feet)

The best equation obtained from the regression analysis was

$$Q_3 = 26.1 y^{2.26} \frac{S^{0.42}}{S_x^{0.66}} \qquad (7.6)$$

Equation 7.6 has a correlation coefficient (R-squared) value of 0.984 and a standard error of 0.025 cfs. The t-values for the variables are

Coefficient	t-value
constant	41.7
y	40.6
S	31.8
S_x	-22.6

This equation is statistically good and can be applied for the cases of low flow behavior. In Figure 7.11, a plot of the measured values of Q_3 versus the predicted values from Equation 7.6 is shown.

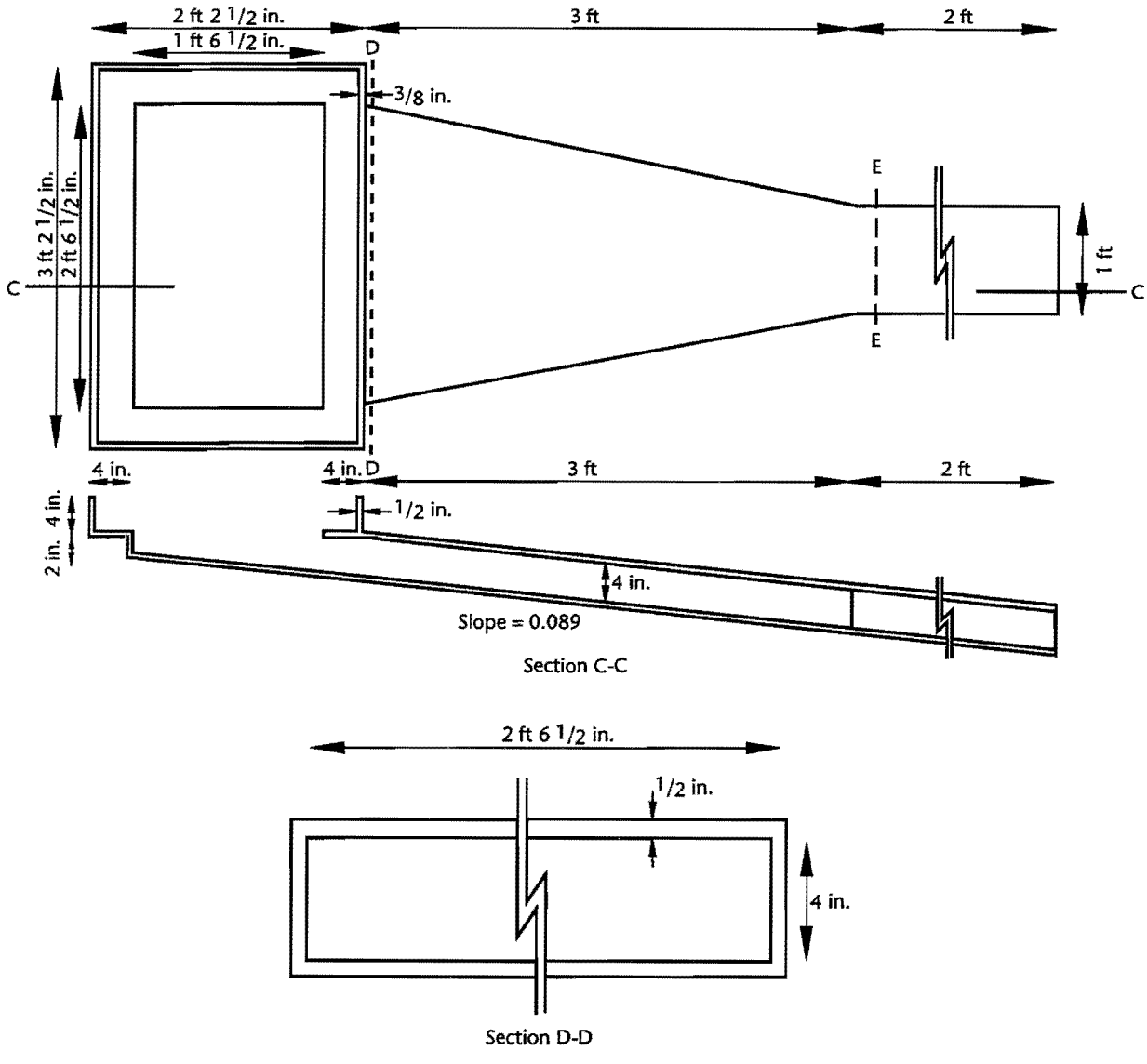

Figure 7.9 Drain 3

7.5.4 Limits of Applicability

It must be emphasized that this equation applies only to the zone of low flow behavior, and therefore its applicability is restricted. As for Drain 2, two approaches were taken for evaluating this limit. The first one came from an observation of flow in the inlet box during the tests. For each set of slopes, the flow depth at which back-pressure effects were first observed was noted. From these results, an approximation to the applicable limit was obtained as

$$y \le 0.2\left(\frac{S_x}{S}\right)^{0.21} \qquad (7.7)$$

Based on Figures 7.10 and 7.11, it seems reasonable that the limit is no greater than a drain flow of 1.6 cfs. Thus, for $0.001 \le S \le 0.08$ and $0.01 \le S_x \le 0.08$, it seems prudent to take the limit as the more restrictive of Equation 7.7 or $Q_2 < 1.6$ cfs until a better definition of the limit is obtained. Equation 7.6 should be used only for these conditions. It is essential that this limit be observed since the capacity of the drain can decrease relative to Equation 7.6 when the low flow range is exceeded.

7.5.5 Comparison of Results for Drain 3 with HEC-12

The empirical results obtained for Drain 3 were compared with predictions from the design method given in HEC-12 (Johnson and Chang, 1984) for grate inlets. None of the grates in HEC-12 is exactly like the grate on Drain 3. Thus, for

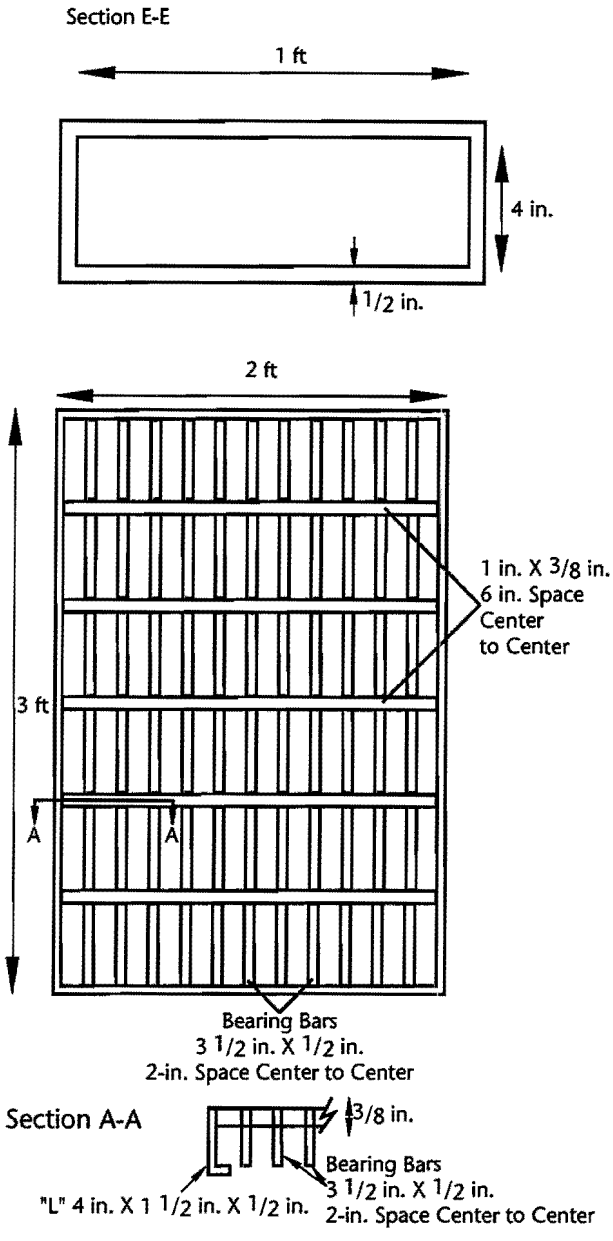

Figure 7.9 Drain 3 (continued)

the calculations, the design method was used for a P-1-7/8-4 grate since this grate seemed to be the most nearly similar to the grate on Drain 3. Based on this type of grate and the length of the grate for Drain 3, a splash-over velocity of 6.2 fps was assumed. Calculations were made for all combinations of Q_a = 0.1, 0.2, 0.4, 0.6, 0.8 cfs; n = 0.015, 0.02; S = 0.005, 0.01, 0.02, 0.03, 0.04, 0.05, 0.06, 0.07, 0.08; and S_x = 0.01, 0.02, 0.03, 0.04, 0.05, 0.06, 0.07, 0.08. For each case, the efficiency (E_{HEC-12}) of the grate was calculated from HEC-12 and compared to the efficiency (E_{emp}) obtained from the empirical results with E_{emp} = Q from Equation 7.6 divided by Q_a. Any conditions which violated the limits of applicability in Section 7.5.4 were eliminated. The results are summarized in Table 7.2. For n = 0.020, except for S_x = 0.01, the averages of the calculated and measured results are very close to each other. However, as the standard deviation, maximum, and minimum show, some of the values had as much as a 11% difference from unity. For most of the cases with n = 0.015, HEC-12 predicts that the flow captured by the grate is much larger than the captured flow obtained from the experiments.

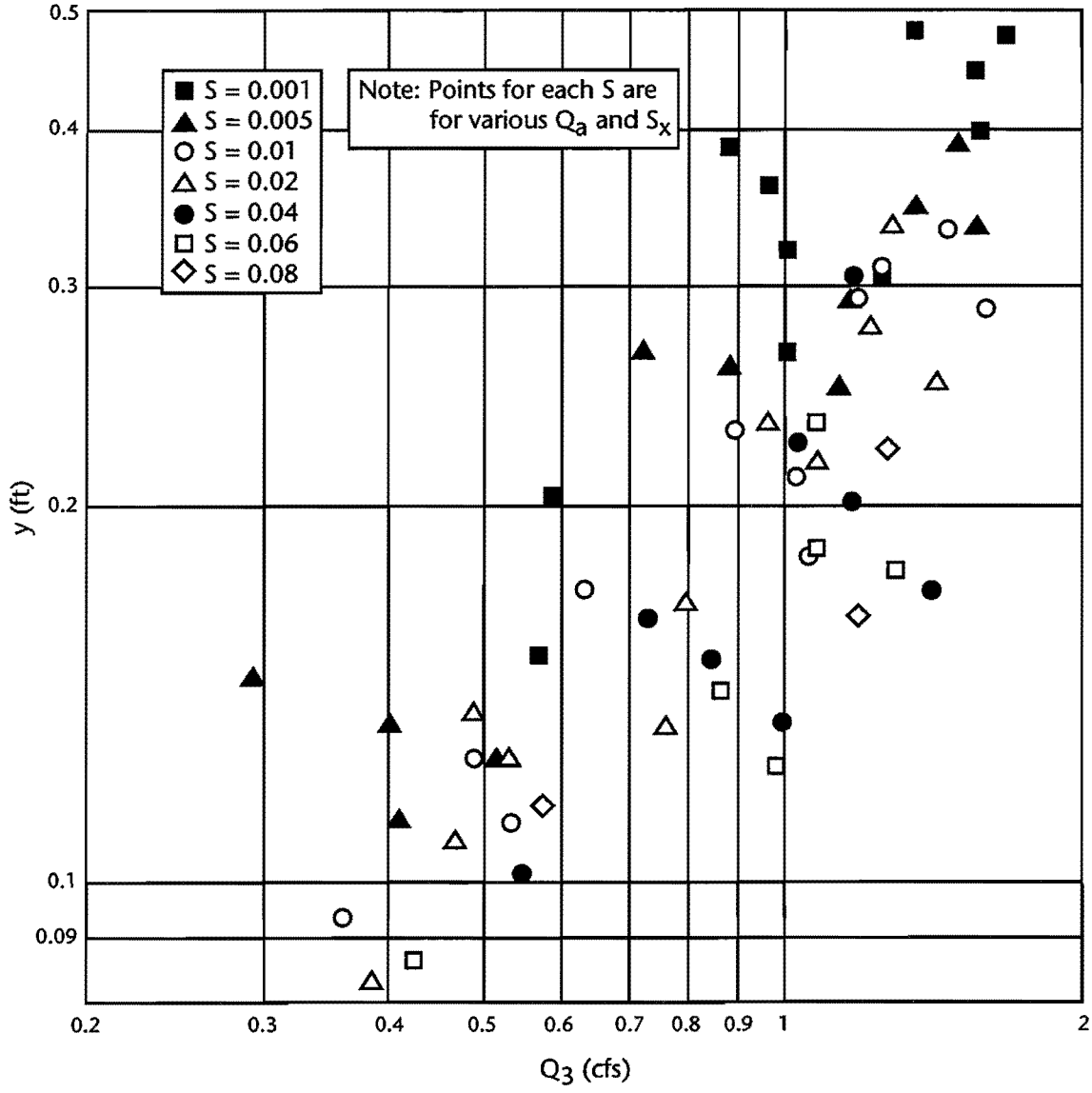

Figure 7.10 Results for Drain 3

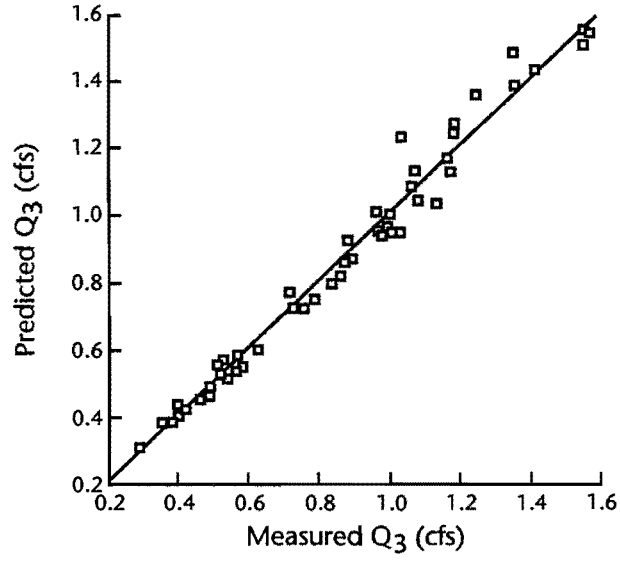

Figure 7.11 Drain 3 flows, measured and predicted from Equation 7.6

Table 7.2 Comparison of calculations from HEC-12 with empirical results for Drain 3

	$\frac{E_{HEC-12}}{E_{emp}}$							
	n=0.020				n=0.015			
S_x	Average	Standard Deviation	Maximum	Minimum	Average	Standard Deviation	Maximum	Minimum
0.01	0.87	0.055	0.98	0.79	1.13	0.072	1.29	1.01
0.02	0.98	0.027	1.03	0.92	1.27	0.049	1.36	1.18
0.03	1.01	0.026	1.06	0.96	1.32	0.050	1.40	1.22
0.04	1.02	0.040	1.08	0.93	1.33	0.066	1.43	1.19
0.05	1.02	0.054	1.09	0.91	1.32	0.081	1.44	1.16
0.06	1.01	0.064	1.10	0.88	1.30	0.091	1.43	1.13
0.07	0.99	0.068	1.07	0.86	1.28	0.096	1.42	1.10
0.08	0.97	0.072	1.06	0.84	1.26	0.098	1.40	1.08
Average	0.98	0.051			1.28	0.075		

CHAPTER 8. CONCLUSIONS FOR BRIDGE DECK DRAINS

This part of the study was concerned with the capacity of three types of bridge deck drains. The ultimate objective was to obtain predictive equations for the capacity of the drains, but a complementary objective was to gain an improved understanding of the hydraulics which control this capacity. To meet these objectives, experiments were conducted in a large laboratory facility constructed especially for this project. This facility represented one lane of a roadway and was built so that both the longitudinal and the cross slopes of the roadway could be easily changed. The surface of the roadway was covered with sand grains to produce a model Manning's n of 0.019. The details of the model are presented in Part I of this report.

Drain 1 was a 4-inch-by-6-inch scupper drain while Drains 2 and 3 were different sizes and types of grated-inlets drains. The two smaller drains (Drain 1 and Drain 2, Figure 7.4) were tested at full scale. Drain 3 (Figure 7.9) was tested at 3/4 scale. Information was previously available for circular scuppers but not for rectangular ones. Likewise, some information was previously available for grated inlets, but primarily for street drains which generally have larger inlet boxes and less restrictive piping systems following the boxes than is the case for bridge drains. That is, the previously available information on grated inlets is applicable primarily for situations where the inlet opening size and the grate itself normally control the capacity. Thus, for Drains 2 and 3, attention was given to investigating the effects of the inlets' boxes and the subsequent piping on the drain capacity. These drains were constructed of plexiglass so that the behavior of the flow inside the inlet box and subsequent piping could be observed. For all three drains, empirical equations were obtained for predicting the capacity for the flow conditions most likely to be encountered on bridges. There generally is not a need to have predictive equations for the higher flow conditions, so these conditions were not tested extensive enough to obtain such equations.

For each drain, many tests (74 for Drain 1, 99 for Drain 2, and 61 for Drain 3) were conducted for a variety of longitudinal slopes (S), cross slopes (S_x), and flow rates (Q_a) upstream of the drains. The graphs showing the capacity of the drains as a function of the upstream uniform flow depth generally showed a change in behavior at some values of depth and flow. From the previously published results for drains and from observing the behavior of the flow during the testing, it could be concluded that the data trend for the smaller depths and the smaller flows corresponded to weir-like behavior for the flow entering the inlets or possibly orifice control at the entrance to the drain piping for Drains 2 and 3. On the other hand, the behavior for larger depths and inlet flow rates corresponded to orifice control for the scupper drain and to back-pressure effects for the other two drains which were followed by piping systems. For the scupper, the change in behavior had to correspond to changing from weir to orifice flow since there is no piping below the scupper to create back-pressure effects. For the other two drains, the change in behavior presumably corresponded to back-pressure effects since visual observation of the flow in the plexiglass drain piping showed that the piping was full when the second type of behavior was obtained. Since the back-pressure effects existed primarily for flows beyond the normally expected range of flow on bridge decks, the testing program did not include enough flow conditions in this back-pressure range to obtain definitive predictive equations. Nevertheless, the testing did allow a reasonable determination of the limit of the range of low flow conditions. For each drain, predictive equations were obtained for the drain capacity for low flow and the limits of applicability for low flow were also specified.

The type of results obtained for the 4-inch-by-6-inch scupper drain are generally comparable to those presented by Chang and Johnson (1984) for 4-inch circular scupper drains. In both types of scuppers, there is a clear difference in the trend

of the results for low flows with weir-like behavior and for higher flows with orifice-like behavior. Because of the larger dimensions of the scupper drain studied in this project, the upper limit of weir-like behavior is for higher flow depths than for a 4-inch circular scupper. Equations 7.1 and 7.2 for the capacity of this rectangular scupper apply only to the zone of weir-like behavior. This zone is limited by Equation 7.3.

An extensive set of preliminary tests was done for Drain 2 to investigate the possible effects of piping below the inlet box on the drain capacity. Different configurations of pipes and elbows in the pipes were tested. The results of these experiments indicated that the most important aspect of the piping was the distance from the inlet to the first elbow; the capacity of the inlet decreased as this distance decreased even when the overall hydraulic conditions were the same (i.e., the same vertical distance to the pipe outlet, the same length of pipe, and the same number of elbows). Thus, the remaining tests were done with the minimum distance between the box and the elbow, namely 12 inches. The control section apparently is at the grate itself for low flows since the capacity (Equation 7.4) is independent of the piping system for these flows. The limit of applicability of this equation is given by Equation 7.5 or is a maximum drain flow of 0.8 cfs (whichever is more restrictive). For higher flows, the control is apparently the back pressure from the piping system. The vertical distance between the inlet box and the elbow has a big influence on the capacity of the drain for higher flows. Again, as for Drain 1, there were not enough data points to obtain flow equations for higher flows.

The analysis of the results for Drain 3 shows that the hydraulic characteristics are similar to those for Drain 2. Drain 3 also had two different types of behavior depending primarily on the flow depth in the gutter, i.e., low flow behavior for low depths and back-pressure effects for higher depths and higher flow rates. Equation 7.6 applies only for low flows, limited by Equation 7.7 or a drain flow of 1.6 cfs (whichever is more restrictive). For the case where the back-pressure effect was important, it was not possible to find a regression equation as a result of few data points.

The ranges of expected design flows fell into the low flow range for all three drains. Also, the transition from low flow conditions to back pressure effects for Drains 2 and 3 may take place at higher flow conditions in the field than in these laboratory tests. In the field, the bottom end of the drain piping is normally much farther below the bridge deck than was the case in the laboratory. This extra vertical drop of the piping may influence the flow conditions for the transition from low flow to back-pressure effects.

REFERENCES

Bauer, W. J., and D. C. Woo, "Hydraulic Design of Depressed Curb-Opening Inlets," *Highway Research Record*, No. 58, 1964, pp 61-80.

Bos, M. G., *Discharge Measurement Structures*, Delft Hydraulics Laboratory, Publication No. 161, Delft, The Netherlands, 1970, pp 168, 464.

Brater, E. F., and H. W. King, *Handbook of Hydraulics*, Sixth Edition, McGraw-Hill, New York, 1976, pp 2.85-2.86, 2.55-2.64.

Conner, N. W., "Design and Capacity of Gutter Inlets," *Bulletin No. 30*, North Carolina State College, Engineering Experiment Station (as cited by Izzard, 1950), 1945.

Corps of Engineers, "Airfield Drainage Structure Investigations," *Hydraulic Laboratory Report No. 54*, U.S. Army Corps of Engineers, St. Paul District Sub-Office (as cited by Izzard, 1950), 1949.

Davis, C. V., and K. E. Sorenson, *Handbook of Applied Hydraulics*, Third Edition, McGraw-Hill, New York, 1969, pp 2.25-2.27.

Forbes, H. J. C., "Capacity of Lateral Stormwater Inlets," *The Civil Engineer in South Africa*, Vol 18, No. 9, 1976, pp 195-205.

Guillou, J. C., "Description of Apparatus and Procedure for Testing Flow in Gutters and Storm Drain Inlets," *Surface Drainage of Highways*, Research Report 6-B, Highway Research Board, 1948, pp 5-8.

Henderson, F. M., *Open Channel Hydraulics*, MacMillan, New York, 1966, pp 493, 98, 126.

Ippen, A. T., "Free Surface Flow," *Engineering Hydraulics* (ed. H. Rouse), 1949, Wiley.

Izzard, C. F., "Hydraulics of Runoff from Developed Surfaces," *Proceedings*, Highway Research Board, Vol 26, 1946, pp 129-150.

Izzard, C. F., "Tentative Results on Capacity of Curb-Opening Inlets," *Highway Research Board*, Research Report No. 11-B, 1950, pp 36-54.

Izzard, C. F., "Simplified Method for Design of Curb-Opening Inlets," *Transportation Research Record*, No. 631, 1977, pp 39-46.

Johns Hopkins University, "The Design of Storm-Water Inlets." Report of the Storm Drainage Research Committee of the Storm Drainage Research Project, 1956, pp 143-181.

Johnson, F. L., and F. F. M. Chang, "Drainage of Highway Pavements," *Hydraulic Engineering Circular No. 12*, FHWA-TS-84-202, Federal Highway Administration, 1984, 136 pp.

Li, W. H., "Hydraulic Theory for Design of Storm-Water Inlets," *Proceedings*, 33rd Annual Meeting, Highway Research Board, 1954, pp 179-189.

Li, W. H., K. K. Sorteberg, and J. C. Geyer, "Hydraulic Behavior of Storm-Water Inlets. II. Flow into Curb-Opening Inlets," *Sewage and Industrial Wastes*, Vol 23, No. 6, 1951, pp 143-159.

Liggett, J. A., Discussion of "Hydrodynamics of Flow into Curb-Opening Inlets," by R. J. Wasley, *Proceedings*, Engineering Mechanics Division, ASCE, Vol 87, No. EM6, December 1961, pp 185-187.

McNown, J. S. , and Y. S. Yu, Discussion of "Hydrodynamics of Flow into Curb-Opening Inlets," by R. J. Wasley, *Proceedings*, Engineering Mechanics Division, ASCE, Vol 88, No. EM2, April 1962, pp. 153-156.

Reagan, D., and E. Friedrich, *Design Training Program*, Manual Course E, Level III, Texas Department of Highways, undated.

Roberson, J. A., J. J. Cassidy, and M. H. Chaudhry, *Hydraulic Engineering*, Houghton Mifflin, Boston, 1988, pp 410-411.

Roberson, J. A., and C. T. Crowe, *Engineering Fluid Mechanics*, Third Edition, Houghton Mifflin, New York, 1985, p 712.

Tapley, G. S., "Hydrodynamics of Model Storm Sewer Inlets Applied to Design," *Proceedings*, ASCE, March 1942, pp 375-409.

Tynes, K. A., "Hydraulics of Side-Channel Weirs For Regional Detention Basins," M.S. Thesis, Department of Civil Engineering, The University of Texas at Austin, 1989, pp 1-4, 26-62.

Wasley, R. J., "Hydrodynamics of Flow into Curb-Opening Inlets," *Technical Report No. 6*, Stanford University, 1960, 108 pp + appendices.

Wasley, R. J., "Hydrodynamics of Flow into Curb-Opening Inlets," *Proceedings*, Engineering Mechanics Division, ASCE, Vol 87, No. EM4, August 1961, pp 1-18.

Wasley, R. J., Closure to "Hydrodynamics of Flow into Curb-Opening Inlets," *Proceedings*, Engineering Mechanics Division, ASCE, Vol 88, No. EM3, June 1962, pp 157-160.

APPENDIX A. DATA FOR RECESSED CURB INLETS

The tables in this appendix summarize the data collected in the model study. All values directly measured are listed.

Each test condition was given a unique designation. Reading from left to right, the first symbol designates the efficiency: * means 100 percent efficiency; < means less than 100 percent efficiency. The first letter designates the type of transition: A = reverse curve; B = linear; C = reverse curve with 20% recessed slope. The first two digits give the size of the inlet opening in feet (prototype). The transverse pavement slope (S_x) in percent is given by the second two digits. The last two digits give the longitudinal gutter slope (S) in percent.

The definitions of variables from left to right for Tables A.1 through A.3 are as follows:

X-SECT = cross section at which the measurement was taken, with the distance measured in the downstream direction from the upstream end of the roadway model.

T = ponded width of flow upstream of the recessed curb inlet.

y_m = measured depth in the approach gutter.

y_c = calculated depth in the approach gutter.

I1 = depth of flow just upstream of the actual inlet opening on the recessed slope.

I2 = depth of flow just downstream of the actual inlet opening on the recessed slope.

Q_a = flow rate in the approach gutter.

Q = flow rate captured by the recessed curb inlet.

All of the values in Tables A.1 through A.3 are model values which have not been scaled to prototype conditions. Measurements at additional cross sections were sometimes taken. At these additional cross sections, only gutter depth and ponded width measurements were made. Blank entries within this appendix indicate no measurements were taken.

Table A.1 Data for reverse curve transitions with 30% recessed slope

Test No.	X-SECT	T (ft)	y_m (ft)	y_c (ft)	I1 (ft)	I2 (ft)	Q_a (cfs)	Q (cfs)
*A15010.5	32	10.5	0.098	0.114	0.25	0.15	0.635	0.635
*A15020.5	32	10.5	0.187	0.216	0.37	0.20	1.743	1.743
*A15040.5	29	8.8	0.375	0.360	0.58	0.18	3.421	3.421
*A150101	29	10.5	0.104	0.090	0.20	0.12	0.484	0.484
*A150201	27	9.0	0.164	0.175	0.33	0.20	1.411	1.411
<A150201	28.5	10.5	0.192	0.212	0.37	0.32	2.363	2.025
*A150401	28.5	7.8	0.292	0.307	0.47	0.27	3.169	3.169
<A150401	25	9.0	0.356	0.351	0.85	0.40	4.517	4.143
	63.0	3.5	0.241					
*A150202	24.5	6.0	0.122	0.116	0.25	0.15	0.663	0.663
<A150202	24.5	8.0	0.158	0.160	0.30	0.22	1.570	1.331
	20.5	8.0	0.165					
<A150402	24.0	8.0	0.312	0.295			4.036	3.329
	32.0	8.0	0.307					
	63.0	4.0	0.168					
*A150602	32.0	6.0	0.364	0.329	0.55	0.27	3.595	3.595
	24.0	6.0	0.331					
	29.0	6.0	0.337					
<A150602	29.0	7.0	0.375	0.380	0.60	0.45	5.246	4.843
	63.0	3.0	0.155					
<A150105	29.0	10.5	0.060	0.069	0.15	0.10	0.525	0.250
	63.0	6.0	0.058					
*A150205	29.0	4.0	0.064	0.066	0.15	0.05	0.238	0.238
<A150205	29.0	4.5	0.092	0.097	0.20	0.10	0.648	0.508
	63.0	2.5	0.054					
<A150205	29.0	7.5	0.132	0.138	0.25	0.20	1.667	0.988
	63.0	4.5	0.098					
*A150405	29.0	3.5	0.131	0.141			0.881	0.881
<A150405	24.5	5.3	0.181	0.193	0.35	0.25	2.063	1.660
	29.0	5.3	0.184					
	63.0	3.0	0.096					
*A150605	29.0	3.5	0.224	0.215	0.35	0.00	1.818	1.818
	24.5	3.5	0.223					
<A150605	25.0	5.0	0.267	0.273	0.50	0.37	3.442	2.882
	29.0	5.0	0.277					
	63.0	3.0	0.133					
<A15017.5	25.0	10.5	0.075	0.073	0.15	0.05	0.754	0.245
	63.0	8.0	0.061					
<A15027.5	29.0	6.5	0.067	0.068	0.15	0.00	0.307	0.221
	63.0	2.0	0.036					
<A15027.5	32.0	8.0	0.106	0.102	0.20	0.10	0.927	0.555
	63.0	3.5	0.069					
*A15047.5	32.0	2.5	0.106	0.107	0.20	0.00	0.521	0.521

Test No.	X-SECT	T (ft)	y_m (ft)	y_c (ft)	I1 (ft)	I2 (ft)	Q_a (cfs)	Q (cfs)
<A15047.5	28.0	4.5	0.176		0.25	0.15	1.871	1.281
	32.0	4.5	0.173					
	63.0	3.5	0.089					
<A15047.5	28.0	5.0	0.230	0.213	0.35	0.25	3.245	1.764
	63.0	4.3	0.143					
	63.0	5.0	0.196					
*A15067.5	28.0	2.5	0.165	0.166			1.123	1.123
<A15067.5	28.0	3.3	0.201	0.204			1.943	1.663
	63.0	2.0	0.104					
<A15067.5	28.0	4.0	0.220	0.221			2.413	1.911
	63.0	2.8	0.118					
	63.0	5.0	0.172					
*A10040.1	32.0	9.6	0.360	0.454	0.50	0.30	2.838	2.838
*A10010.5	32.0	9.0	0.086	0.088	0.20	0.05	0.321	0.321
*A10020.5	32.0	9.5	0.181	0.195	0.37	0.20	1.326	1.326
*A10040.5	32.0	8.0	0.313	0.323	0.50	0.30	2.557	2.557
<A10040.5	32.0	9.4	0.360	0.369	0.50	0.40	3.639	3.349
	63.0	3.5	0.132					
*A100101	32.0	8.5	0.086	0.073	0.20	0.10	0.273	0.273
<A100101	32.0	10.5	0.101	0.097			0.590	0.545
*A100201	32.0	7.5	0.156	0.170	0.30	0.20	1.307	1.307
	25.5	7.5	0.158					
<A100201	25.5	10.0	0.197	0.200	0.35	0.30	2.005	1.632
	63.0	4.5	0.117					
*A100401	32.0	6.5	0.273	0.259	0.45	0.25	2.006	2.006
<A100401	32.0	7.5	0.310	0.296	0.45	0.35	2.870	2.650
	63.0	2.5	0.110					
*A100102	32.0	6.0	0.080	0.058	0.15	0.10	0.210	0.210
<A100102	32.0	10.5	0.122	0.098	0.20	0.20	0.846	0.530
	63.0	6.5	0.079					
*A100202	25.5	5.5	0.111	0.113	0.25	0.15	0.624	0.624
<A100202	31.0	8.0	0.141	0.146	0.30	0.25	1.242	0.991
	63.0	4.0	0.086					
<A100202	31.0	10.5	0.182	0.199	0.35	0.30	2.812	1.486
	63.0	7.0	0.162					
*A100402	31.0	5.0	0.193	0.204	0.40	0.20	1.504	1.504
	25.5	5.0	0.198					
<A100402	31.0	6.5	0.244	0.251	0.40	0.35	2.624	2.150
	63.0	3.3	0.138					
<A100402	31.5	8.5	0.317	0.325	0.50	0.50	5.218	3.094
	63.0	5.0	0.203					
*A100602	31.0	5.0	0.283	0.281	0.45	0.30	2.357	2.357
<A100602	31.0	5.5	0.338	0.332	0.55	0.44	3.661	3.159
	63.0	2.5	0.163					
<A100105	31.0	10.5	0.074	0.076	0.15	0.10	0.676	0.298
	63.0	7.0	0.059					

Test No.	X-SECT	T (ft)	y_m (ft)	y_c (ft)	I1 (ft)	I2 (ft)	Q_a (cfs)	Q (cfs)
*A100205	31.0	3.5	0.069	0.074	0.15	0.05	0.316	0.316
<A100205	31.0	6.5	0.129	0.127	0.25	0.20	1.339	0.701
	63.0	3.0	0.060					
*A100405	28.5	3.5	0.120	0.129	0.25	0.10	0.699	0.699
<A100405	28.0	5.0	0.176	0.188	0.30	0.30	1.902	1.288
	63.0	4.0	0.099					
<A100405	28.0	6.0	0.262	0.245	0.40	0.35	3.881	1.882
	63.0	5.0	0.181					
*A100605	28.5	3.0	0.179	0.188	0.30	0.20	1.268	1.268
<A100605	28.5	4.5	0.239	0.251	0.40	0.40	2.749	2.078
	63.0	3.3	0.140					
<A10017.5	31.0	10.5	0.059	0.055	0.10	0.05	0.346	0.126
	63.0	6.0	0.046					
<A10027.5	32.0	8.3	0.168	0.152	0.25	0.20	2.647	0.778
	63.0	7.0	0.139					
*A10047.5	32.0	2.4	0.103	0.098	0.20	0.05	0.412	0.412
<A10047.5	32.0	4.5	0.175	0.179	0.30	0.20	2.047	1.177
	63.0	4.0	0.107					
<A10047.5	31.5	5.0	0.220	0.201	0.35	0.25	2.799	1.169
	63.0	3.5	0.142					
<A10047.5	31.5	6.0	0.288	0.252	0.40	0.30	5.118	1.683
	63.0	5.0	0.190					
*A10067.5	32.0	2.5	0.146	0.151	0.25	0.10	0.873	0.873
<A10067.5	32.0	3.5	0.207	0.206	0.40	0.30	1.990	1.368
	63.0	2.5	0.119					
<A10067.5	29.0	4.5	0.251	0.256	0.45	0.35	3.536	1.875
	63.0	4.5	0.152					
*A05020.1	31.5	10.0	0.201	0.223	0.35	0.20	0.856	0.856
*A05040.1	31.5	8.2	0.319	0.393	0.50	0.30	1.932	1.932
*A05020.5	31.5	8.5	0.166	0.162	0.30	0.25	0.810	0.810
<A05020.5	31.5	10.5	0.201	0.193	0.35	0.30	1.295	1.108
	63.0	3.2	0.075					
*A05040.5	31.5	6.5	0.261	0.262	0.40	0.30	1.462	1.462
<A05040.5	31.5	7.5	0.296	0.292	0.50	0.40	1.958	1.801
	63.0	2.5	0.880					
<A05040.5	31.5	9.3	0.360	0.357	0.50	0.45	3.343	2.493
	63.0	5.0	0.174					
*A05060.5	31.5	6.0	0.352	0.348	0.50	0.35	2.079	2.079
<A050101	31.5	10.5	0.126	0.107	0.20	0.20	0.763	0.525
	63.0	6.0	0.073					
*A050201	31.5	6.5	0.152	0.133	0.25	0.20	0.677	0.677
<A050201	31.5	8.0	0.172	0.151	0.30	0.25	0.951	0.839
	63.0	2.5	0.064					
<A050201	31.5	9.3	0.200	0.177	0.30	0.30	1.455	1.094
	63.0	4.5	0.101					
*A050401	31.5	5.0	0.222	0.204	0.35	0.25	1.069	1.069

Test No.	X-SECT	T (ft)	y_m (ft)	y_c (ft)	I1 (ft)	I2 (ft)	Q_a (cfs)	Q (cfs)
<A050401	31.5	6.5	0.279	0.257	0.40	0.40	1.958	1.642
	63.0	3.3	0.112					
<A050401	31.5	8.5	0.361	0.325	0.50	0.50	3.691	2.404
	63.0	5.0	0.205					
*A050601	31.5	4.7	0.305	0.288	0.40	0.30	1.777	1.777
<A050601	31.5	5.7	0.370	0.337	0.50	0.45	2.711	2.327
	63.0	2.5	0.137					
<A050102	31.5	9.0	0.103	0.084	0.20	0.20	0.559	0.303
<A050102	31.5	10.5	0.111	0.106	0.20	0.20	1.036	0.491
*A050202	31.5	4.5	0.110	0.098	0.20	0.15	0.424	0.424
<A050202	31.5	6.6	0.142	0.134	0.25	0.20	0.982	0.697
	63	4.0	0.076					
<A050202	31.5	8.5	0.162	0.164	0.30	0.30	1.676	0.954
	63	4.5	0.098					
*A050402	31.5	4.0	0.166	0.164	0.30	0.20	0.840	0.840
<A050402	31.5	5.4	0.219	0.217	0.35	0.30	1.762	1.315
	63	3.0	0.118					
<A050402	31.5	6.5	0.262	0.251	0.40	0.40	2.618	1.472
	63.0	4.0	0.145					
<A050402	31.5	8.0	0.292	0.295	0.50	0.50	4.036	1.945
	63.0	5.0	0.192					
*A050602	31.5	3.8	0.229	0.230	0.40	0.30	1.372	1.372
<A050602	31.5	4.5	0.276	0.270	0.45	0.40	2.122	1.688
	63.0	2.0	0.132					
<A050602	31.5	5.2	0.332	0.310	0.50	0.50	3.054	2.041
	63.0	3.2	0.194					
<A050602	31.5	5.6	0.335	0.320	0.50	0.50	3.321	2.106
	63.0	4.0	0.202					
<A050105	31.5	5.5	0.053	0.053	0.10	0.05	0.265	0.115
	63.0	3.5	0.027					
<A050105	31.5	10.5	0.090	0.095	0.20	0.20	1.236	0.307
	63.0	8.0	0.070					
<A050205	31.5	4.5	0.092	0.096	0.20	0.15	0.635	0.340
	63.0	3.2	0.049					
<A050205	31.5	6.4	0.129	0.133	0.25	0.20	1.524	0.556
	63.0	4.5	0.096					
<A050205	31.5	10.0	0.184	0.175	0.30	0.30	3.155	0.647
	63.0	7.3	0.150					
*A050405	31.5	2.2	0.093	0.093	0.30	0.05	0.294	0.294
<A050405	31.5	4.0	0.155	0.165	0.30	0.20	1.343	0.909
	63.0	3.5	0.084					
*A050605	31.5	2.4	0.140	0.147	0.25	0.20	0.667	0.667
<A050605	31.5	3.6	0.232	0.226	0.40	0.40	2.074	0.996
	63.0	3.5	0.123					
<A050605	31.5	5.3	0.277	0.281	0.50	0.50	3.714	1.019
	63.0	5.3	0.181					

Test No.	X-SECT	T (ft)	y_m (ft)	y_c (ft)	I1 (ft)	I2 (ft)	Q_a (cfs)	Q (cfs)
<A05027.5	31.5	5.0	0.099	0.102	0.20	0.10	0.917	0.342
	63.0	3.5	0.066					
<A05027.5	31.5	8.0	0.159	0.154	0.25	0.20	2.761	0.536
	63.0	6.0	0.123					
<A05027.5	31.5	10.5	0.177	0.168	0.30	0.20	3.485	0.555
	63.0	7.0	0.139					
<A05047.5	31.5	3.5	0.143	0.149	0.25	0.20	1.248	0.626
	63.0	3.0	0.082					

Table A.2 Data for linear transitions

Test No.	X-SECT	T (ft)	y_m (ft)	y_c (ft)	I1 (ft)	I2 (ft)	Q_a (cfs)	Q (cfs)
*B150201	31.5	10.0	0.194	0.177	0.30	0.20	1.453	1.453
*B150401	31.5	8.0	0.347	0.312	0.45	0.20	3.31	3.327
*B150202	31.5	6.5	0.143	0.129	0.30	0.15	0.891	0.891
<B150202	31.5	8.2	0.173	0.166	0.30	0.20	1.74	1.468
	63.0	4.0	0.091					
<B150202	31.5	10.0	0.192	0.184	0.30	0.30	2.27	1.665
	63.0	5.5	0.110					
*B150402	31.5	6.0	0.254	0.232	0.35	0.10	2.127	2.127
<B150402	31.5	7.0	0.285	0.272	0.40	0.30	3.24	3.051
	63.0	2.7	0.107					
<B150402	31.5	8.0	0.310	0.303	0.40	0.40	4.33	3.720
	63.0	4.5	0.141					
*B150204	31.5	3.5	0.080	0.077	0.15	0.05	0.313	0.313
<B150204	31.5	7.0	0.137	0.140	0.25	0.15	1.56	1.082
	63.0	4.5	0.087					
<B150204	31.5	9.2	0.185	0.179	0.30	0.25	2.99	1.526
	63.0	6.5	0.146					
<B150204	31.5	10.5	0.194	0.187	0.30	0.30	3.36	1.618
	63.0	7.7	0.158					
*B150404	31.5	4.0	0.163	0.166	0.25	0.05	1.222	1.222
<B150404	31.5	7.0	0.273	0.265	0.35	0.40	4.28	2.834
	63.0	5.0	0.144					

Table A.3 Data for reverse curve transitions with 20% recessed slope

Test No.	X-SECT	T (ft)	y_m (ft)	y_c (ft)	I1 (ft)	I2 (ft)	Q_a (cfs)	Q (cfs)
*C150401	31.5	8.0	0.326	0.297	0.45	0.20	2.889	3.001
<C150401	31.5	9.0	0.376	0.340	0.50	0.30	4.149	1.892
	63.0	2.5	0.153					
*C150202	31.5	6.0	0.131	0.126	0.25	0.05	0.834	0.834
<C150202	31.5	9.5	0.167	0.169	0.30	0.25	1.814	1.413
	63.0	4.0	0.103					
<C150402	31.5	7.0	0.264	0.261	0.45	0.30	0.000	2.718
	63.0	2.5	0.123					
<C150402	31.5	8.0	0.290	0.298			4.117	3.262
	63.0	4.0	0.155					
*C150402	31.5	5.5	0.228	0.225	0.35	0.15	1.949	1.892
<C150402	31.5	7.5	0.274	0.284	0.50	0.30	3.632	2.984
	63.0	3.0	0.152					
	63.0	4.5	0.155					
*C150204	31.5	3.5	0.078	0.079	0.15	0.05	0.344	0.344
<C150204	31.5	6.5	0.127	0.134	0.25	0.10	1.377	0.851
	63.0	3.5	0.090					
<C150204	31.5	8.5	0.172	0.174	0.30	0.15	2.785	1.320
	63.0	6.0	0.142					
*C150404	31.5	3.5	0.152	0.162	0.25	0.05	1.143	1.104
<C150404	31.5	6.0	0.220	0.236	0.50	0.35	3.127	2.170
	63.0	4.0	0.128					
<C150404	31.5	6.5	0.268	0.275	0.45	0.40	4.734	2.865
	63.0	5.0	0.182					

Table A.4 Data for field tests (100% efficiency)

Test	L ft	S	S_x	Q cfs	qL cfs/ft	y ft	n	Fr
1	10.1	0.023	0.023	1.66	0.059	0.178	0.022	1.4
2	15.1	0.040	0.041	2.54	0.077	0.208	0.016	2.6
3	10.2	0.004	0.032	3.03	0.108	0.344	0.021	0.7
4	10.1	0.023	0.044	2.21	0.079	0.208	0.013	2.4
5	10.0	0.027	0.033	0.87	0.031	0.146	0.019	1.7
6	9.8	0.129	0.040	2.01	0.072	0.156	0.018	4.1
7	10.0	0.040	0.043	3.15	0.113	0.250	0.021	2.1
8	10.0	0.027	0.033	0.87	0.031	0.146	0.019	1.7
9	10.1	0.121	0.020	0.87	0.031	0.098	0.023	2.9
A	10.0	0.026	0.028	0.87	0.031	0.144	0.021	1.5
B	14.9	0.047	0.020	1.02	0.031	0.119	0.020	2.1
C	9.8	0.0210	0.045	1.33	0.048	0.214	0.022	1.4
D	15.2	0.0304	0.069	2.99	0.090	0.269	0.014	2.7

APPENDIX B. DATA FOR BRIDGE DECK DRAINS

The tables in this appendix summarize the data collected in the model study for bridge deck drains. All values directly measured are listed.

The definitions of variables for Tables B.1 through B.3 are as follows:

S = longitudinal gutter slope
Sx = transverse pavement slope
T us = ponded width of flow upstream of the drain
y us = measured depth in the approach gutter
T ds = ponded width of flow downstream of the drain
y ds = measured depth downstream of the drain
Qa = flow rate in the approach gutter
Q1 = flow rate captured by Drain 1
Q2 = flow rate captured by Drain 2
Q3 = flow rate captured by Drain 3
Qiw = carryover flow rate (iw = inside weir)

For Drains 2 and 3 the flows entering the drain (Q2 and Q3) were not measured directly. Instead, they were calculated as the difference between Qa and Qiw:

$$Q2 = Qa - Qiw$$
$$Q3 = Qa - Qiw$$

All of the values in Tables B.1 through B.3 are model values which have not been scaled to prototype conditions. Blank entries within this appendix indicate no measurements were taken.

Table B.1 Summary of model data for Drain 1

Test No.	S	Sx	T us (ft)	y us (ft)	T ds (ft)	y ds (ft)	Qa (cfs)	Q1 (cfs)	Qiw (cfs)
1	0.001	0.01	7.0	0.097	7.0	0.089	0.359	0.084	0.286
2	0.001	0.01	5.7	0.074	5.0	0.068	0.338	0.053	0.124
3	0.001	0.01	5.5	0.079	5.0	0.070	0.149	0.055	0.130
4	0.001	0.01	7.0	0.094	6.8	0.085	0.288	0.079	0.248
5	0.001	0.01		0.091		0.084	0.281	0.072	0.230
6	0.001	0.02	5.6	0.114	5.0	0.094	0.281	0.109	0.194
7	0.001	0.04	3.4	0.137	2.8	0.101	0.281	0.148	0.148
8	0.001	0.06	2.8	0.154	1.8	0.105	0.281	0.173	0.129
9	0.001	0.08	2.4	0.175	1.4	0.101	0.281	0.195	0.105
10	0.001	0.02	3.5	0.081	2.6	0.069	0.121	0.057	0.073
11	0.001	0.01	5.5	0.064	5.0	0.065	0.121	0.044	0.096
12	0.001	0.04	2.8	0.104	1.6	0.068	0.121	0.084	0.056
13	0.001	0.06	2.2	0.117	1.1	0.064	0.121	0.095	0.037
14	0.001	0.08	1.9	0.129	0.8	0.055	0.121	0.104	0.025
15	0.001	0.08	2.5	0.189	1.6	0.116	0.354	0.225	0.139
16	0.001	0.08	3.5	0.262	2.5	0.185	0.890	0.392	0.463
17	0.001	0.08	5.0	0.373	4.0	0.302	2.028	0.577	1.529
18	0.001	0.02	6.3	0.129	5.8	0.120	0.482	0.149	0.346
19	0.001	0.02	8.7	0.165	8.0	0.155	1.000	0.232	0.733
20	0.001	0.04	6.0	0.213	4.5	0.175	0.991	0.322	0.649
21	0.001	0.04	6.0	0.232	5.0	0.197	1.230	0.362	0.850
22	0.001	0.04	8.5	0.324	8.0	0.292	2.903	0.534	2.319
23	0.001	0.06	6.6	0.377	5.7	0.329	2.903	0.573	2.319
24	0.001	0.06	4.6	0.245	3.5	0.195	1.019	0.377	0.621
25	0.005	0.01	7.6	0.089	7.0	0.070	0.444	0.076	0.329
26	0.005	0.01	7.5	0.089	7.5	0.068	0.429	0.077	0.318
27	0.005	0.02	5.0	0.108	4.0	0.079	0.321	0.109	0.239
28	0.005	0.02	7.0	0.148	7.0	0.115	0.835	0.187	0.618
29	0.005	0.04	3.3	0.128	2.6	0.080	0.264	0.136	0.154
30	0.005	0.04	5.8	0.237	5.0	0.191	1.443	0.361	1.090
31	0.005	0.06	3.0	0.183	2.0	0.120	0.511	0.240	0.274
32	0.005	0.06	5.5	0.337	4.7	0.274	2.090	0.453	1.704
33	0.005	0.08	4.6	0.372	4.0	0.301	2.090	0.459	1.682
34	0.010	0.01	8.5	0.078	8.0	0.072	0.517	0.087	0.437
35	0.010	0.01	6.0	0.066	5.8	0.054	0.201	0.050	0.180
36	0.010	0.02	3.8	0.086	3.8	0.072	0.268	0.091	0.200
37	0.010	0.04	3.0	0.134	2.5	0.099	0.407	0.167	0.244
38	0.010	0.04	5.8	0.215	5.4	0.210	1.765	0.360	1.443
39	0.010	0.06	3.3	0.191	2.6	0.141	0.714	0.285	0.403
40	0.010	0.06	4.4	0.249	4.1	0.227	1.646	0.383	1.351

Test No.	S	Sx	T us (ft)	y us (ft)	T ds (ft)	y ds (ft)	Qa (cfs)	Q1 (cfs)	Qiw (cfs)
41	0.010	0.08	4.5	0.318	4.0	0.285	2.300	0.442	1.889
42	0.010	0.08	2.9	0.213	2.0	0.159	0.681	0.321	0.447
43	0.020	0.01	8.4	0.095	8.0	0.099	1.019	0.149	0.940
44	0.020	0.01	6.5	0.071	6.5	0.068	0.420	0.081	0.357
45	0.020	0.02	5.2	0.101	5.0	0.098	0.674	0.155	0.505
46	0.020	0.02	6.0	0.123	5.8	0.123	1.084	0.216	0.853
47	0.020	0.04	6.0	0.240	6.0	0.254	2.880	0.276	2.499
48	0.020	0.04	2.7	0.106	1.9	0.085	0.349	0.155	0.208
49	0.020	0.06	2.9	0.158	2.1	0.140	0.816	0.284	0.503
50	0.020	0.06	4.3	0.258	4.1	0.259	2.261	0.359	1.959
51	0.020	0.08	3.6	0.296	3.2	0.286	2.462	0.387	2.104
52	0.020	0.08	1.7	0.128	1.1	0.072	0.281	0.190	0.111
53	0.040	0.01	6.8	0.064	6.0	0.063	0.367	0.072	0.302
54	0.040	0.02	4.0	0.089	4.0	0.090	0.522	0.131	0.384
55	0.040	0.02	4.5	0.103	4.2	0.108	0.784	0.168	0.588
56	0.040	0.04	2.4	0.091	1.9	0.080	0.315	0.139	0.186
57	0.040	0.04	4.7	0.192	4.5	0.203	1.915	0.275	1.682
58	0.040	0.06	2.5	0.160	2.1	0.144	0.901	0.237	0.636
59	0.040	0.06	2.6	0.161	2.0	0.144	0.746	0.238	0.764
60	0.060	0.01	9.0	0.086	8.3	0.091	0.925	0.131	0.754
61	0.060	0.01	7.0	0.060	6.0	0.059	0.288	0.066	0.237
62	0.060	0.02	4.3	0.100	4.0	0.108	0.748	0.170	0.704
63	0.060	0.02	4.8	0.122	4.3	0.129	1.165	0.186	0.928
64	0.060	0.04	4.2	0.185	4.0	0.187	1.812	0.240	1.591
65	0.060	0.04	2.2	0.090	1.6	0.070	0.281	0.132	0.159
66	0.001	0.02		0.056		0.042	0.034	0.025	
67	0.001	0.02		0.069		0.045	0.058	0.042	
68	0.001	0.06		0.073		0.001	0.033	0.033	
69	0.020	0.01		0.032		0.026	0.035	0.012	
70	0.040	0.01		0.034		0.033	0.068	0.023	
71	0.060	0.01	5.5	0.041	4.0	0.035		0.035	0.100
72	0.060	0.01	2.4	0.029	1.8	0.028		0.020	0.041

Table B.2 Summary of model data for Drain 2

Test No.	S	Sx	T us (ft)	y us (ft)	T ds (ft)	y ds (ft)	Qa (cfs)	Qiw (cfs)	Configu-ration
1	0.001	0.08	5.0	0.475	3.2	0.241	2.305	0.720	A
2	0.001	0.08	5.0	0.469	4.0	0.299	2.296	1.341	B
3	0.001	0.08	4.6	0.411	3.2	0.271	1.982	1.086	B
4	0.001	0.06	5.5	0.360	4.4	0.224	1.782	0.894	B
5	0.001	0.06	6.3	0.417	5.1	0.288	2.569	1.581	B
6	0.001	0.06	6.0	0.397	4.9	0.265	2.301	1.356	B
7	0.001	0.08	5.0	0.433	4.2	0.298	2.301	1.356	B
8	0.001	0.08	5.0	0.418	3.0	0.205	2.010	0.603	A
9	0.001	0.08	5.3	0.441	3.5	0.239	2.305	0.842	A
10	0.001	0.06	6.2	0.401	4.6	0.226	2.305	0.913	A
11	0.001	0.06	5.8	0.370	4.0	0.183	1.787	0.544	A
12	0.001	0.06	6.4	0.421	4.8	0.249	2.562	1.103	A
13	0.001	0.06	5.5	0.376	3.5	0.200	1.819	0.674	C
14	0.001	0.06	6.2	0.409	4.5	0.250	2.350	1.159	C
15	0.001	0.06	6.4	0.423	4.9	0.266	2.581	1.346	C
16	0.001	0.08	5.0	0.423	3.4	0.235	1.967	0.803	C
17	0.001	0.08	5.3	0.450	3.7	0.272	2.338	1.141	C
18	0.001	0.06	5.7	0.364	3.5	0.176	1.771	0.492	D
19	0.001	0.08	5.0	0.422	3.0	0.187	1.996	0.484	D
20	0.001	0.08	5.3	0.444	3.0	0.225	2.288	0.713	D
21	0.001	0.06	6.1	0.401	4.2	0.229	2.288	0.861	D
22	0.001	0.06	6.5	0.419	4.6	0.246	2.607	1.061	D
23	0.001	0.06	6	0.363	4.2	0.222	1.727	0.764	E
24	0.001	0.08	5.2	0.420	4.0	0.268	2.010	1.040	E
25	0.001	0.08	5.4	0.445	3.9	0.291	2.292	1.280	E
26	0.001	0.06	6.3	0.399	5.0	0.273	2.292	1.267	E
27	0.001	0.06	6.6	0.416	5.5	0.289	2.566	1.519	E
28	0.001	0.06	5.8	0.385	3.6	0.226	1.705	0.737	F
29	0.001	0.08	5.3	0.455	3.3	0.284	1.991	0.991	F
30	0.001	0.08	5.8	0.489	4.0	0.330	2.451	1.390	F
31	0.001	0.06	6.3	0.435	4.5	0.294	2.451	1.394	F
32	0.001	0.06	6.4	0.445	5.1	0.306	2.614	1.550	F
33	0.001	0.06	5.6	0.375	4.0	0.240	1.612	0.835	G
34	0.001	0.08	5.3	0.463	4.0	0.311	2.081	1.267	G
35	0.001	0.08	5.6	0.481	4.2	0.331	2.313	1.468	G
36	0.001	0.06	6.4	0.431	5.0	0.299	2.363	1.504	G
37	0.001	0.06	6.5	0.442	5.1	0.325	2.551	1.661	G
38	0.001	0.06	4.0	0.249	1.3	0.074	0.649	0.043	E
39	0.001	0.06	4.0	0.276	1.3	0.077	0.838	0.046	E
40	0.001	0.06	4.9	0.307	1.7	0.107	1.071	0.105	E
41	0.001	0.08	3.5	0.289	1.0	0.091	0.423	0.058	E

Test No.	S	Sx	T us (ft)	y us (ft)	T ds (ft)	y ds (ft)	Qa (cfs)	Qiw (cfs)	Configu-ration
42	0.001	0.08	3.2	0.323	1.2	0.108	0.950	0.064	E
43	0.001	0.06	4.0	0.230	1.4	0.084	0.635	0.043	A
44	0.001	0.06	4.2	0.254	1.5	0.089	0.757	0.057	A
45	0.001	0.06	4.8	0.280	2.2	0.132	1.048	0.194	A
46	0.001	0.08	2.8	0.226	1.0	0.077	0.520	0.042	A
47	0.001	0.08	3.5	0.289	1.4	0.115	0.923	0.103	A
48	0.001	0.06	4.0	0.283	1.0	0.077	0.601	0.028	G
49	0.001	0.06	4.5	0.311	1.5	0.104	0.796	0.072	G
50	0.001	0.08	3.3	0.316	1.0	0.092	0.725	0.060	G
51	0.001	0.08	3.3	0.305	1.0	0.090	0.435	0.053	G
52	0.001	0.08	4.2	0.371	2.0	0.176	1.011	0.304	G
53	0.001	0.04	5.0	0.264	1.3	0.071	0.785	0.035	G
54	0.001	0.02	6.5	0.190	2.3	0.071	0.416	0.077	G
55	0.005	0.01	6.5	0.118	3.5	0.057	0.590	0.083	G
56	0.005	0.01	7.5	0.135	6.0	0.078	0.590	0.146	G
57	0.005	0.02	5.5	0.157	2.3	0.062	0.572	0.078	G
58	0.005	0.02	5.8	0.165	2.7	0.081	0.572	0.104	G
59	0.005	0.04	4.2	0.210	1.3	0.073	0.821	0.056	G
60	0.005	0.04	4.6	0.225	2.0	0.100	0.927	0.157	G
61	0.005	0.06	3.0	0.211	1.0	0.075	0.636	0.050	G
62	0.005	0.06	3.5	0.241	1.2	0.078	0.866	0.060	G
63	0.005	0.06	4.1	0.275	2.8	0.172	1.201	0.418	G
64	0.005	0.08	2.2	0.210	0.9	0.071	0.460	0.047	G
65	0.005	0.08	3.0	0.266	1.2	0.102	0.746	0.090	G
66	0.010	0.01	7.3	0.114	6.9	0.062	0.537	0.161	G
67	0.010	0.02	5.2	0.133	2.0	0.058	0.493	0.075	G
68	0.010	0.02	5.6	0.152	2.8	0.078	0.760	0.142	G
69	0.010	0.02	5.8	0.159	3.3	0.085	0.855	0.181	G
70	0.010	0.04	3.3	0.158	1.0	0.052	0.572	0.041	G
71	0.010	0.04	3.7	0.185	1.2	0.060	0.760	0.047	G
72	0.010	0.06	3.1	0.207	1.1	0.072	0.601	0.056	G
73	0.010	0.06	3.3	0.239	1.8	0.133	0.938	0.244	G
74	0.010	0.08	2.1	0.190	0.9	0.072	0.519	0.053	G
75	0.010	0.08	2.9	0.244	1.3	0.110	0.920	0.123	G
76	0.020	0.01	6.5	0.113	6.5	0.059	0.602	0.133	G
77	0.020	0.02	4.2	0.129	2.1	0.059	0.594	0.080	G
78	0.020	0.02	5.1	0.145	3.4	0.080	0.793	0.152	G
79	0.020	0.04	2.6	0.133	0.9	0.050	0.400	0.038	G
80	0.020	0.04	3.3	0.166	1.2	0.063	0.771	0.053	G
81	0.020	0.04	4.1	0.206	3.4	0.145	1.322	0.597	G
82	0.020	0.06	2.0	0.147	0.9	0.059	0.414	0.041	G

Test No.	S	Sx	T us (ft)	y us (ft)	T ds (ft)	y ds (ft)	Qa (cfs)	Qiw (cfs)	Configu-ration
83	0.020	0.06	2.6	0.181	1.0	0.076	0.688	0.065	G
84	0.020	0.08	2.2	0.197	1.0	0.089	0.688	0.089	G
85	0.020	0.08	2.7	0.225	1.4	0.121	0.960	0.215	G
86	0.040	0.02	3.8	0.095	1.5	0.042	0.433	0.042	G
87	0.040	0.02	4.3	0.109	3.0	0.053	0.717	0.091	G
88	0.040	0.02	6.0	0.158	6.0	0.126	1.625	0.940	G
89	0.040	0.04	2.8	0.119	1.1	0.054	0.522	0.056	G
90	0.040	0.04	3.5	0.152	1.9	0.077	0.890	0.174	G
91	0.040	0.06	3.1	0.194	2.1	0.122	1.154	0.463	G
92	0.040	0.06	2.7	0.165	1.2	0.080	0.806	0.129	G
93	0.040	0.08	1.5	0.126	0.8	0.060	0.315	0.050	G
94	0.060	0.02	3.4	0.083	1.6	0.038	0.398	0.049	G
95	0.060	0.04	3.0	0.136	1.6	0.065	0.808	0.206	G
96	0.060	0.04	3.5	0.162	2.3	0.111	1.137	0.445	G
97	0.060	0.06	1.7	0.105	0.8	0.050	0.312	0.049	G
98	0.060	0.06	2.3	0.149	1.2	0.075	0.723	0.140	G
99	0.080	0.04	2.4	0.112	1.1	0.053	0.548	0.086	G
100	0.080	0.04	3.0	0.144	1.8	0.083	0.796	0.241	G
101	0.080	0.04	3.7	0.193	3.3	0.157	1.747	1.073	G

Table B.3 Summary of model data for Drain 3

Test No.	S	Sx	T us (ft)	y us (ft)	T ds (ft)	y ds (ft)	Qa (cfs)	Qiw (cfs)
1	0.001	0.02	5.5	0.153	1.6	0.048	0.315	0.028
2	0.001	0.02	6.4	0.192	3.9	0.087	0.638	0.144
3	0.001	0.02	8.0	0.223	5.6	0.114	0.922	0.310
4	0.001	0.04	5.5	0.270	2.2	0.106	0.923	0.154
5	0.001	0.04	6.3	0.327	4.7	0.188	1.498	0.681
6	0.001	0.04	4.5	0.213	0.9	0.045	0.517	0.021
7	0.001	0.06	3.5	0.238	0.0	0.000	0.476	0.000
8	0.001	0.06	4.1	0.293	1.3	0.082	0.824	0.062
9	0.001	0.08	2.8	0.244	0.0	0.000	0.433	0.000
10	0.001	0.08	3.3	0.308	1.3	0.106	0.761	0.097
11	0.005	0.01	6.0	0.111	4.5	0.053	0.281	0.083
12	0.005	0.01	6.5	0.119	5.0	0.059	0.376	0.125
13	0.005	0.02	3.5	0.118	1.1	0.034	0.223	0.028
14	0.005	0.02	4.2	0.130	1.7	0.049	0.312	0.036
15	0.005	0.04	2.4	0.122	0.0	0.000	0.142	0.000
16	0.005	0.04	3.8	0.192	1.1	0.051	0.583	0.028
17	0.005	0.06	2.7	0.191	0.0	0.000	0.429	0.000
18	0.005	0.06	3.1	0.216	0.5	0.000	0.587	0.010
19	0.005	0.06	3.7	0.249	1.4	0.090	0.862	0.101
20	0.005	0.06	4.5	0.293	3.0	0.180	1.281	0.553
21	0.005	0.08	2.1	0.196	0.0	0.000	0.354	0.000
22	0.005	0.08	2.8	0.254	1.0	0.079	0.709	0.043
23	0.010	0.01	5.1	0.096	3.2	0.042	0.243	0.068
24	0.010	0.01	5.6	0.108	5.2	0.054	0.393	0.134
25	0.010	0.02	3.8	0.114	1.4	0.038	0.268	0.030
26	0.010	0.02	5.3	0.158	3.5	0.075	0.713	0.192
27	0.010	0.04	2.8	0.137	0.0	0.000	0.309	0.000
28	0.010	0.04	3.4	0.162	0.9	0.038	0.527	0.023
29	0.010	0.04	4.9	0.228	3.1	0.126	1.183	0.408
30	0.010	0.06	3.8	0.258	2.5	0.154	1.183	0.468
31	0.010	0.06	2.4	0.167	0.0	0.000	0.440	0.000
32	0.010	0.08	2.4	0.216	0.9	0.062	0.630	0.050
33	0.010	0.08	2.6	0.230	1.2	0.091	0.727	0.114
34	0.020	0.01	5.0	0.078	4.0	0.039	0.257	0.071
35	0.020	0.02	3.5	0.091	1.2	0.031	0.257	0.030
36	0.020	0.02	4.3	0.104	2.1	0.048	0.450	0.078
37	0.020	0.04	2.4	0.104	0.0	0.000	0.239	0.000
38	0.020	0.04	2.9	0.124	0.8	0.031	0.400	0.013
39	0.020	0.06	2.5	0.156	0.6	0.033	0.541	0.012
40	0.020	0.06	3.0	0.185	1.3	0.079	0.793	0.099
41	0.020	0.08	2.1	0.163	0.6	0.038	0.491	0.018

Test No.	S	Sx	T us (ft)	y us (ft)	T ds (ft)	y ds (ft)	Qa (cfs)	Qiw (cfs)
42	0.020	0.08	2.5	0.202	1.3	0.106	0.779	0.183
43	0.020	0.08	3.1	0.247	2.2	0.189	1.288	0.655
44	0.040	0.02	3.2	0.083	1.4	0.035	0.306	0.042
45	0.040	0.02	4.3	0.107	2.3	0.058	0.635	0.148
46	0.040	0.02	5.7	0.145	5.2	0.101	1.219	0.533
47	0.040	0.04	2.1	0.094	0.6	0.025	0.268	0.012
48	0.040	0.04	2.6	0.113	0.8	0.032	0.433	0.023
49	0.040	0.06	1.9	0.120	0.0	0.000	0.356	0.000
50	0.040	0.06	2.3	0.149	0.8	0.050	0.623	0.049
51	0.040	0.08	2.0	0.163	1.0	0.079	0.623	0.116
52	0.040	0.08	2.9	0.237	2.3	0.180	1.423	0.850
53	0.060	0.02	2.8	0.076	1.1	0.034	0.243	0.036
54	0.060	0.02	4.0	0.104	2.0	0.052	0.613	0.133
55	0.060	0.04	2.4	0.113	0.8	0.036	0.454	0.031
56	0.060	0.04	3.0	0.146	1.6	0.077	0.809	0.177
57	0.060	0.06	2.1	0.144	0.9	0.056	0.601	0.073
58	0.060	0.06	2.9	0.192	2.2	0.128	1.122	0.597
59	0.080	0.04	2.0	0.095	0.7	0.031	0.303	0.023
60	0.080	0.04	2.7	0.138	1.4	0.069	0.752	0.169
61	0.080	0.04	3.8	0.194	3.7	0.158	1.733	1.111

APPENDIX C. PHOTOGRAPHS

Figure C.1 Recessed curb inlet

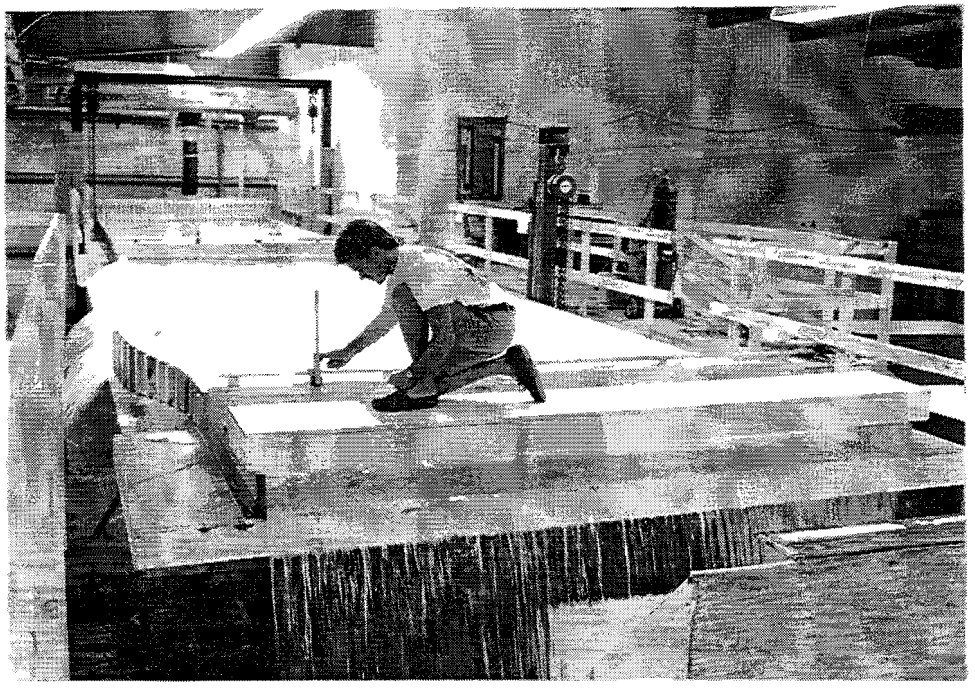

Figure C.2 Overall view of roadway model looking upstream

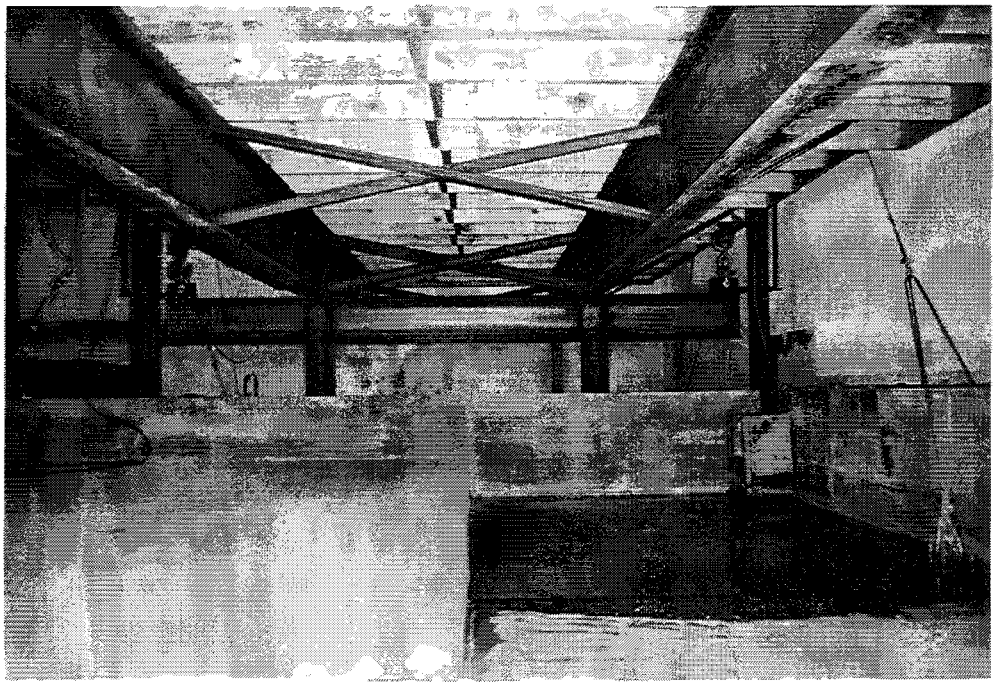

Figure C.3 Underside of model looking upstream

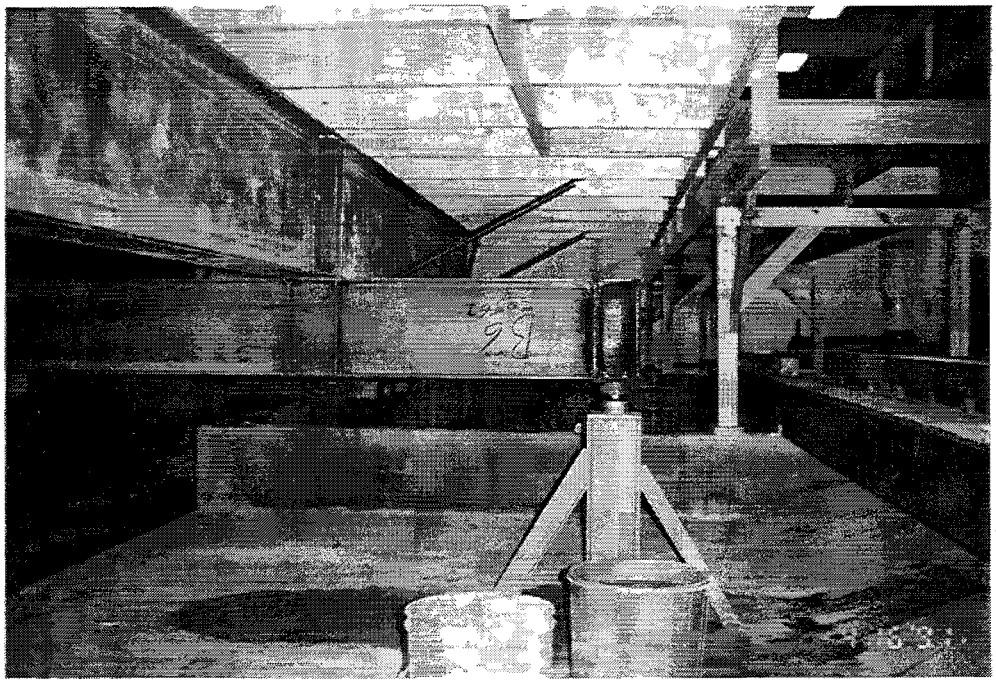

Figure C.4 Ball-bearing support looking downstream

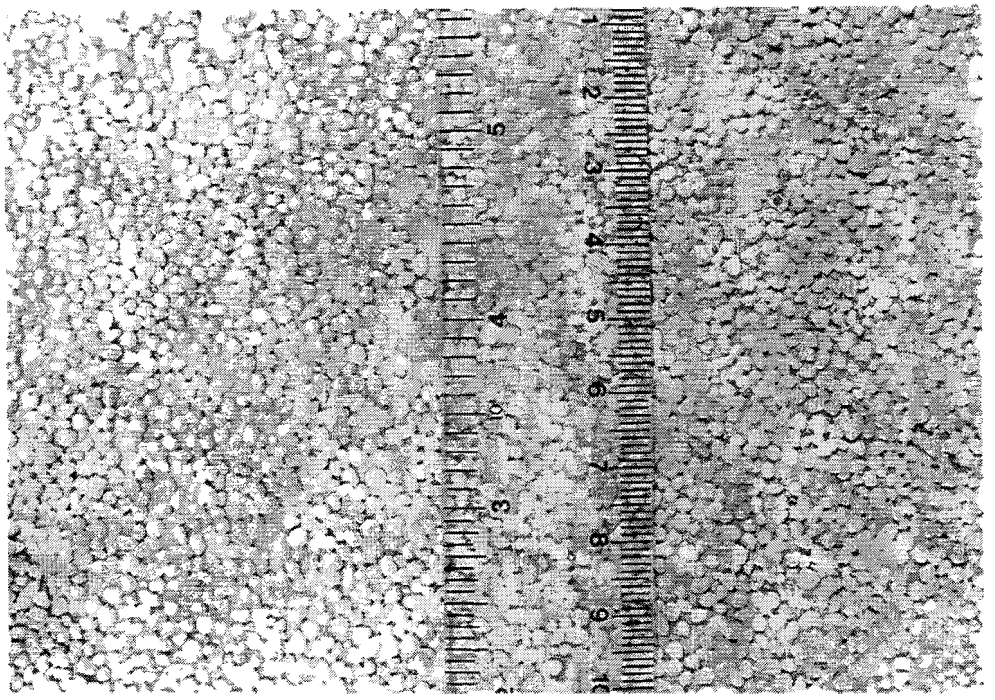

Figure C.5 Surface roughness on the model roadway

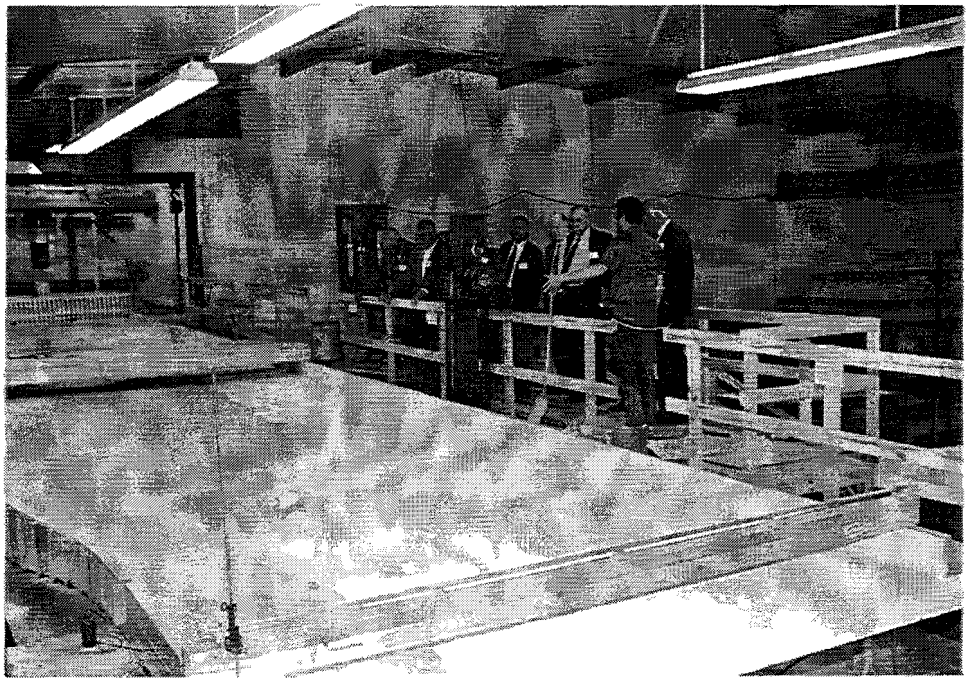

Figure C.6 View of ponded width for efficiency less than 100%

Figure C.7 Initiation of standing wave at downstream end of inlet opening for efficiency less than 100%

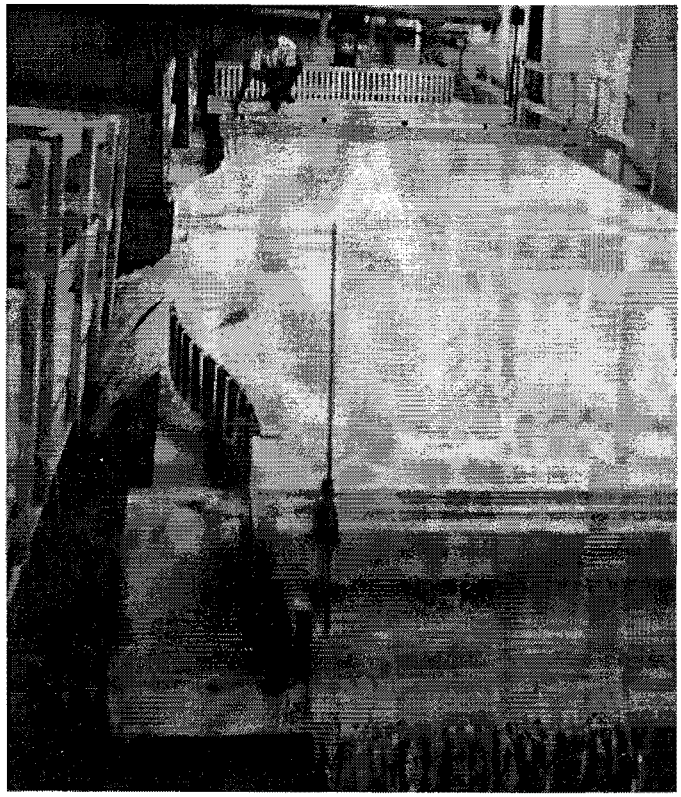

Figure C.8 Standing wave moving from downstream transition back into roadway for efficiency less than 100%

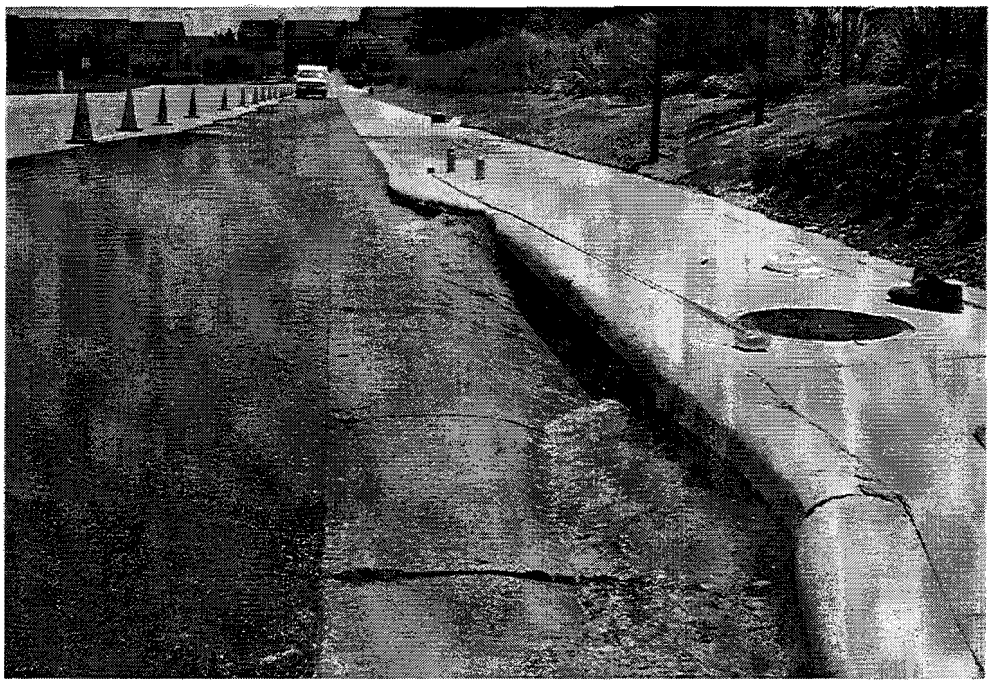

Figure C.9 Overall view of field test 3

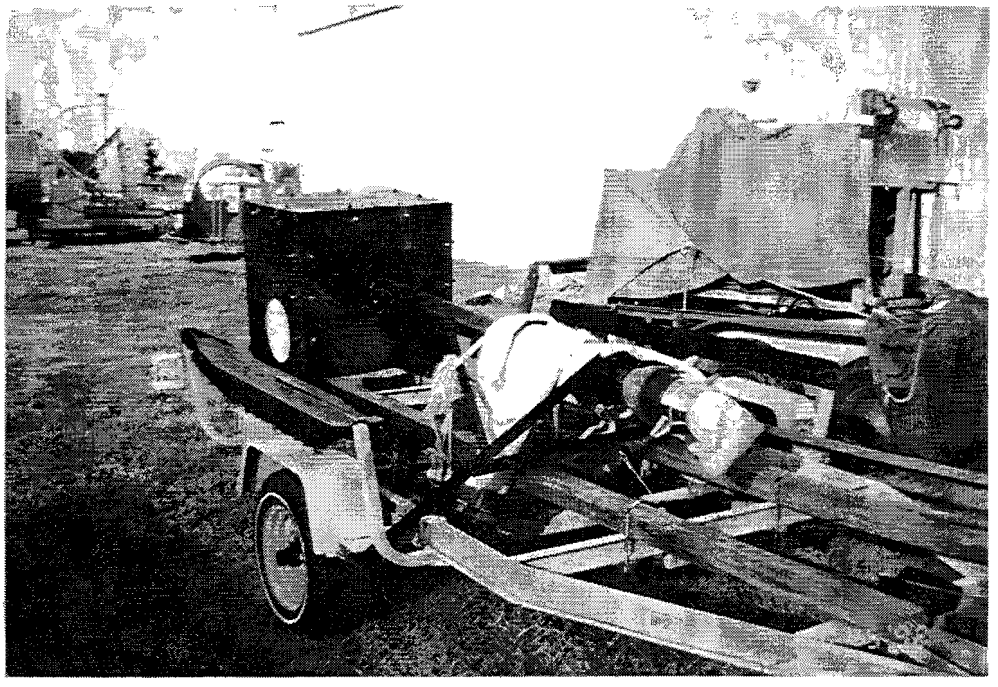

Figure C.10 Flow measurement device for field tests

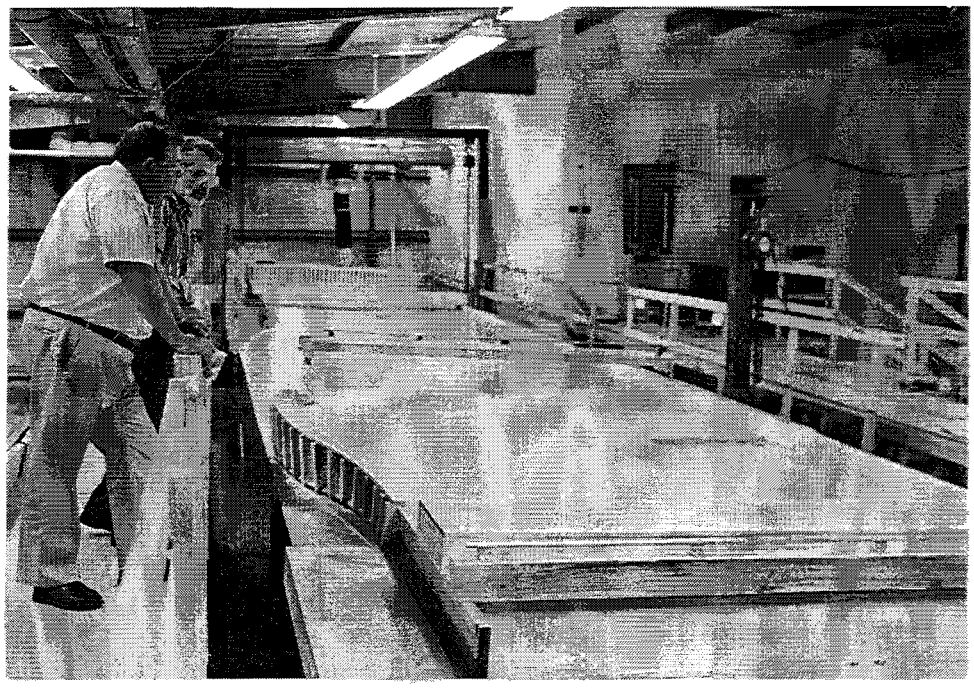

Figure C.11 Model tilted to the left for bridge deck drain studies (with drain 2 installed)

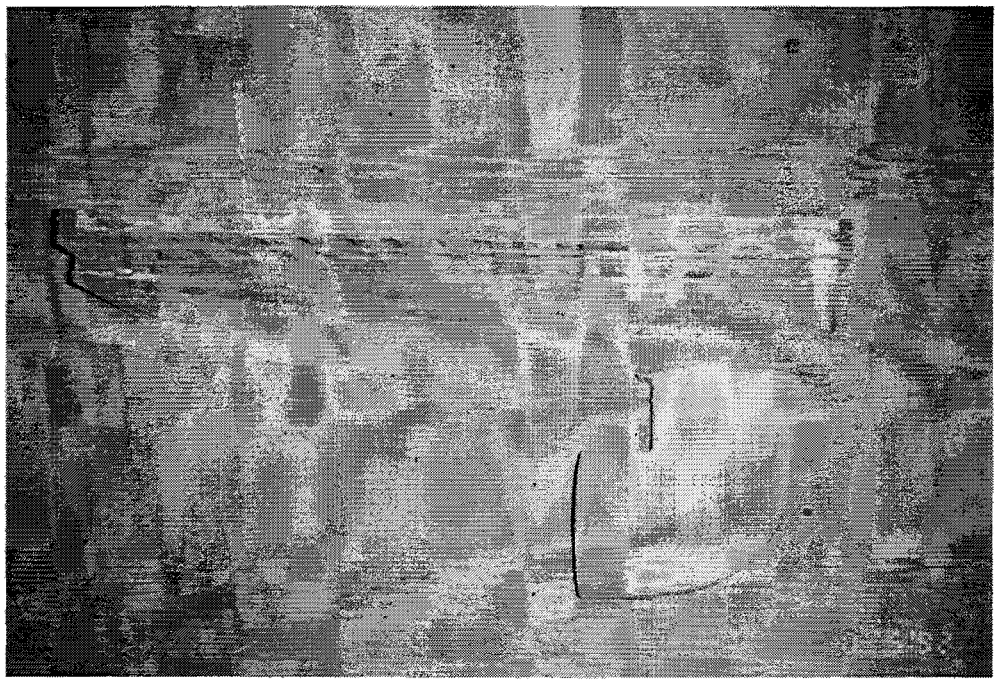

Figure C.12 Drain 2

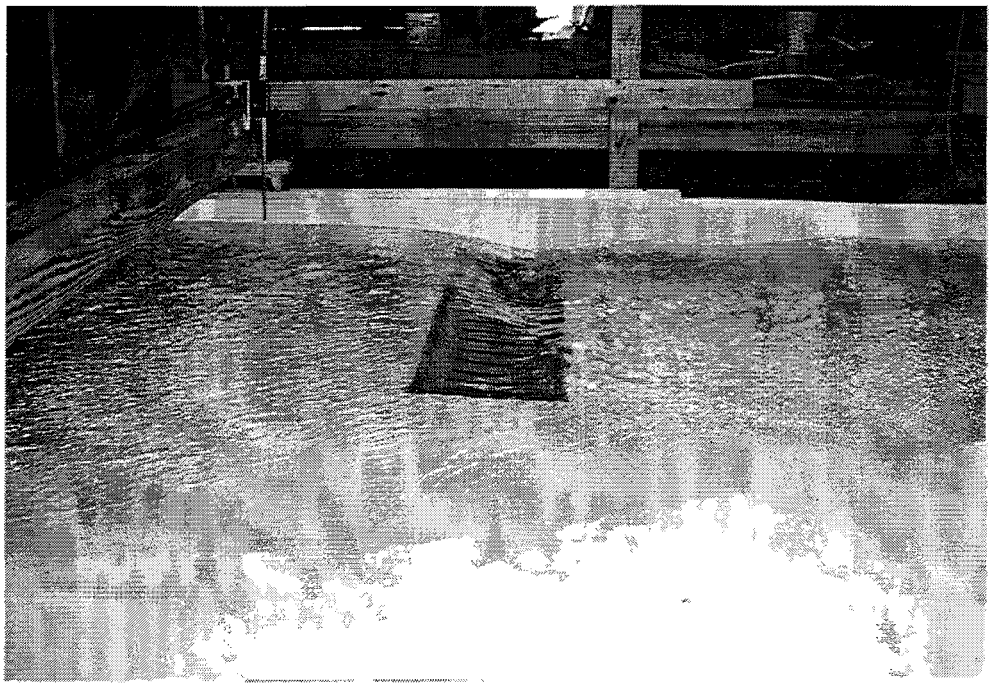

Figure C.13 Drain 2 for back-pressure conditions

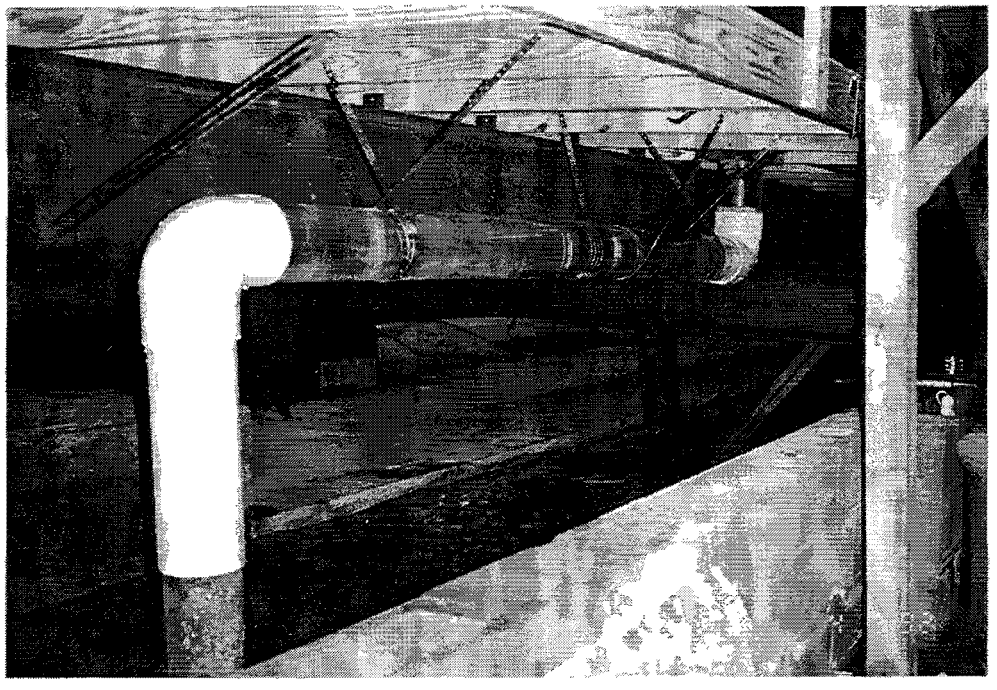

Figure C.14 Piping configuration B for Drain 2

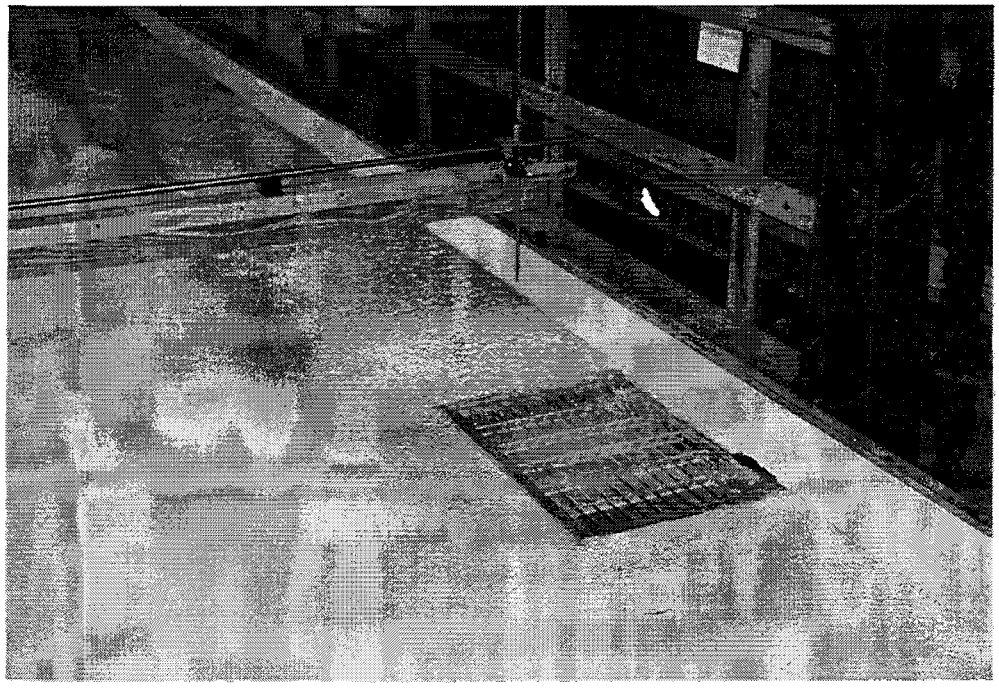

Figure C.15 Drain 3

Figure C.16 Drain 3 for back-pressure conditions